U.PORTO
FACULDADE DE CIÊNCIAS
UNIVERSIDADE DO PORTO

INSTITUTO DE CIÊNCIAS BIOMÉDICAS ABEL SALAZAR
UNIVERSIDADE DO PORTO

U.PORTO
FACULDADE DE FARMÁCIA
UNIVERSIDADE DO PORTO

HELSINGIN YLIOPISTO
HELSINGFORS UNIVERSITET
UNIVERSITY OF HELSINKI

# *In vitro - in silico* approach for the prediction of *in vivo* performance of drugs


Cristiana do Vale Correia
Master Degree in Biochemistry
Department of Drug Sciences, FFUP
2018

**Supervisor**
Prof. Dr. Nuno Filipe de Sousa Vale,
Faculty of Pharmacy of the University of Porto

**Co-supervisors**
Prof. Dr. Arto Urtti and Prof. Dr. Marjo Yliperttula,
Faculty of Pharmacy of the University of Helsinki

INSTITUTO DE CIÊNCIAS BIOMÉDICAS ABEL SALAZAR
UNIVERSIDADE DO PORTO

U.PORTO

FACULDADE DE CIÊNCIAS
UNIVERSIDADE DO PORTO

Todas as correções determinadas pelo júri, e só essas, foram efetuadas.

O Presidente do Júri,

Porto, _____/_____/_____

# AGRADECIMENTOS (ACKNOWLEDGEMENTS)

Em primeiro lugar quero agradecer ao Prof. Nuno Vale pelo desafio lançado, pela constante procura em inovar, pela oportunidade de ir para fora do país estudar algo novo para nós e pela confiança que depositou em mim.

Quero também agradecer à minha co-orientadora Marjo Ylipertulla por me ter recebido e integrado na sua equipa e ao professor Arto pela ajuda e supervisão quer na fase de aprendizagem quer na fase de desenvolvimento do projeto.

Um enorme agradecimento à técnica de laboratório Leena por toda a orientação dada no laboratório, por estar sempre disponível a ajudar e por garantir constantemente que nada me faltasse. Agradeço também ao Feng Deng pela enorme ajuda que me deu na aprendizagem de manipulação dos programas assim como na superação dos obstáculos que foram aparecendo.

Obrigada a toda a equipa da Marjo não só por estarem sempre disponíveis para me ajudar no que quer que precisasse, como pelos agradáveis momentos de lazer.

Quero agradecer à Shahba, ao Jhon, à Sara e a todo o Antti Korpien, pelos bons momentos passados em casa, e por me ajudarem a descontrair depois de um dia de trabalho.

Por fim, mas não menos importante, queria agradecer a todos os meus amigos, família e namorado por me terem acompanhado sempre, mesmo que à distância!

# RESUMO

O uso de modelos farmacocinéticos permite uma seleção, e posterior exclusão, de compostos com potencial toxicidade, levando a tomadas de decisões mais informadas em estados iniciais de desenvolvimento de novos fármacos, bem como a formulação de regimes de dosagem e estudos de farmacocinética. Estes estudos podem ser feitos a partir da construção de modelos em softwares de simulação como o STELLA® ou com recurso a programas mais sofisticados especificamente criados para estudos farmacocinéticos como o GastroPlus™.

No tratamento de cancro, onde o tecido a ser tratado é composto por várias subpopulações de células e onde várias vias de crescimento celular podem estar desreguladas, o tratamento com um único fármaco anticancerígeno é insuficiente para um tratamento efetivo, o que pode levar à implementação de terapias de combinação.

Na realização deste trabalho foi principal preocupação a utilização de abordagens *in vitro* como ponto de partida para o desenvolvimento de modelos *in silico,* no âmbito de combinações de fármacos para o tratamento de cancro*.* Por sua vez, esta ligação tem por base o objetivo posterior de prever a performance da combinação de fármacos *in vivo*. Para isso, dois fármacos de referência para o tratamento de cancro [gemcitabina e 5-fluorouracil (5-FU)] foram estudados, *in vitro*, em combinação com um fármaco reaproveitado, ou seja, um fármaco já licenciado e bem caracterizado para uma dada indicação terapêutica e cuja aplicabilidade na área do cancro pode ser incluída. As combinações de fármacos foram testadas nas linhagens celulares humana e cancerígena da próstata PNT2 e PC-3, e na linhagem celular também humana e cancerígena de pulmão A549. Depois, com recurso ao software de simulação STELLA ® foram desenvolvidos modelos farmacocinéticos de dois compartimentos que mimetizam o efeito das combinações de fármacos previamente testadas nos ensaios *in vitro* e que acoplam essa informação ao seu perfil farmacocinético em humanos.

Considerando o parâmetro de quantificação do efeito das combinações a área sobre a curva do efeito ($AUC_{efeito}$), verificou-se que as combinações de fármacos com maior AUC (o que é um indicador direto de maior % de inibição da proliferação celular), foram as do itraconazole em combinação com qualquer um dos fármacos anticancerígenos de referência. Além disso, verificou-se que a % de inibição celular tem uma relação de dependência com a dose de itraconazole e que se a administração do itraconazole for

continuada (intervalo de dosagem de 24h) prevê-se um aumento na % de inibição celular.

# ABSTRACT

Pharmacokinetic models enables filtering out molecules with high potential for toxicity, improving decision making in clinical drug development in early drug development stage, the design of dosing regiments and pharmacokinetic (PK) studies. This studies may be done through the development of models in simulation softwares as STELLA® or using more sophisticated programs specifically created for pharmacokinetic studies as GastroPlus™.

In cancer treatment, where tissue to be treated is composed by several cell sub-populations and where several cell growth pathways may be disrupted, single-agent treatment is insufficient for an effective treatment, which can lead to implementation of drug combination therapies.

In this work the main concern was the use of *in vitro* approaches as a starting point for the development of *in silico* models, in the context of drug combinations for the treatment of cancer. In turn, this linkage is based on the later goal of predicting the performance of the drug combination *in vivo*. For this, two reference drugs for the treatment of cancer [gemcitabine and 5-fluorouracil (5-FU)] were studied, *in vitro*, in combination with a repurposed drug, that is, an existing licensed and well-characterized drug for a certain therapeutic indication and whose applicability in the area of cancer may be included. Combinations of drugs were tested in human and prostate cancer cell lines PNT2 and PC-3, and in the human cell line and lung cancer A549. Then, using the STELLA® simulation software, two-compartment pharmacokinetic models were developed that mimic the effect of drug combinations previously tested in the *in vitro* assays and which couple this information to their pharmacokinetic profile in humans.

Considering the combinations effect quantification parameter area under the effect curve ($AUC_{effect}$), it was found that combinations of drugs with higher AUC (which is a direct indicator of greater % inhibition of cell proliferation) were the itraconazole in combination with any of the reference anticancer drugs. In addition, it was found that % cell inhibition is itraconazole-dose dependent and that if itraconazole administration is continued (24 hour dosing interval) an increase in % cell growth inhibition is predicted.

# KEYWORDS

Cancer treatment, compartmentally based pharmacokinetic models, drug combination, drug repurposing, GastroPlus™, *in silico* modeling and simulation, pharmacokinetics, STELLA®.

# INDEX

# LIST OF FIGURES

# LIST OF TABLES

# LIST OF ABBREVIATIONS

14DM: lanosterol 14-demethylase

5'-NT: 5'-nucleotidase

5-FU: 5-fluorouracil

ACAT: advanced compartmental absorption and transit

ACD: anticancer drug

AD: Alzheimer disease

ADME: absorption, distribution, metabolism, and elimination

ADMET: absorption, distribution, metabolism, elimination, and toxicity

ATL: alanine aminotransaminase

AUC: area under the curve

Bax: Bcl-2 associated X

Bcl-2: B-cell lymphoma 2

CDA: cytidine deaminase

CL: plasma clearance

CNT: concentrative nucleoside transporters

$C_p$-time: plasma concentration versus time

CV: coefficient of variation

CYP: cytochrome P450

DCTD: deoxycytidylate deaminase

dFdCDP: gemcitabine diphosphate

dFdCMP: gemcitabine monophosphate

dFdCTP: gemcitabine triphosphate

dFdU: 2',2'-difluorodeoxyuridine

dFdUMP: 2',2'-difluorodeoxyuridine monophosphate

DHFU: dihydrofluorouracil

DMSO: dimethyl sulfoxide

DNA: deoxyribonucleic acid

DPD: dihydropyrimidine dehydrogenase

$EC_{50}$: half maximal effect concentration

ENT: equilibrative nucleoside transporters

FBS: fetal bovine serum

FDA: food and drug administration

FdUDP: fluorodeoxyuridine diphosphate

FdUMP: fluorodeoxyuridine monophosphate

FdUTP: fluorodeoxyuridine triphosphate

FUDP: fluorouridine diphosphate

FUDR: fluorodeoxyuridine

FUMP: fluorouridine monophosphate

FUR: fluorouridine

FUTP: fluorouridine triphosphate

Gem: gemcitabine

GLI: glioma

I.v.: intravenous

$IC_{50}$: half maximal inhibitory concentration

JNK: c-JUN N-terminal kinase

$k_{10}$: elimination rate constant

$k_{12}$: transfer rate constants to describe the movement of drug from central to peripheral compartment

$k_{21}$: transfer rate constants to describe the movement of drug from peripheral to central compartment

$k_a$: absorption rate constant

$k_e$: kidney elimination rate constant

$k_m$: liver elimination rate constant

logP: logarithmic partition coefficient

MDR: multidrug resistance

mtDNA: mitochondrial deoxyribonucleic acid

mTOR: mammalian target of rapamycin

MTT: methylthiazolyldiphenyl-tetrazolium bromide

MW: molecular weight

OD: optical density

OPRT: orotate phosphoribosyltransferase

P.o.: per oral

p38 MAPK: p38 mitogen-activated protein kinase

p38: protein 38

p53: protein 53

PBPK: physiologically based pharmacokinetic

PBS: phosphate buffered saline

PD: pharmacodynamic

PEAR: population estimates for age-related physiology

P-gp: p-glycoprotein

PK: pharmacokinetic

$pK_a$: acid dissociation constant at a logarithmic scale

PRPP: phosphoribosyl pyrophosphate

Q: rate of blood perfusion

R&D: research and development

RD: repurposed drug

RET: rapidly equilibration tissue

RNA: ribonucleic acid

RPMI-1640: Roswell park memorial institute 1640

RR: ribonucleotide reductase

SET: slowly equilibrating tissue

SMO: smoothened

SP: side population

SRB: sulforhodamine B

STELLA: structural thinking experimental learning laboratory with animation

$t_{1/2\beta}$: elimination half-life time

TK: thymidine kinase

Topo II: topoisomerase type II

TP: thymidine phosphorylase

TrypLE: trypsin-like enzyme

TS: thymidylate synthase

UK: uridine kinase

UMP/CMP kinase: nucleoside monophosphate kinase

UP: uridine phosphorylase

$V_d$: volume of distribution

$V_{d1}$: volume of distribution in the central compartment

$V_{d2}$: volume of distribution in the tissue compartment

VEGF: vascular endothelial growth factor

VEGFR2: vascular endothelial growth factor receptor 2

$V_{ss}$: steady-state volume of distribution

# LIST OF EQUATIONS

# 1. INTRODUCTION

## 1.1. Drug development process

Drugs are xenobiotics, which means that they are not naturally produced in the body, thus being foreign to it. They can heal, but they can harm too, depending on the circumstances in which they are used and in which dose. Citing the physician/alchemist Paracelsus statement: “All things are poisons, for there is nothing without poisonous qualities. It is only the dose which makes a thing poison”.[1-2]

Pharmaceutical development has numerous phases (Figure 1). Firstly, there is the discovery period, where the target to “attack” is defined and several compounds are tested against that specific target. The most promising ones (lead compounds) may suffer chemical modifications (lead optimization) to improve their potency and then continue to the preclinical phase. At this stage, the drug candidate’s pharmacology is well characterized through *in vitro* and *in vivo* tests, and that includes its pharmacokinetics (PK), which refers to what the body does to the drug [absorption, distribution, metabolism, and elimination (ADME)] and pharmacodynamics (PD), which is more related to what the drug does to the body and places particular emphasis on dose-response relationships, that is, the relationships between drug concentration and effect.[3] Thus, important parameters can be evaluated, such as dosing regimen, efficacy degree, and possible toxicity. It is also at this stage where the therapeutic window of the new drug formulation is determined, which is a crucial step in drug development. In other words, it’s imperative to establish the dose at which drug starts to be therapeutic and when it starts to be toxic. If new drug candidate successfully overcomes the preclinical stage, it enters in clinical trials where parameters like efficacy, safety, and dose selection are determined in healthy and non-healthy humans.[2] The small percentage of new drug candidates that successfully pass in all the previous stages can then be submitted to approval and market phases.[4-5] Regarding all the variables to consider and all the tests that need to be performed to a new drug formulation, new drugs approval takes on average 7 to 9 years. Moreover, the cost of introducing a new drug can range from 600 million to 1 billion euros.[2, 6]

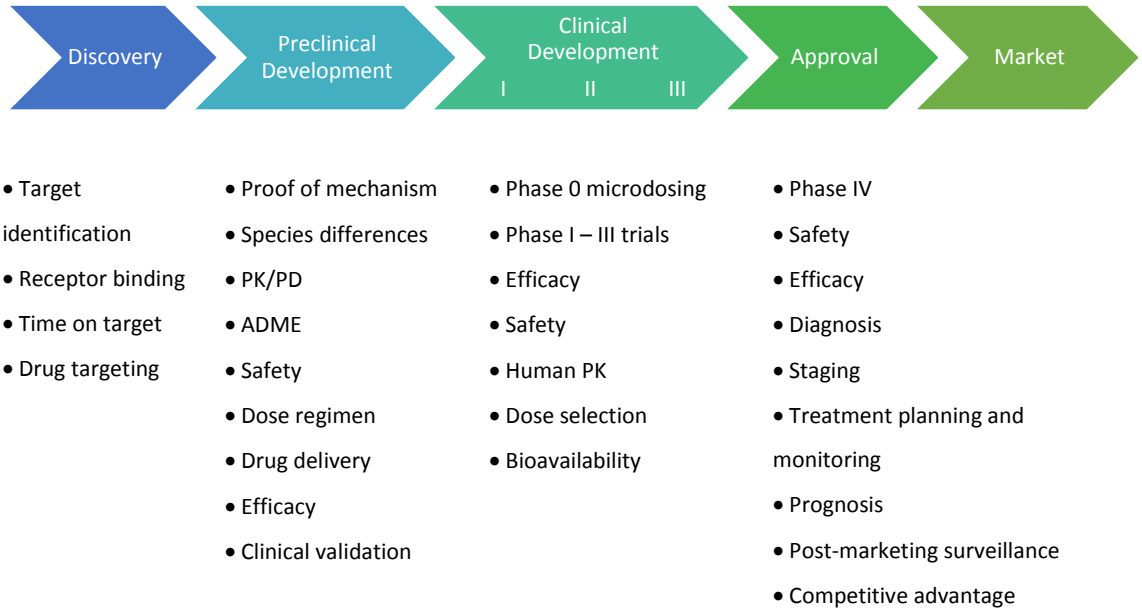


Figure 1 - **Drug development process.** Adapted from https://goo.gl/images/L5REQT.

## 1.2. Pharmacokinetics

PK refers to the study of the drug's behavior in the body, like their pharmacologic, therapeutic and toxic responses in either man or animals. This is the area of the pharmacology where the kinetics of ADME of a certain drug are studied (Figure 2). The study of PK involves both theoretical and experimental approaches. On the one hand, in experimental approaches, one aims for the development of techniques and analytical methods to measure drug and metabolites in biological samples, such as plasma, serum or blood, tissues, urine, feces, saliva or any other relevant biologic specimens, and procedures that facilitate data collection and manipulation. On the other hand, theoretical approaches aim the development of PK models to predict drug disposition, which includes drugs distribution and elimination, after its administration.[2, 7]

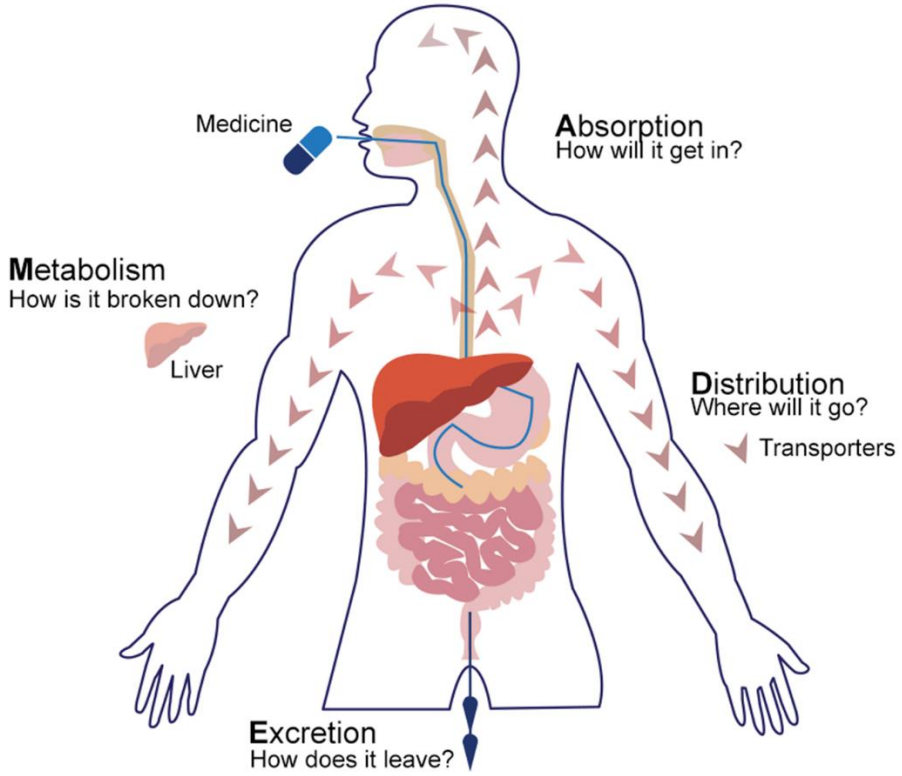


Figure 2 - **General scheme of pharmacokinetic principles** (ADME). Adapted from https://goo.gl/images/Cq1XAz.

With PK studies, one can measure the drug's bioavailability, which is the fraction of unaltered drug that reaches systemic circulation after administration, and thus one can make dosage adjustments in order to maintain drug plasma concentration within the therapeutic window. Moreover, it enables the evaluation of the effects of physiological and pathologic conditions on drug disposition and absorption as well as to correlate the pharmaceutical responses with the administered doses.[2, 7]

## 1.3. Pharmacokinetic models

PK models describe the absorption, distribution, metabolism, and the elimination of molecules (drugs, compounds under development…) in an organism, thus providing useful information to foster efficient and informative drug development. These models not only improve decision making in clinical drug development but also enable the design of dosing regimens that have the highest probability for the drug to reach its target with the desired concentration.[8-10]

PK models may comprise three categories of models, empirically, physiologically and compartmentally based PK models.[7] An empirically based model is used when limited information is available. In this case, the model only interpolates the data and allows an empirical formula to predict the drug level over time, without taking in consideration the mechanism by which the drug is absorbed, distributed and eliminated in the body.[7] On the opposite side, there is the physiologically based PK (PBPK) model, the most complex type of model and the model that more accurately describes a drug PK. In this model, sample tissues and blood flow monitoring to the liver *in vivo* are needed, which makes it more frequently used to describe drug distribution in animals, rather than in humans. When making physiologic PK models for the human body, since tissue sampling is not practical, the drug concentration in each tissue may be estimated based on previous knowledge of the physiologic and biochemical composition of the body human organs.[7, 11] Ultimately, the most commonly used PK model is the compartmentally based, which represents a very simple and useful tool in PK. In this model type tissues are grouped into compartments, depending on their blood flow and drug binding (tissues with similar blood flow and drug tissue binding are grouped in the same compartment).[7, 12]

### 1.3.1. Compartment models

After drug administration, intravenously, peroral or by any other administration route, plasma drug concentration changes all the time and this change can be described by analytical equations. ADME processes are complex, so, an accurate mathematical description of these processes often leads to heavy calculations for a computer which is not practical. Thus, simple models, such as the compartmental models, are usually used in PK studies.[1-2, 7]

In compartment models, the body is distributed in one or more compartments. A compartment is not a real anatomic or physiologic region but it is a group of tissues or organs that behave similarly with a certain drug. The compartments of the model communicate with each other in a reversible way through rate constants.[7, 13]

Compartment models allow the description of the drug plasma concentration over time and, consequently, an accurate estimation of important PK parameters such as clearance, volume of distribution, half-life elimination and elimination rate constants of a drug. Through plasma concentration profile analysis, the compartment model that best describes the profile can be chosen. The profile will depend not only on the drug in study

but also on the administration route. Thus, the equations that characterize the profile are also dependent on these factors.[2, 7]

Independently on the administration route, the main factor that will influence the number of compartments in a model is the ability of the drug to distribute in the body. In other words, a drugs distribution time is relative to the time period needed to achieve an equilibrium between the drug that is in plasma and the drug in the tissues. If the drug is rapidly distributed, all the tissues will behave similarly with the drug and the drug in plasma will equilibrate with the tissues or organs almost instantaneously. Thus, its plasma profile is easily described by a one-compartment model, where there's only one compartment to describe the drug concentration in all body. On the opposite side is a drug that is slowly distributed. In this case, additional compartments are needed to separate central compartment from groups of tissues or organs with lower capacity to equilibrate with plasma. Summarily, the longer is the distribution period, the higher is the number of compartments needed to describe the system.[2, 7]

In Figure 3 are depicted one- and two-compartment models following oral and intravenous administration. Plasma and tissues with high flux of fluids from circulatory or lymphatic systems (well-perfused tissues), such as liver and kidney, are usually grouped in central compartment (or plasma compartment) – Box 1. Systems with lower perfusion degree, such as bones, cartilage or fat tissue are usually grouped together in a peripheral compartment (or tissue compartment) – Box 2.

When a drug is given intravenously, the drug enters directly into the central compartment (Figure 3, Model 1 and Model 3). When a drug is administered per oral, the drug has to be absorbed from gastrointestinal tract and enters in blood circulation at a rate determined by absorption rate constant $k_a$ (Figure 3, Model 2 and Model 4). Two-compartment models (Figure 3, Models 3 and 4) have two extra transfer rate constants to describe the movement of drug from central to peripheral compartment and vice versa ($k_{12}$ and $k_{21}$, respectively). Elimination of drug occurs from the central compartment because the organs involved in primary drug elimination are kidney and liver. The elimination is regulated by an elimination rate constant k. Compartment models don't usually describe tissue drug levels well but are very useful to predict drug plasma levels.

Knowing the parameters of the compartment model, one can estimate the amount of drug in the body and the amount of drug eliminated at any time. The compartmental models are particularly useful when little information is known about the tissues.[7]

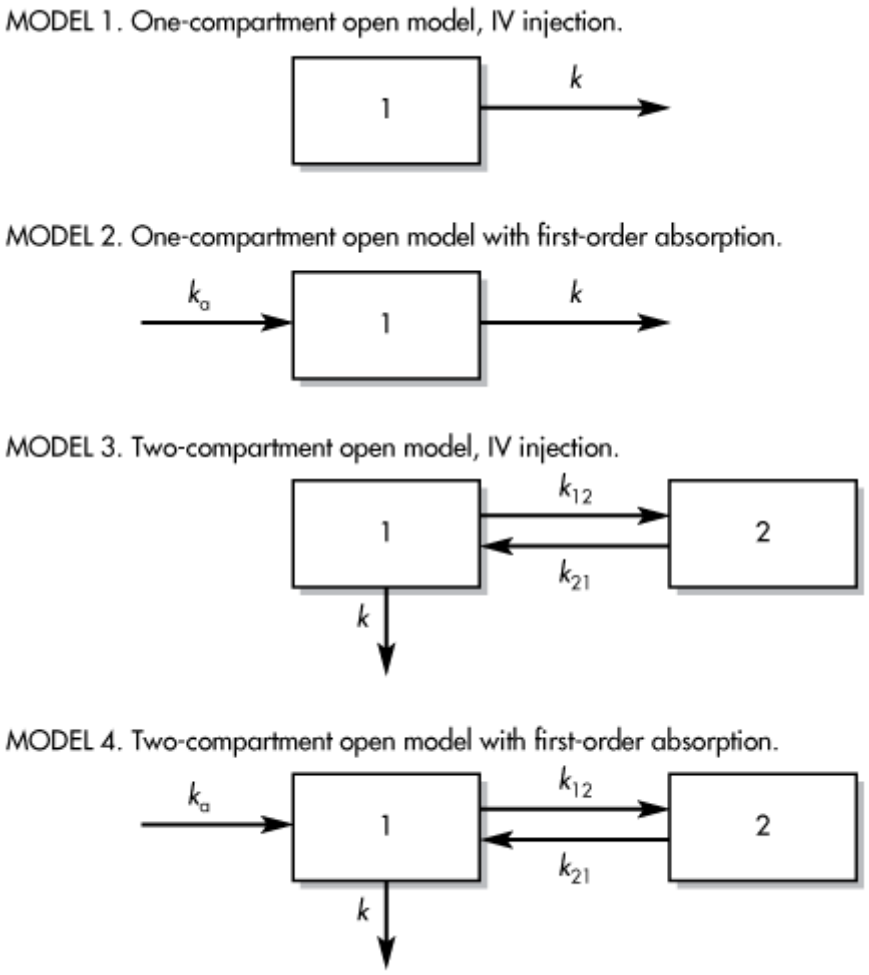


Figure 3 - **Schematic representation of compartment models.** Model 1 is a one-compartment model for IV injection. The drug is administered directly to the central compartment and eliminated at a rate defined by elimination rate constant k. Model 2 is a one-compartment model for oral administration. The drug enters central compartment at a rate defined by absorption rate constant $k_a$. Model 3 is a two-compartment model for IV injection. After drug administration drug amount in central compartment reaches equilibrium with the peripheral compartment. $k_{12}$ and $k_{21}$ are the transfer rate constants that define mass transfer from central compartment to peripheral compartment and vice-versa, respectively. Model 4 is a two-compartment model for oral administration. Adapted from Ref. 7.

### 1.3.2. Physiologically based pharmacokinetic model

The concept of PBPK models first appeared in 1937, introduced by Teorell Torsten, the father of Pharmacokinetics.[14-15] The mathematical framework is similar to the one used in compartment model but in this models, besides the inclusion of a higher number of compartments, known anatomic and physiologic data are included. Thus, in case example where a pathology affects the physiology of an organ or tissue, the new physiology will be taken into consideration. In PBPK models, contrarily to compartment

models, relevant organs or tissues for the model are realistically represented and more accurate drug distribution predictions are achieved.[7, 16]

Model development requires many experimental data collection. In order to realistically predict drug distribution to every part of the body, blood flow in every tissue is required. Besides that, real organ volume and its tissue drug concentration have to be described. The number of compartments included in the model is variable since tissues with no drug penetration are excluded (usually brain, bones and other parts of the central nervous system).[7] In Figure 4 an example of a PBPK model for drug perfusion after intravenous injection is shown. Relevant organs or tissues for drug absorption are shown separately, such as heart, muscle, kidney, and liver, while other tissues are grouped according to their ability to equilibrate with plasma. Tissues that equilibrate rapidly were included in the RET group (rapidly equilibration tissue) and tissues that take longer to reach equilibrium were put in the SET group (slowly equilibrating tissue). The rate of blood perfusion in every organ or tissue is known and represented by Q. Kidney and liver elimination rate constants are also included in the model ($k_e$ and $k_m$, respectively).

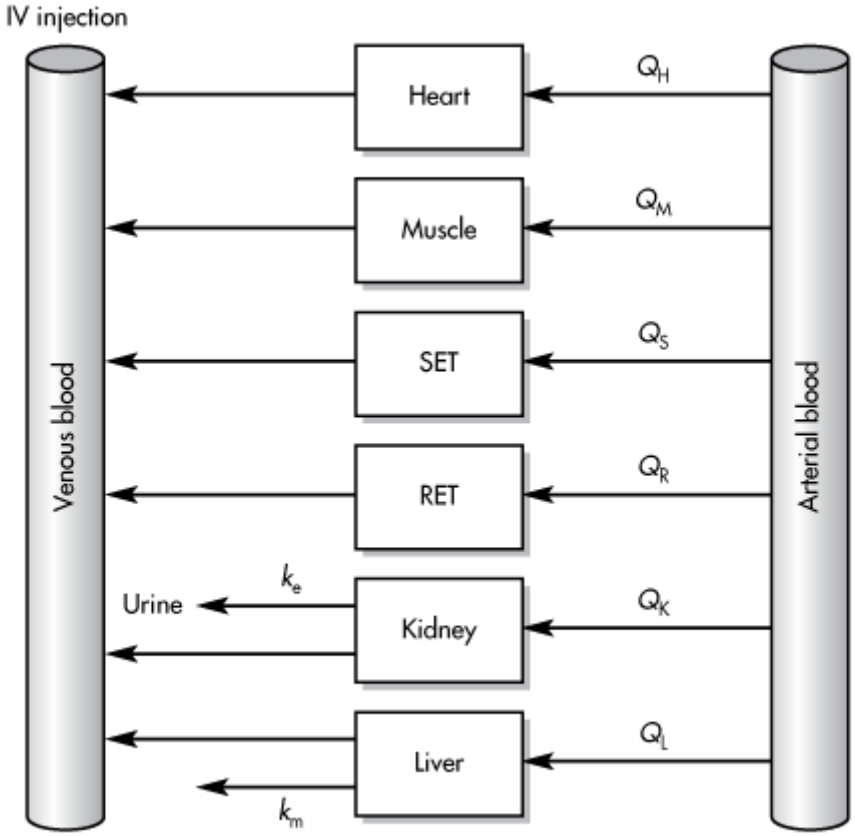


Figure 4 - **Representative example of a PBPK model for IV injection.** Q's represent the rate of blood perfusion in every compartment represented in the model. The compartment may be an organ or a group of tissues with similar blood perfusion rate. Heart, Muscle, SET (slowly equilibrating tissue), RET (rapidly equilibrating tissue), Kidney and Liver represent are the different compartments of the model. k's represent kinetic constants: $k_e$ is the rate constant for drug excretion in kidney and $k_m$ is the rate constant for hepatic elimination. This model construction requires knowledge about the size or mass of each tissue compartment, which is experimentally determined. Adapted from Ref. 7.

In Figure 4 the model is not complete because there is no way that the drug would go from injection IV to the tissues. All the arrows point to the left. From venous blood the blood (and drug) goes through the lungs and heart to the arterial blood and from there through the tissues.

Unfortunately, much of the data required for model development is experimentally difficult to obtain, especially for human models. Therefore, this kind of approach is usually used to describe drug distribution in animal models, since experimental data is easier to obtain, and then distribution comparison between animal models can be done. In other words, varying animal model, insight into how physiologic and anatomic differences can affect drug distribution can be obtained and extrapolation data to human model may be possible.

## 1.4. *In silico* tools for PK studies

### 1.4.1. STELLA®

STELLA® is a simulation software application that enables the study of systems through its graphical representation. The program uses Compartments, Flows, Converters, and Connectors as building blocks. Compartments accumulate whatever flows into them, net of whatever flows out of them. Flows fill and drain accumulations. The unfilled arrowhead on the flow pipe indicates the direction of positive flow. The converter serves a utilitarian role in the software. It holds values for constants, defines external inputs to the model and calculates algebraic relationships. In general, it converts inputs into outputs. Hence, the name "converter." Connectors, as its name suggests, connects model elements. Moreover, the use of built-in time functions in converters, such as AND, OR, IF…THEN…ELSE or PULSE, allows a set of rules to be established which the program uses to control flow through the model, enabling the construction of more complex models. When the model is complete the user has only to establish a simulation time period and a time increment (h). This time increment is the interval of time between calculations. For example, if h=0.25 then every round of calculations (calculation of the value of every parameter in the model) is made every ¼ of time. Each value calculation can be made using either Euler's, 2$^{nd}$ or 4$^{th}$ order Runge-Kutta methods, being Euler's the simplest version of Runge-Kutta method. These are integration methods that estimate a new value ($y_{i+1}$) through the extrapolation of an old value ($y_i$) following Equation 1. In Euler's method, φ is the slope in $x_i$ (first derivate in $x_i$). In Runge-Kutta method, instead of one single derivation, one or more representative slopes (depending on the order of the method) are determined during h to estimate the new value. This equation can be applied step by step and trace out the trajectory of the solution.[17] Figure 5 is presented for a better interpretation of the method.

**Equation 1**

$$y_{i+1} = y_i + \varphi h$$

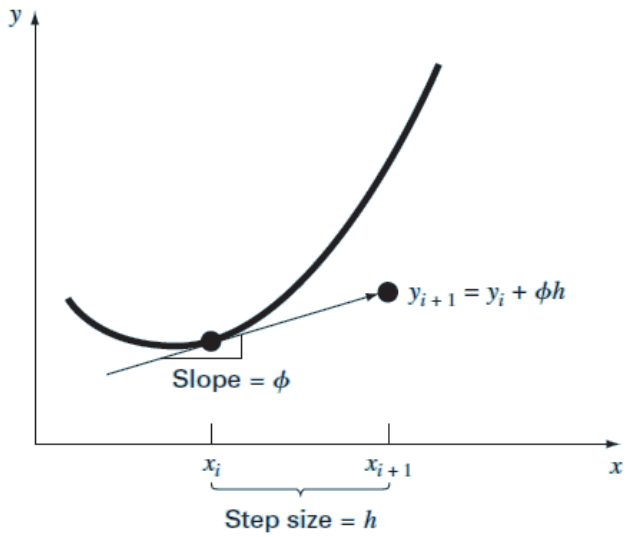


Figure 5 - **Graphical depiction of a one-step Runge-Kutta method.** Adapted from Ref. 17.

For systems with inherent oscillatory tendencies, Euler's method incurs in integration errors that accumulate throughout the simulation giving rise to results far from reality. In this cases, higher order Runge-Kutta methods represent better integration options, in a way that the greater the order is and the more accurate the results are. However, the simulation is slower.

A representative model built in STELLA® software is shown in Figure 6. The mass amount in Compartment 1 is determined by the difference between the amount that comes from Compartment 2 (mass transferred through Flow 2) and the amount that leaves Compartment 1 (mass transferred through Flow 1). The rate at each Flow building block transfers from one Compartment to the other is dependent on both the convertor and the stock to which is connected by connecting arrows. Therefore, knowing all the factors controlling the rate of transfer between the Compartments a model can be constructed and run.

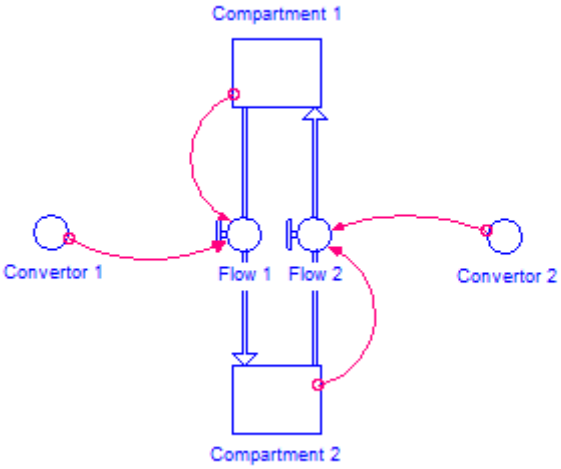


Figure 6 - **Schematic representation of a model built in STELLA® modeling program.** In this model, mass flows from compartment 1 to compartment 2 and from compartment 2 to compartment 1. Flow rates 1 and 2 are determined by convertor 1 and 2 respectively.

Many pharmaceutically related systems have been simulated using STELLA®. These have included models to predict *in-vivo* oral pharmacokinetic profiles for new drug formulations, ocular drug distribution or even gene expression.[18-20] One of the main advantages is the flexibility the user has to build and modify a model. Only the graphical interpretation has to be changed.

### 1.4.2. GastroPlus™

GastroPlus™ is an advanced technology computational program used in drug R&D. Contrary to STELLA®, GastroPlus™ has an absorption model incorporated which enables the simulation of intravenous, gastrointestinal, ocular, nasal and pulmonary absorption of new molecules. This absorption model is the Advanced Compartmental Absorption and Transit (ACAT) model, which is based on the original Compartmental Absorption and Transit model published by Yu and Amidon in 1999[21], but ACAT includes, for example, stomach and colon absorption. Thus, the physiological variables of each segment of the digestive tract are well characterized for different animal models or human from Fasted to Fed states. The physiological variables include pH, length and volume, enzymes and transporter protein distributions in the gut in the different species and for human, scaled to body weight for less than 77.5 kg.

Apart from ACAT model, which enables the user to obtain a detailed absorption profile of the molecule in study, GastroPlus simulations consist of the numerical integration of differential equations that coordinate a set of well-characterized physical phenomena that occur and interact as a result of drug transport, dissolution/precipitation, lumenal degradation, absorption/exsorption, excretion, gut metabolism, distribution, hepatic metabolism, enterohepatic circulation, renal clearance, and other clearance mechanisms. Therefore, if appropriate inputs about the compound in study are provided, such as lipophilicity, acid dissociation constant at logarithmic scale ($pK_a$), solubility, diffusion coefficient and gastrointestinal permeability and permeability in the ocular and pulmonary tissues, new drug plasma profile prediction, for a certain dose and administration route, is possible.

Furthermore, ten extra models are available to extend the capabilities of the basic GastroPlus™ beyond absorption and pharmacokinetic simulations. One of GastroPlus™ additional modules is ADMET Predictor™ module. With this model, physicochemical and pharmacokinetic parameters prediction of a new compound is possible through its molecular structure import. For deeper insight into the pharmacokinetics of a drug, PKPlus™ and PBPKPlus™ modules are very useful. The former can find the compartment model (up to three compartments) that best fits existing experimental $C_p$-time data of a drug. As an output gives the PK parameters that characterize the plasma profile. The latter enables prediction of drug distribution into various tissues as well as simulation of clearance profiles specific to given tissues. Additionally, an internal module called PEAR (Population Estimates for Age-Related Physiology) allows studies of human models with different organ physiologies, such as American, Japanese or Chinese population organs any age from 0 to 85 years old. Furthermore, coupling PBPK module to Metabolism and Transporter module one can input specific metabolizing enzymes and the extension of drug metabolization in any tissue or organ of the PBPK model and evaluate the effect of this metabolization in drug's plasma profile.

In spite of its sophistication, GastroPlus™ is relatively easy for someone with a background in ADME to learn and to use because GastroPlus™ incorporates an intuitive and modern graphical user interface that enables rapid and smooth transition from setting up inputs to evaluating results.

### 1.4.3. *In silico* tools for drug combination studies

The lack of satisfactory results with single-agent therapy in patients led to the introduction of drug combination therapies in health care. The use of drugs with different mechanisms or modes of action enables multiple targeting, either within the same cell or in multiple cell subpopulations, or the targeting of multiple diseases simultaneously, providing more effective treatments. This strategy's possible favorable outcome includes enhancement of the efficacy of the therapeutic effect, reducing the dosage but increasing or maintaining the efficacy, minimizing or avoiding possible toxicity and reducing or slowing down the development of drug resistance. Due to these therapeutic benefits, drug combinations have been widely used and became the leading choice for treating of very dreadful diseases, such as cancer and infectious diseases, including AIDS.[22-24]

Several *in silico* tools have been developed for theoretical drug combination studies. Some research areas are more focused in predicting if the combined effect may be synergistic, additive or antagonistic, where, by definition, synergism is more than an additive effect and antagonism is less than an additive effect, while others are more interest in predicting drug-drug interactions, which aims the evaluation of the influence of one drug in another's drug disposition. For this, several PK modeling programs like Simcyp® or GastroPlus™ have now specific modules to predict drug-drug interaction, using previous knowledge on main metabolizing enzymes of each one of the drugs in study. [25-27]

Although a wide variety of *in silico* tools is already available for drug combination studies, new approaches can be proposed and drug combination effect coupled with drug disposition simulation is an example of a gap in the existing resources.

## 1.5. Cancer

### 1.5.1. Anticancer drugs

Cancer treatment by chemotherapy is one of the most commonly used methodologies in cancer therapy, either as primary treatment or as an adjunt to another treatment modalities, such as surgery, radiotherapy or immunotherapy. This approach involves the use of low-molecular-weight drugs to destroy or reduce the proliferation of cancer cells.[28]

Antineoplastic drugs can be classified according to whether they need the cell to be in cycle (cycle-specific agents) or not (cycle-nonspecific agents). When they depend on the cell to be in cycle they can be divided into phase-specific agents, when their activity is greater at a specific phase of the cycle or nonphase-specific agents. Because cells are not usually in the same phase of the cycle at the same time, cell cycle phase specific agents need to be administered in separated doses or as a continuous infusion. Nevertheless, these classifications are not absolute since more than one mechanism may be involved.[28]

Cycle specific agents that are not dependent on the phase include alkylating agents, the antitumor antibiotics, and some miscellaneous agents and they are effective as long as the cell is in cycle, independently on the phase. Cycle nonspecific agents, which include mechlorethamine (nitrogen mustard) and the nitrosoureas, are effective through all phases of the cell cycle since their mechanism of action is not related to the cycle.[28]

Many of the cell cycle phase-specific drugs are antimetabolites chemically synthesized to mimic purines, pyrimidines or folates indispensable for nucleic acid and DNA synthesis. Two examples of pyrimidine analogs are gemcitabine and 5-fluorouracil (5-FU), that will be used in this project.[28]

#### 1.5.1.1. Gemcitabine

Gemcitabine is a chemotherapeutic drug, a nucleoside analog, which acts against an extensive range of solid tumors such as pancreatic, non-small cell lung cancer, breast, and ovarian cancers.[29]

This anticancer drug has several mechanisms of action including the inhibition of thymidylate synthetase, important to the inhibition of DNA synthesis and cell death, and the activation of the c-JUN N-terminal kinase (JNK) and p38 mitogen-activated protein kinase (p38 MAPK), that are key kinases in two major stress-activated signaling pathways.[30]

Gemcitabine is a prodrug whose activity occurs as a result of intracellular conversion to two active metabolites, gemcitabine diphosphate and gemcitabine triphosphate by the enzyme deoxycytidine kinase. Gemcitabine diphosphate also inhibits ribonucleotide reductase, the enzyme responsible for catalyzing the synthesis of deoxynucleoside triphosphates required for DNA synthesis. Finally, gemcitabine triphosphate

(difluorodeoxycytidine triphosphate) competes with endogenous deoxynucleoside triphosphates for incorporation into DNA.[29]

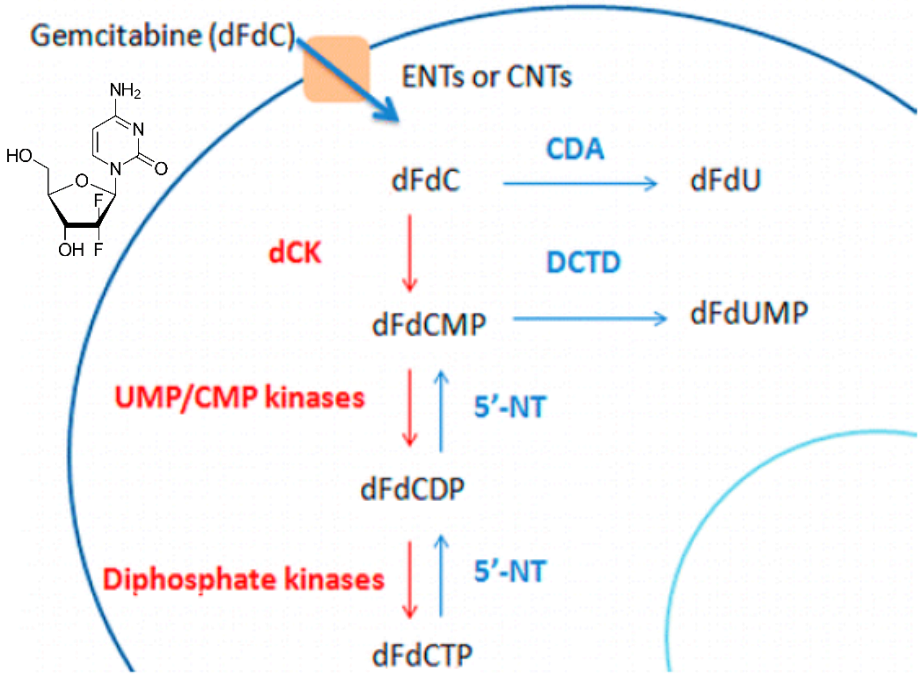


Figure 7 - **Phosphorylation and dephosphorylation of gemcitabine (dFdC) in the cell.** ENT: equilibrative nucleoside transporters, CNT: concentrative nucleoside transporters, dFdCMP: gemcitabine monophosphate, dFdCDP: gemcitabine diphosphate, dFdCTP: gemcitabine triphosphate, dFdU: 2',2'-difluorodeoxyuridine, dFdUMP: 2',2'-difluorodeoxyuridine monophosphate, CDA: cytidine deaminase, DCTD: deoxycytidylate deaminase, 5'-NT: 5'-nucleotidase, UMP/CMP kinase: nucleoside monophosphate kinase. Up left corner is gemcitabine molecular structure. Adapted from Ref. 29.

Nevertheless, treatment with gemcitabine has limited efficacy due to its high toxicity and inactivation in the serum, through deamination of its N-4 amine. Another important disadvantage associated with gemcitabine therapy is that, after initial tumor regression, some tumor cells may develop different forms of drug resistance, such as resistance related to nucleoside transporter deficiency. Indeed, the expression of human equilibrative nucleoside transporter-1 (hENT-1), which plays a key role in gemcitabine intracellular uptake, was found decreased in resistant cells lines.[31]

To improve its metabolic stability and cytotoxic activity and to limit drug resistance many alternatives have emerged, such as the synthesis of prodrugs.[29, 32-34] Chemical modifications could potentially lead to new therapeutic strategies. Various modifications have already been done in the 4-(*N*)- and 5'-positions of gemcitabine (Figure 8), such as the incorporation of poly(ethylene glycol) (PEG), valproic acid, 1,1',2-tris-nor-squalenoic acid (squalene) or valeroyl, heptanoyl, lauroyl and stearoyl linear acyl derivates in the 4-

(*N*) site or the addition of fatty acid chains or phosphate function protecting groups to the 5'-position.[29]

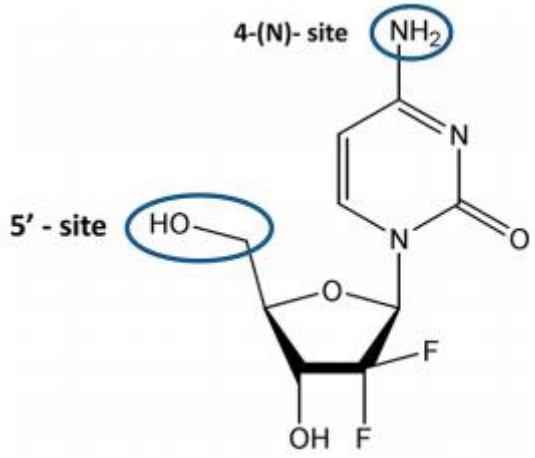


Figure 8 - **Principal modification sites in gemcitabine molecule.**

Additionally, in a recent work developed in our research group, an hexapeptide was conjugated to 4-(*N*)- site through anhydride succinic linker (Figure 9). Another strategy commonly used in cancer treatment to overcome drug resistance and improve efficiency is drug combination.[35]


Figure 9 - **Schematic structure of cell-penetrating hexapeptide (CPP6) gemcitabine conjugates.** Manuscript for submission: Correia et al, Bioorg. Med. Chem. Lett.

#### 1.5.1.2. 5-Fluorouracil

5-Fluorouracil (5-FU) is an anticancer drug, uracil analog, whose mechanism of action has been ascribed to the inhibition of thymidylate synthase (TS) and stoppage of DNA and RNA synthesis. This drug is not only first choice for the treatment of several

malignancies, such as colorectal, breast, gastric and head and neck cancer, but it is also being studied in the treatment of other conditions and types of cancer.[36]

5-FU-based chemotherapy improves overall and disease-free survival of the patients. Nonetheless, response rates for 5-FU-based chemotherapy as a first-line treatment is limited essentially due to the short half-life of this drug and the significant toxicity which requires dose reduction in 30-40% of the patients.[37]

Using the same facilitated transport mechanism as uracil, 5-FU enters the cell rapidly and is intracellularly converted in fluorodeoxyuridine monophosphate (FdUMP), fluorodeoxyuridine triphosphate (FdUTP) and fluorouridine triphosphate (FUTP). These are the 5-FU active metabolites that inhibit TS and disrupt DNA and RNA synthesis, respectively.[38-39]

The rate-limiting enzyme in 5-FU catabolism is dihydropyrimidine dehydrogenase (DPD), which converts 5-FU to dihydrofluorouracil (DHFU) (Figure 10). More than 80% of administered 5-FU is normally catabolized primarily in the liver, where DPD is abundantly expressed.[38] The remaining 20% enters the cell and can either be catabolized by DPD or anabolized. There are three pathways by which 5-FU may be anabolized and form cytotoxic nucleotides. The first is through uridine phosphorylase (UP) and uridine kinase (UK) for conversion to the ribonucleotide 5-fluorouridine-5'-monophosphate (FUMP). The second involves orotidine-5'-monophosphate phosphoribosyltransferase (OPRT) and its cofactor phosphoribosyl pyrophosphate (PRPP) to generate FUMP directly. The third, which is quantitatively less important, uses thymidine phosphorylase and thymidine kinase for conversion of 5-fluorouracil to FdUMP.[38]

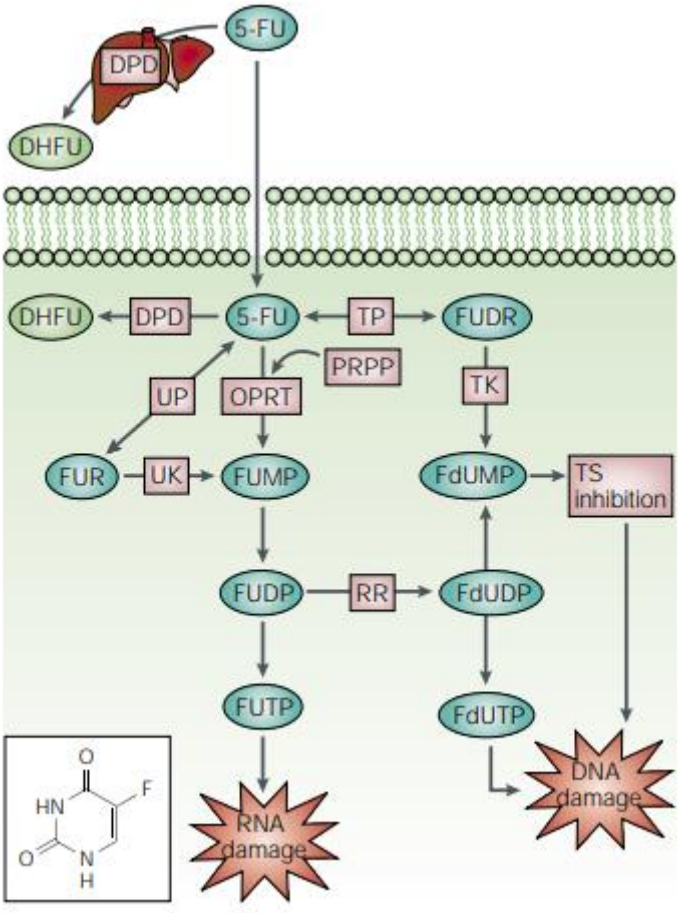


Figure 10 - **5-Fluorouracil (5-FU) metabolism**. Catabolism pathway: 5-FU is broken down in dihydrofluorouracil (DHFU) by dihydropyrimidine dehydrogenase (DPD) in the liver or intracellularly. Anabolism pathways: 5-FU can be converted in three main active metabolites: fluorodeoxyuridine monophosphate (FdUMP), which can inhibit thymidylate synthase (TS), fluorodeoxyuridine triphosphate (FdUTP), that can be incorporated in the DNA strand and stop chain progression, and fluorouridine triphosphate (FUTP), which will be involved in RNA damage. The first is originated through thymidine phosphorylase (TP) catalyzed the conversion of 5-FU to fluorodeoxyuridine (FUDR) which is then phosphorylated by thymidine kinase (TK). The second results from double phosphorylation of FdUMP. The last one derives from double phosphorylation of fluorouridine monophosphate (FUMP), which can either be directly converted from 5-FU by orotate phosphoribosyltransferase (OPRT) with phosphoribosyl pyrophosphate (PRPP) as the cofactor, or indirectly via fluorouridine (FUR) through the sequential action of uridine phosphorylase (UP) and uridine kinase (UK). The intermediate fluorouridine diphosphate (FUDP) metabolite can either be phosphorylated and originate FUTP or can be converted in fluorodeoxyuridine diphosphate (FdUDP) by ribonucleotide reductase (RR). Down left corner is 5-FU molecular structure. Adapted from Ref. 36.

Over the years, strategies to increase the anticancer activity of 5-FU and to overcome clinical resistance have been developed. One of them is the combination of 5-FU with other cytotoxic drugs that will act on targets distinct from 5-FU, like methotrexate, which will interfere with purine biosynthesis through disruption of tetrahydrofolate synthesis.[40] Other approaches are relative to the reduction of 5-FU degradation or increase of 5-FU activation, through inhibition of DPD or up-regulation of the anabolic enzymes, respectively. Despite these improvements, higher response rates and decreased toxicity still need to be accomplished.[36]

### 1.5.2. Drug repurposing in cancer

Although the existence of a wide variety of anticancer drugs approved and used in clinics, lack of effectiveness and good outcomes in many cancer patients incites to continuous hunt for new anticancer drug candidates. New drugs discovery, as stated in section 1.1, incurs to high investments and time to the pharmaceutical industry. Recently, drug repurposing has emerged as a strategy to reduce development times and cancer treatment cost, speeding up the access to new cancer therapies.[41-42]

Drug repurposing is a drug development strategy to reuse existing licensed and well-characterized drugs for new medical indications. In the cancer context, this represents research in finding the untapped anticancer potential on non-anticancer drugs, which may result in potential new clinical applications in cancer therapy. Thus, even if new dosage regimens have to be established, one can rely on previous pharmacokinetic, toxicological, and safety data from years of widespread clinical use.[41-42]

Between wide range of non-cancer drugs currently in study to integrate cancer treatment are itraconazole and verapamil, with at least one peer-reviewed paper supporting its use against cancer.[43-45] Both have shown a survival benefit in at least one randomized trial. For example, itraconazole has shown survival benefit against metastatic non-squamous non-small-cell lung cancer while verapamil has been reported to increase the survival of patients with anthracycline-resistant metastatic breast carcinoma.[44-45] However, itraconazole has been proven to be more relevant than verapamil for cancer treatment, with more success cases and application in a wider range of cancer types.[46-47] Verapamil's clinical evidence of ACD activity enhancement has been revealed more limited.[48-49]

In this work, itraconazole's and verapamil's effect in combination with well-known anticancer agents was evaluated against several cancer cell lines. Based on previous work in cancer research with tacrine developed in our group, tacrine's potential for cancer treatment in combination with well-known anticancer agents was also evaluated.

#### 1.5.2.1. Itraconazole

Itraconazole is an azole antifungal drug commonly used for the treatment of a broad range of fungal infections, such as aspergillosis, blastomycosis, candidiasis or histoplasmosis.[50] This drug acts inhibiting lanosterol 14-demethylase (14DM), which

catalyzes an essential step in the biosynthesis of ergosterol, an important sterol required for the membrane integrity of fungal cells. Although itraconazole preferably inhibits the fungal 14DM over its human equivalent enzyme, they do inhibit the human enzyme at high concentrations, which will interfere with cholesterol biosynthesis, the most familiar type of animal sterol, vital to cell membrane structure and precursor of fat-soluble vitamins and steroid hormones.[51-52]

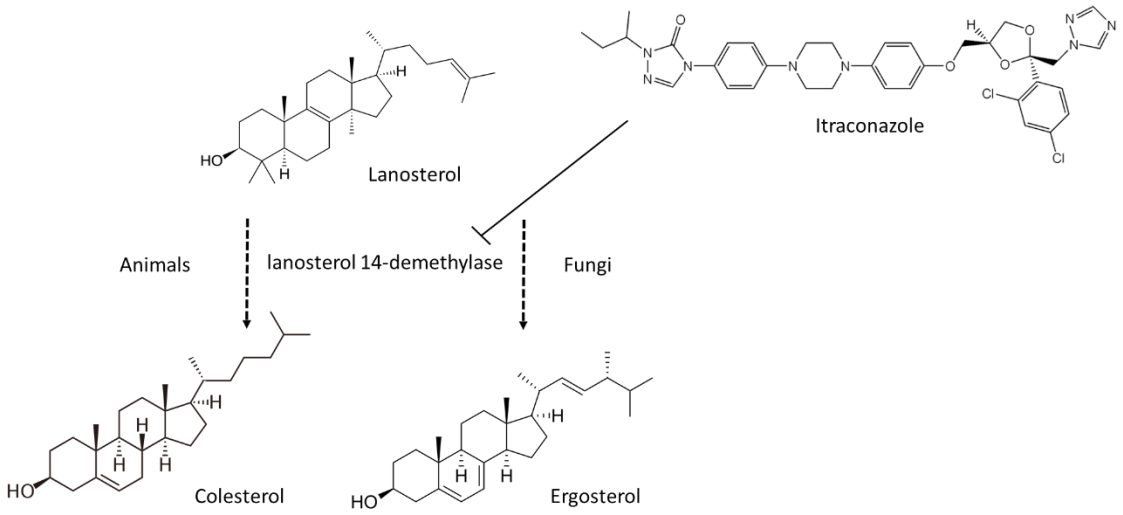


Figure 11 - **Mechanism of action of itraconazole in sterol's ergosterol and cholesterol biosynthesis.**

Besides itraconazole's capability of lanosterol 14-demethylase inhibition, in a screening recently performed by Food and Drug Administration (FDA) approved drugs, this drug showed promising anticancer results. Some of the multiple anticancer mechanisms of action include the ability to inhibit Hedgehog pathway and angiogenesis,[53-56] both mechanisms related to cancer development (Figure 12), autophagy induction[57] and reversal of multidrug resistance.[58]

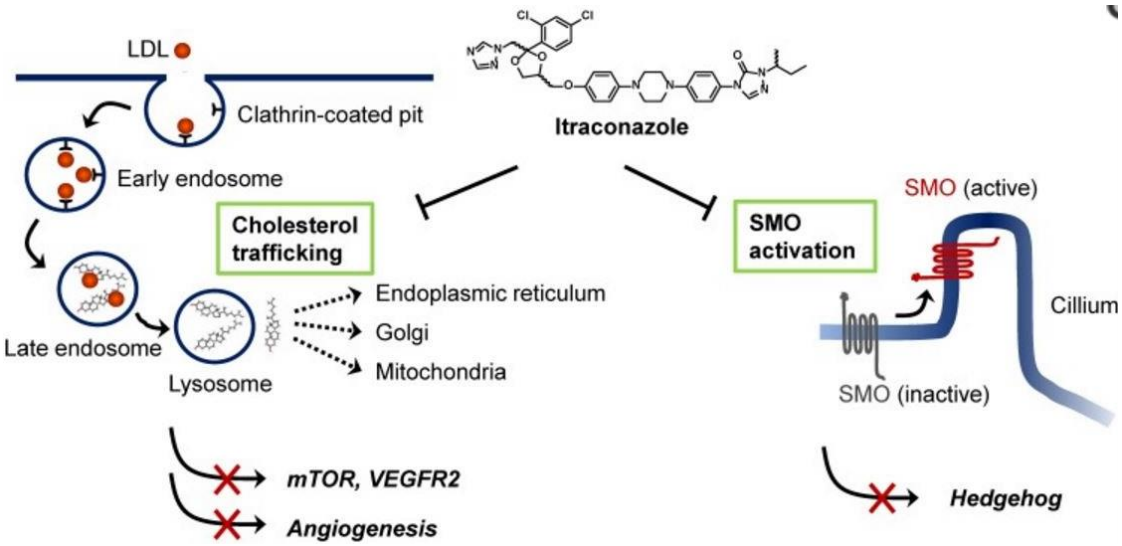


Figure 12 - **Itraconazole's cell targets in cancer.** Itraconazole inhibits cholesterol trafficking through cholesterol trapping within late endosomal and lysosomal compartments.[59] Therefore, proper cholesterol trafficking essential for mammalian target of rapamycin (mTOR) activation in endothelial cells is inhibited, leading to mTOR pathway inhibition.[59] Furthermore, mTOR pathway inactivation will also contribute to endothelial cells cycle arrest consequently inhibiting angiogenesis.[59] Itraconazole can also bind directly to vascular endothelial growth factor receptor 2 (VEGFR2) preventing binding to its endogenous ligand vascular endothelial growth factor (VEGF) and reducing endothelial cell proliferation.[56] Another signaling pathway affected by itraconazole is the Hedgehog pathway. Itraconazole can reversibly bind to SMO protein preventing nuclear translocation of the GLI transcription factors (not shown), which would activate downstream targets that affect cell growth, survival and differentiation.[54, 60] Figure adapted from https://goo.gl/images/6MT9Dg.

#### 1.5.2.2. Tacrine

Tacrine is an anticholinesterase drug and acts reversibly inhibiting this enzyme (Figure 13). In Alzheimer Disease (AD), where presynaptic cholinergic neurons in the basal forebrain are destroyed, its main role is to prevent the breakdown of acetylcholine, a neurotransmitter needed for memory processing and known to be diminished in this pathology.[61-62] Although tacrine was the first drug approved for AD treatment, after other acetylcholinesterase inhibitors were introduced, it was discontinued because of its liver toxicity and attendant requirement for monitoring liver function.[63] In fact, at therapeutic doses, tacrine has been reported to induce reversible increases in serum alanine aminotransaminase (ATL), a biomarker of liver injury, in 30 to 50% of the patients, which severely limited its clinical use.[64-66]

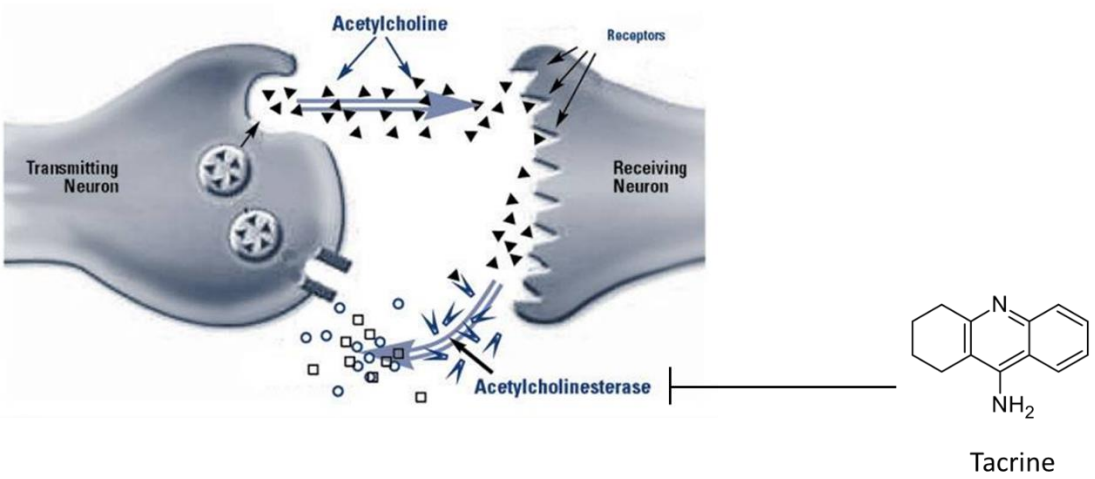


Figure 13 - **The life cycle of acetylcholine.** After signaling acetylcholine is released from receptors and broken down by acetylcholinesterase to be recycled in a continuous process. Tacrine reversibly inhibits acetylcholinesterase. Figure adapted from https://goo.gl/images/Lsv6mr.

Tacrine's hepatotoxicity is known but the molecular basis of the toxicity is incompletely understood. An explanation for tacrine-Induced liver dysfunction was proposed by Alain Berson and his collaborators in 1996, where the weak base tacrine was suggested to exert a protonophoric effect in mitochondria, which means that it will transport protons across lipid layer (Figure 14), and thus waste energy without concomitant formation of adenosine triphosphate in rat and human cells, causing cell death at high doses and cell dysfunction at lower doses.[67] Later, studies performed in mouse liver revealed that tacrine is a relatively weak catalytic inhibitor of Topo II, a dimer enzyme that transiently cleaves and then quickly religates the 2 DNA strands.[68] mtDNA was identified as an important target in tacrine toxicity, causing mtDNA depletion and apoptosis in this animal model.[69] Furthermore, in the same study tacrine was found to enhance p53, Bax and caspase activity, all mechanisms favorable to tumor supresson.[69]

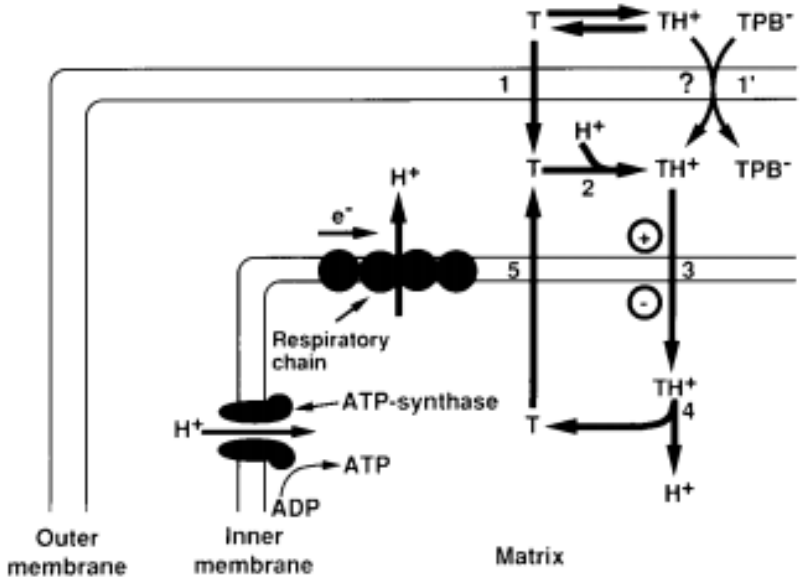


Figure 14 - **Proposed mechanism for the mitochondrial effects of tacrine.** The flow of electrons ($e^-$) through the respiratory chain extrudes protons from the mitochondrial matrix and creates a large membrane potential across the inner membrane. Normally, the reentry of protons through ATP synthase then allows ATP synthesis. In the cytosol, the weak base tacrine exists as the unprotonated form (T) and the protonated species ($TH^+$). The lipophilic, unprotonated tacrine crosses the outer membrane (step 1) and is protonated in the intermembranous space because of the abundance of protons in this space (step 2). Protonated tacrine is positively charged and is ''pushed'' by the membrane potential into the matrix (step 3). In the relatively more alkaline matrix, protonated tacrine dissociates (step 4) into a proton and unprotonated tacrine that can cross back through the inner membrane (step 5), ready for another cycle of proton translocation. The exact site of action of tetraphenylborate ($TPB^-$) is unknown. It may initially speed up the uptake by also allowing the entry of protonated tacrine (in the form of an ion pair) through the outer membrane (step 1). Figure adapted from Ref. 65.

#### 1.5.2.3. Verapamil

Verapamil is a calcium antagonist that acts slowing $Ca^{2+}$ entry through voltage-activated, ion-selective channels (calcium channels) in cardiac and vascular smooth muscle cells.[70-71] Therefore, it is commonly used in the management of a variety of cardiac disorders, such as cardiac arrhythmia and angina pectoris.[72-73]

Although its extensive first-pass hepatic metabolism, verapamil is commonly administered orally, at doses ranging from 40 to 480 mg, depending on the dosing regimen, reaching plasma concentrations up to 900 $\mu g.L^{-1}$ without showing adverse effects.[74-76]

Apart from its cardiac disorders related applications, verapamil has been known to inhibit P - glycoprotein (P-gp), an energy-dependent drug efflux pump responsible for multidrug resistance (MDR) in multiple experimental models and human tumors.[77-78]

# 2. OBJECTIVES

The objective of the present study was to predict the performance of drugs in humans, through *in vitro* and *in silico* approaches. In a nutshell, the drug combinations effect was evaluated through *in vitro* methodologies and then the results were reproduced and analyzed *in silico* in more detail.

The project started with the study of GastroPlus™ modeling and simulation program, in the Faculty of Pharmacy of the University of Porto. Then, in the Faculty of Pharmacy of the University of Helsinki, deep insight into STELLA® simulation software application was acquired and work plan was methodically delineated.

In the first study (*in vitro* approach), MTT cell viability assay was performed in healthy and cancer human prostate cell lines (PNT2 and PC-3, respectively), and non-small cell lung cancer human cell line. Six different drug combinations were tested, where one of the drugs is a clinically used ACD (gemcitabine or 5-fluorouracil) and the other is a RD with promising qualities for cancer treatment:

Drug combinations:

- Gemcitabine + Itraconazole
- Gemcitabine + Tacrine
- Gemcitabine + Verapamil
- 5-FU + Itraconazole
- 5-FU + Tacrine
- 5-FU + Verapamil

At this stage, the main goal was to understand if ACD's anticancer activity is enhanced in the presence of one of this RD in those cell lines.

In the second study, (*in silico* approach) the aim was the development of two-compartment PK models in STELLA® simulation software that mimic the drug combination effect previously assessed *in vitro* and couple it to human drug's PK. Thus, a general analysis of drug combination's performance in the human body can be done over time, doses can be varied and its influence can be evaluated.

# 3. EXPERIMENTAL

Gemcitabine and 5-FU are very potent in *in vitro* cell growth inhibition assays. Many are the variables that influence $IC_{50}$ value (in this case, the $IC_{50}$ value is relative to the concentration of an anticancer agent that inhibits cell growth by half). Depending on the tumor type, cell line, time of exposure to the drug, number of cells per well or cell viability assay chose to perform the experiments, $IC_{50}$ of the drugs will be different (Table 1). Therefore, reported $IC_{50}$ values may help in a way that one can find a range of concentration to test expecting to find one's $IC_{50}$ value for that drug when used in that specific conditions.

Table 1 - Growth inhibition effect of gemcitabine (Gem) and 5-fluorouracil (5-FU) in lung and prostate cancer cell lines.

| Drug | Organ | Cell line | Treatment / h | Cells per well | $IC_{50}$ / µM | Cell viability assay | Ref |
|---|---|---|---|---|---|---|---|
| **Gem** | Lung | A549 | 72 | 4000 | 0.01038 | MTT | [79] |
| | | A549 | 72 | 4000 | 11.54 | MTT | [80] |
| | | A549 | 72 | - | 0.002 | MTT | [81] |
| | Prostate | PC-3 | 48 | - | 54.47 | Cell Counting Kit-8 | [82] |
| | | PC-3 | - | - | 0.5 | - | [83] |
| | | PC-3 | 72 | - | 1.47 | Fluorescence based cell availability assay | [84] |
| **5-FU** | Lung | A459 | 48 | 1000 | 10.32 | MTT | [85] |
| | | A549 | 48 | 3000 | 8.21 | SRB | [86] |
| | Prostate | PC-3 | 120 | 2000 | 1.5 | MTT | [87] |
| | | PC-3 | 72 | - | 13.9 | Fluorescence based cell availability assay | [84] |

Besides $IC_{50}$ data collection, before experimental work start, extensive literature research about each drug intended to integrate the project was done. In Table 2, general physicochemical properties are shown. These include molecular weight (MW), drug's

solubility in water, logarithmic partition coefficient (logP) and logarithmic acidic dissociation constant ($pK_a$).

Table 2 - Physicochemical properties of the ACDs 5-FU and gemcitabine and the RD for cancer treatment verapamil, itraconazole, and tacrine.

| | 5-FU | Gemcitabine | Verapamil | Itraconazole | Tacrine |
|---|---|---|---|---|---|
| MW ($g.mol^{-1}$) | 130.08[a] | 263.20[a] | 454.60[a] | 705.63[a] | 198.26[a] |
| Water solubility ($mg.mL^{-1}$) | 11.10[88] | 22.30[a] | 0.44[89] | < 0.005[90] | 0.217[a] |
| logP | -0.83[88] | -1.40[a] | 4.47 - - 5.69[89] | 5.66[90] | 2.40[91] |
| $pK_a$ | 8.10[38] | 3.60[a] | 8.60[89] | 3.70[90] | 9.94[91] |

a: values obtained from DrugBank, https://www.drugbank.ca/, January of 2018.

Besides their physicochemical properties, PK data was collected. Table 3 depicts drugs elimination half-life time ($t_{1/2\beta}$), plasma clearance (CL), volume of distribution ($V_d$) and % protein binding.

Table 3 - Clinical pharmacokinetics of the ACDs 5-FU and gemcitabine and the RD for cancer treatment verapamil, itraconazole, and tacrine.

| | 5-FU | Gemcitabine | Verapamil | Itraconazole | Tacrine |
|---|---|---|---|---|---|
| $t_{1/2\beta}$ (h) | 0.13 - 0.37[38] | 0.31[92] | 2.7 - 4.8[74] | 21[90] | 1.4 - 2.5[93] |
| plasma clearance ($L.h^{-1}$) | 48 - 114[38] | 89.8[92] | 52.5[74] | 22.86[90] | 145 - 168[93] |
| $V_{d\ area}$ (L) | 14 - 54[38] | 140.8[92] | 162 - 380[74] | 800[90] | 259 - 350[93] |
| % Protein binding | 8 - 12[a] | < 10[a] | 90[74] | 99.8[90] | 55[a] |

a – values obtained from DrugBank, https://www.drugbank.ca/, January of 2018.

Moreover, additional research was done regarding their most relevant metabolizing enzymes. These comprise some of the cytochrome P450 (CYP) isoenzymes, when RDs are concerned, cytidine deaminase (CDA) and nucleoside kinases that inactivate and activate, respectively, gemcitabine and dihydropyrimidine dehydrogenase (DPD), that

catabolizes 5-FU, and uridine kinase (UK) and Urdpase, responsible for 5-FU anabolism. The enzymes and respective substrate are presented in Table 4.

Table 4 - Metabolizing enzymes of the ACDs 5-FU and gemcitabine and the RD for cancer treatment verapamil, itraconazole, and tacrine.

| | Enzymes | 5-FU | Gemcitabine | Verapamil | Itraconazole | Tacrine |
|---|---|---|---|---|---|---|
| **CYP's** | 3A5 | | | √[a] | | |
| | 3A4 | | | √[a] | √[a] | |
| | 2C8 | | | √[a] | | |
| | 2C9 | | | √[a] | | |
| | 1A2 | | | √[a] | | √[65] |
| **In.** | CDA | | √[a] | | | |
| **Act.** | Nucleoside kinases | | √[a] | | | |
| **C** | DPD | √[94] | | | | |
| **A** | UK | √[94] | | | | |
| | Urdpase | √[94] | | | | |

CYP's - cytochrome P540 family enzymes; CYP isoforms: 3A5, 3A4, 2C8, 2C9, 1A2; In - inactivation; Act - activation; C - catabolism; A - anabolism; CDA - cytidine deaminase; DPD - dihydropyrimidine dehydrogenase; UK - uridine kinase; Urdpase - uridine phosphorylase; a - data obtained from DrugBank, https://www.drugbank.ca/, January of 2018.

Lastly, the list of known cellular transporters for each drug was collected and presented in Table 5.

Table 5 - Cellular transporters and maximum plasma concentration ($C_{max}$) for single dose oral administration (p.o.) and multiple dose p.o. and intravenous (i.v.) administration.

| | | | 5-FU | Gemcitabine | Verapamil | Itraconazole | Tacrine |
|---|---|---|---|---|---|---|---|
| **Transporters** | | | 1[95], 2[96] | 2[a], 3[a] and 4,[97-99] 5,[99] 6,[100] 7,[101] 8[102] | 7[a], 8[a], 10[a], 11[a], 12[a], 13[a], 14[a], 15[a], 16[a], 17[a], 18[a], 19[a], 20[a] | 7[103] | 7[a] and 21[104] |
| **$C_{max}$ ($\mu g.L^{-1}$)** | Single dose | p.o. | - | - | 900[74] | 127[105] | 24[93] |
| | Multi dose | p.o. | - | - | - | 1980[105] | 167[93] |
| | | i.v. | - | - | - | 4554[106] | - |

1 - Solute carrier family 22 member 7; 2 - ENT1 - Equilibrative nucleoside transporter 1; 3 - ENT2 - Equilibrative nucleoside transporter 2; 4 - CNT - Concentrative nucleoside transporter; 5 - Sodium/nucleoside cotransporter 1; 6 - Solute carrier family 28 member 3; 7 - MDR1 - Multidrug resistance protein 1; 8 - MRP7 - multidrug resistance-associated protein 7; 10 - Solute carrier family 22 member 1; 11 - canalicular multispecific organic anion transporter 2; 12 - MRP4 - Multidrug resistance-associated protein 4; 13 - Solute carrier family 22 member 5; 14 - bile salt export pump; 15 - MRP1 - Multidrug resistance-associated protein 1; 16 - solute carrier organic anion transporter family member 1A2; 17 - canalicular multispecific organic anion transporter 1; 18 - solute carrier family 22 member 4; 19 - ATP-binding cassete sub-family G member 2; 20 - solute carrier organic anion transporter family member 1B1; 21 - MDR2 - multidrug resistance protein 2; a - data obtained from DrugBank, https://www.drugbank.ca/, January of 2018.

## 3.1. Drugs

Gemcitabine, 5-FU, itraconazole, tacrine, and verapamil were obtained from Sigma-Aldrich® and dissolved in sterile dimethyl sulfoxide (DMSO) at 50, 100, 17, 10 and 10 mM, respectively, as a stock solution. The drugs were stored at -20 and diluted with culture medium prior to use.

## 3.2. Cell culture

Cell lines

The normal human prostate epithelium cell line PNT-2, human prostate adenocarcinoma cell line PC-3 and human lung carcinoma cell line A549 were obtained from the American Type Culture Collection and maintained in RPMI-1640 medium with 2mM L-glutamine

(Gibco™, Life Technologies) supplemented with 10% heat-inactivated fetal bovine serum (FBS) (Gibco™, Life Technologies) at 37˚C in a 5% $CO_2$ atmosphere.

All the cell culture procedures were carried out under very clean conditions in biological safety cabinets, using sterile reagents and materials. Cells were routinely kept exponentially growing and were sub-cultured by trypsinization twice a week.

Sub-culturing

Sub-culturing consists in the removal of the media and passaging the cells to a new culture vessel with fresh culture medium, thus enabling the further propagation of the cell line. In more detail, this process consists in the detachment of the (adherent) cells from the culture plate upon the action of TrypLE™ Express (Gibco™, Life Technologies) solution (cleaves peptide bonds on the C-terminal sides of lysine and arginine). Briefly, after removing the cell culture medium, cells were washed with 1x PBS (Gibco™, Life Technologies) and 500 µL of TrypLE Express were added to the cells for around 5 minutes at 37 ºC until the cells were detached from the culture plate. Cells were then in suspension and with a round morphology.

Evaluation of the cell culture viability with the trypan blue exclusion assay

Cell viability of the cell culture was routinely evaluated using the trypan blue exclusion assay. After trypsinization, the total number of viable cells was determined by adding to 50 µL of cell suspension the same amount of trypan blue reagent (Gibco™, Life Technologies). The viable cells were distinguished from dead cells by microscopic observation since dead cells incorporate the trypan blue reagent (due to the holes in the cell membrane characteristic of dead cells) and thus will appear blue. The number of viable cells was calculated by counting cells in a Neubauer chamber and was expressed as a number of viable cells / mL of cellular suspension. All experiments were carried out with exponentially growing cells having over 90% of cell viability.

## 3.3. Cell viability assay

### 3.3.1. Evaluation of cell growth inhibition with the MTT assay

The MTT cell proliferation assay allows the measurement of cell proliferation rate based on the capacity of metabolically active cells to reduce the yellow tetrazolium MTT (3-(4, 5-dimethylthiazolyl-2)-2, 5-diphenyltetrazolium bromide). Then, the resulting purple formazan crystals can be solubilized and quantified by spectrophotometric means. Thus, in order to evaluate the effect of several drugs on cell growth, the MTT assay was performed.

Optimal cell concentration

Firstly, the optimal cell concentration of each cell line (PC-3, A459, and PNT-2) to be plated for this assay had to be determined for 72 h incubation; this concentration would correspond to the concentration of cells that would provide a good detection signal following 72 h of cell growth in the incubator, while simultaneously allowing cells to be in exponential growth throughout that incubation period. Therefore, to establish the optimal cell concentration to be plated for 72 h incubation periods, cells were seeded into a 96-well plate at a range of concentrations from 1000 to 100000 cells per well, by plating a total volume of 100 µL/well and incubated for 24 h to allow cells to adhere to the plate. The day after (24 h later), 100 µL/well of culture medium (RPMI-1640 medium + 10% FBS) were added to the cells and cells were further incubated for another 72 h (the same incubation period as the one to be used in the experiments with the drugs). Following the 72 h incubation period, the media was removed by aspiration, 100 µL/well of MTT (Sigma-Aldrich®) solution (0.5 mg/mL in media) was added to each well and cells were incubated for further 3 h. After the incubation period, the MTT solution was removed by aspiration, the cells were washed with 100 µL/well of 1x PBS and 100 µL/well of DMSO were added to dissolve the formazan crystals. The fluorescence was read using a Varioskan™ LUX multimode microplate reader, at 540 nm. Results were treated in Microsoft Excel and the optimal cell concentration was determined.

Dose-Response curve determination for the anticancer drugs alone

The optimal cell concentration determined, as described above, was $4x10^4$ cells/mL (for all the cells lines) and was then used in the MTT assay. Cells were therefore seeded into a 96-well plate at a concentration of $3x10^4$ cells/mL by plating 100 µL/well and incubated for 24 h to allow cells to adhere to the plate. The following day (24 h later), 100 µL/well of different concentrations of the anticancer drug (gemcitabine or 5-FU) were added to the cells and these were further incubated for 72 h. The multiple serial dilutions tested of each anticancer drug were prepared in culture medium (RPMI-1640 medium + 10% FBS). The ranges of concentrations tested were: for gemcitabine (Gem) from 0.01 to 50 µM; for the 5-FU from 0.05 to 100 µM. DMSO control was also included in the experiments, even though the maximum concentration used was previously considered to be a non-toxic concentration to the cells (0.2% DMSO). Following the 72 h cellular treatment, the media was removed by aspiration, 100 µL/well of MTT solution (0.5 mg/mL in media) was added to each well and cells were incubated for further 3 h. After the incubation period, the MTT solution was removed by aspiration, the cells were washed with 100 µL/well of 1x PBS and 100 µL/well of DMSO were added to dissolve the formazan crystals. The fluorescence was read in a spectrometer (Varioskan™ LUX multimode microplate reader), at 540 nm. Results were treated in Microsoft Excel and GraphPad Prism 6. The dose-response curves for each treatment were then plotted in appropriate graphs, differences between treatments were compared and the $IC_{50}$ value, indicating the concentration resulting in inhibition of 50% of the maximal cell growth, was determined. The percentage of cell growth inhibition resulting from each drug was calculated as: [(OD 540 control cells - OD 540 treated cells)/OD 540 control cells] x 100. This assay was repeated in at least three independent experiments.

Dose-Response curve determination for the anticancer drugs in combination with a RD

The optimal cell concentration determined, as described above, was $4x10^4$ cells/mL (for all the cell lines) and was then used in the MTT assay. Cells were, therefore, seeded into a 96-well plate at a concentration of $4x10^4$ cells/mL by plating 100 µL/well and incubated for 24 h to allow cells to adhere to the plate. The following day (24 h later), 50 µL/well of different concentrations of the anticancer drug (gemcitabine or 5-FU) were added to the cells and an extra 50 µL/well of a fixed concentration of RD. Cells were further incubated for 72 h. The multiple serial dilutions tested of each anticancer drugs were prepared in RPMI-1640 medium + 10% FBS. The ranges of concentrations tested were: for Gem from 0.01 to 50 µM; for the 5-FU from 0.05 to 100 µM. The chosen concentration of each

RD was based on the maximum plasma concentration ($C_{max}$) found in the literature. The concentrations used in the study were then 1, 8.5 and 0.24 μM for verapamil, itraconazole, and tacrine, respectively.[74, 90, 93, 107] DMSO control was also included in the experiments, even though the maximum concentration used was previously considered to be a non-toxic concentration to the cells (0.2 % DMSO). Following the 72 h cellular treatment, the media was removed by aspiration, 100 μL/well of MTT solution (0.5 mg/mL in media) was added to each well and cells were incubated for further 3h. After the incubation period, the MTT solution was removed by aspiration, the cells were washed with 100 μL/well of 1x PBS and 100 μL/well of DMSO were added to dissolve the formazan crystals. The fluorescence was read in a spectrometer (Varioskan™ LUX multimode microplate reader), at 540 nm. Results were treated in Microsoft Excel and GraphPad Prism 6. The dose-response curves for each treatment were then plotted in appropriate graphs and differences between treatments were compared. The percentage of cell growth inhibition resulting from each drug treatment was calculated as: [(OD 540 nm control cells - OD 540 nm treated cells)/OD 540 nm control cells] x 100. This assay was repeated in at least three independent experiments.

Further studies with itraconazole in combination with 5-FU or gemcitabine

To study in which way the drug combination response is affected by itraconazole concentration, further studies were performed. For this purpose, only the human lung carcinoma cell line A549 was used for simplification purpose.

Two studies were then performed:

1) Range of itraconazole concentrations + ACD (gemcitabine or 5-FU) at a fixed concentration;
2) Range of ACD (gemcitabine or 5-FU) concentrations + fixed concentration of itraconazole (three different concentrations were tested).

Cells were seeded into a 96-well plate at a concentration of $4x10^4$ cells/mL by plating 100 μL/well and incubated for 24 h to allow cells to adhere to the plate.

1) The following day (24 h later), 50 μL/well of different concentrations of itraconazole were added to the cells and an extra 50 μL/well of a fixed concentration of anticancer drug (gemcitabine or 5-FU). Cells were further incubated for 72 h. The multiple serial dilutions tested for itraconazole were

prepared in RPMI-1640 medium + 10% FBS. The concentrations tested ranged from 0.07 to 4.25 μM since the concentration used in the previous experiments was 8.5 μM and the serial dilutions had a dilution factor of 2. The concentration chosen for gemcitabine and 5-FU was one of the concentrations that showed the lowest effect in the previous experiments: 0.01 and 1 μM respectively (concentrations also prepared in RPMI-1640 + 10% FBS). The ACD was also tested alone for control purposes. Furthermore, DMSO control was included in the experiments, even though the maximum concentration used was previously considered to be a non-toxic concentration to the cells (0.2 % DMSO);

2) The following day (24 h later), 50 μL/well of different concentrations of ACD (gemcitabine or 5-FU) were added to the cells and an extra 50 μL/well of a fixed concentration of itraconazole. Cells were further incubated for 72 h. The multiple serial dilutions tested for ACD were prepared in RPMI-1640 medium + 10% FBS. The concentrations tested ranged from 0.005 to 10 μM for gemcitabine, since in the previous experiments the resulting dose-response curve didn't have the ideal shape, and for 5-FU the range was maintained (0.01-100 μM). The concentrations chosen for itraconazole were 2, 4 and 6 μM (concentrations within the range of concentrations that showed an effect when administered with a very low concentration of ACD). itraconazole was also tested alone for control purposes. Furthermore, DMSO control was included in the experiments, even though the maximum concentration used was previously considered to be a non-toxic concentration to the cells (0.2 % DMSO).

Following the 72 h cellular treatment, the media was removed by aspiration, 100 μL/well of MTT solution (0.5 mg/mL in media) was added to each well and cells were incubated for further 3 h. After the incubation period, the MTT solution was removed by aspiration, the cells were washed with 100 μL/well of 1x PBS and 100 μL/well of DMSO were added to dissolve the formazan crystals. The fluorescence was read in a spectrometer (Varioskan™ LUX multimode microplate reader), at 540 nm. Results were treated in Microsoft Excel and GraphPad Prism 6. The dose-response curves for each treatment were then plotted in appropriate graphs and differences between treatments. The percentage of cell growth inhibition resulting from each drug treatment was calculated as: [(OD 540 nm control cells - OD 540 nm treated cells)/OD 540 nm control cells] x 100. This assay was repeated in at least three independent experiments.

## 3.4. Model development

From data available in the literature and the results of experimental work, pharmacokinetic models were built in the simulation software STELLA® 10.0.3 (ISEE Systems).

The structure of the model is described in detail in following chapters, as well as all the equations, variables and constants used for this purpose.

### 3.4.1. WinNonLin: PK analysis

Compartmentally based PK STELLA models require the input of PK parameters of each drug, such as the volume of distribution in central and tissue compartment ($V_{d1}$ and $V_{d2}$ respectively), clearance (CL) and transfer rate constants from central compartment to tissue compartment and from tissue compartment to central compartment ($k_{12}$ and $k_{21}$, respectively). The ideal situation would be where all the parameters would belong to the same source: human plasma concentration versus time data ($C_p$-time data), belonging to the same ethnicity, gender, age. Due to lack of data available in the literature concerning this issue, the only mandatory condition for the data to be collected was to be human, and that all the PK data for each drug belonged to the same literature source.

Phoenix WinNonLin (64-bit, version 7.00) is a pharmacokinetic/pharmacodynamic (PK/PD) modeling program that, through the analysis of the $C_p$-time data of a certain drug, can generate its PK parameters. Thus, based in only three literature sources (one for each drug) all the PK parameters were obtained.

For gemcitabine, the data collected came from non-small-cell lung cancer Chinese patients[108] (Table 6). Gemcitabine was intravenously infused for 120 minutes at a rate of 15.7 $mg.min^{-1}$. Plasma samples were collected until 210 minutes after infusion start.

Table 6 - $C_p$-time data of gemcitabine in Chinese non-small-cell lung cancer patients.

| Time (min) | Gemcitabine plasma concentration (μg.mL$^{-1}$) |
|---|---|
| 30 | 2.60 |
| 120 | 4.90 |
| 130 | 2.60 |
| 140 | 0.85 |
| 150 | 0.50 |
| 165 | 0.25 |
| 180 | 0.15 |
| 210 | 0.00 |

For 5-FU, $C_p$-time data collected belongs to English cancer patients,[109] and is presented in Table 7. 5-FU was administered over 1 minute, by intravenous bolus injection, at a dose of 900 mg. Plasma samples were collected for 90 minutes.

Table 7 - $C_p$-time data of 5-FU in English cancer patients.

| Time (min) | 5-FU plasma concentration (μg.mL$^{-1}$) |
|---|---|
| 5 | 54.61 |
| 8 | 40.23 |
| 12 | 28.20 |
| 20 | 14.82 |
| 30 | 8.56 |
| 45 | 2.98 |
| 60 | 1.35 |
| 90 | 0.65 |

For itraconazole, the data is relative to healthy subjects, from The Netherlands.[106] 100 mg of drug were administered intravenously, over 1 hour, and plasma samples were collected during 96 hours.

Table 8 - Cp-time data of itraconazole in healthy subjects from The Netherlands.

| Time (min) | Itraconazole plasma concentration (μg.mL$^{-1}$) |
|---|---|
| 30 | 3.12 |
| 60 | 3.90 |
| 120 | 0.34 |
| 150 | 0.29 |
| 180 | 0.23 |
| 300 | 0.21 |
| 420 | 0.14 |
| 540 | 0.12 |
| 1440 | 0.04 |
| 1920 | 0.03 |
| 2880 | 0.02 |
| 4320 | 0.01 |
| 5760 | 0.01 |

### 3.4.2. Model Structure

Several models were built, depending on the case study. In each case study, each drug has a specific route of administration. Therefore, the structure of the model is different for all the situations, varying the variables, the constants and some equations corresponding to each particular case.

Drugs in each drug combination are not metabolized through the same CYP's (Table 4), don't have transporters in common (Table 5) and in each drug combination, only one of the drugs is highly protein bonded (Table 3). Knowing this, one admits that no drug interaction will occur and each drug disposition will not be affected. Thus, the compartment model is developed for each drug separately, but they are connected in the same human model.

The layout of each model is shown in the following chapters.

#### 3.4.2.1. Determination of the AUC for each drug combination effect, in humans

AUC is usually calculated when bioavailability is concerned, to compare two different drug formulations, routes of administration or the effect of food on the bioavailability of a certain drug, for example.[110-112] In this models, "AUC plasma concentration" was calculated for model validation purposes. "AUC effect" was determined to evaluate the overall effect of each drug combination tested in the non-small cell lung cancer cell line A549. In current STELLA® model, AUC is recorded using a separate compartment but it follows a principle which is mathematically expressed in Equation 2.

**Equation 2** $$AUC = AUC(t - dt) + "variable\ in\ study" * dt$$

Gemcitabine + Itraconazole

The model built for gemcitabine is a two-compartmental model since its $C_p$-time profile has a two-compartmental distribution. Using gemcitabine $C_p$-time data for intravenous infusion obtained from literature and the PK/PD modeling program Phoenix WinNonLin (64-bit, version 7.00), the curve that best fitted the experimental values was achieved and the values for each PK parameter ($V_{d1}$, $V_{d2}$, CL, $k_{12}$ and $k_{21}$) were obtained. Thus, with the input of the parameters obtained through WinNonLin, the model describes the disposition of gemcitabine over time, after intravenous infusion. The input dose is also the same as the one reported in the literature source used (infusion of 15.7 $mg.min^{-1}$ for 120 min).

As a result of the previous *in vitro* studies, where a range of concentration of gemcitabine was tested, gemcitabine concentration-dependent % of cell growth inhibition is known. Therefore, in the model, gemcitabine tissue concentration was linked to % of cell growth inhibition in cancer cells. In other words, the % of cell growth inhibition is given depending on the concentration of anticancer drug in the tissue compartment over time. It is assumed that tumor tissue behaves the same way as other tissues grouped in tissue compartment, for simplification purposes.

With the *in vitro* studies in A549 cell line, dose-response curves were obtained, as reported above. With the constants obtained from those curves, such as the lowest and highest effect achieved ("Bottom" and "Top" respectively), the steepness of the curve ("Steepness factor") and the drug concentration at which 50% of the maximum effect was obtained ("$EC_{50}$"), the effect over time can be determined through Equation 3 (because tissue concentration will vary over time).

The parameters from all the 4 dose-response curves were used in this model (one at a time) and for each, the AUC effect was evaluated:

- Gemcitabine alone
- Gemcitabine + Itraconazole 2 μM
- Gemcitabine + Itraconazole 4 μM
- Gemcitabine + Itraconazole 6 μM

**Equation 3**

$$\%\,Effect = (Bottom) + \frac{(Top) - (Bottom)}{1 + \left(\frac{tissue\ concentration}{EC_{50}}\right)^{-stepness\ factor}}$$

All the variables, such as drug plasma concentration, drug tissue concentration, drug amount eliminated and % effect can be plotted in graph or table and evaluated over time.

For the simulation, 4 Runge–Kutta integration method was used, since it's the most accurate integration method available in STELLA®. Simulation length and h were chosen in a way that h was low enough to give accurate results and without compromising the speed of the simulation and simulation length long enough to allow the lower effect value to be reached. Therefore, h=0.02 and 400 min of simulation length were used.

In Figure 15 is shown the model for gemcitabine without itraconazole (I=0 μM). For the three combinations of gemcitabine with itraconazole, the exact same layout was used and only the "Bottom", "Top", "Steepness factor" and "$EC_{50}$" variables were changed, according to each situation.

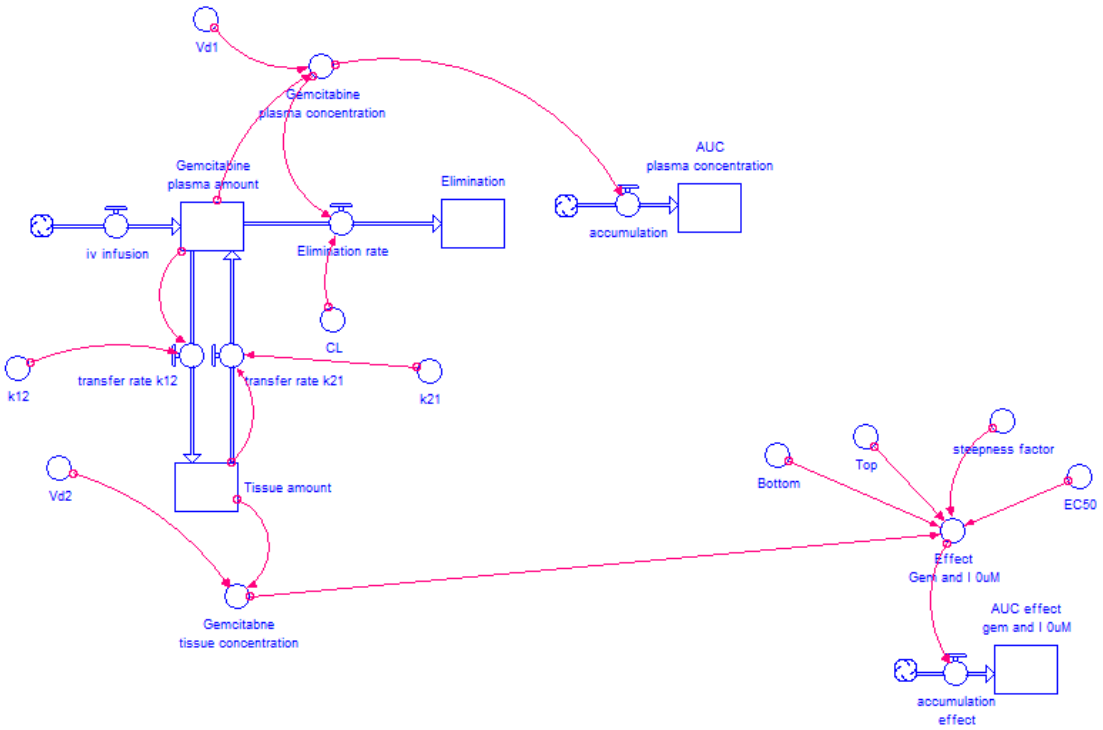


Figure 15 - **Two-compartment model of gemcitabine intravenous infusion administration.** The drug is infused to plasma compartment at a rate of 15.7 $mg.min^{-1}$ for 120 minutes. The drug is transferred from plasma compartment to tissue compartment and vice versa at a rate defined by "$k_{12}$"*"Gemcitabine plasma amount" and "$k_{21}$"*"Tissue amount", respectively, where "$k_{12}$" and "$k_{21}$" are transfer rate constants. The drug is eliminated from plasma compartment to elimination compartment at a rate defined by "CL"*"Gemcitabine plasma concentration", where "CL" is a constant and "Gemcitabine plasma concentration" is a variable that changes over time. "Gemcitabine plasma concentration" is the result of "Gemcitabine plasma amount" divided by "$V_{d1}$" while "Gemcitabine tissue concentration" results from "Tissue amount" divided by "$V_{d2}$". "Gemcitabine plasma amount" is the net result of the amount of drug that leaves plasma compartment (to elimination and tissue compartment) and the amount that enters in this compartment (coming from the infusion and tissue compartment). "AUC plasma concentration" is generated through Equation 2 where the variable in study is "Gemcitabine plasma concentration". Considering Equation 3, "Gemcitabine tissue concentration" and the four parameters obtained from gemcitabine without itraconazole dose-response curve ("Bottom", "Top", "Steepness factor" and "$EC_{50}$"), the effect of gemcitabine alone is modeled over time.

## 5-FU + Itraconazole

The model built for 5-FU is a two-compartmental model since its $C_p$-time profile has a two-compartmental distribution. Using 5-FU $C_p$-time data for intravenous injection obtained from literature and the PK/PD modeling program Phoenix WinNonLin (64-bit, version 7.00), the curve that best fitted the experimental values was achieved and the values for each PK parameter ($V_{d1}$, $V_{d2}$, CL, $k_{12}$ and $k_{21}$) were obtained. Thus, with the input of the parameters obtained through WinNonLin, the model describes the disposition of 5-FU over time, after intravenous injection. The input dose is also the same as the one reported in the literature source used (injection of 900 mg).

As a result of the previous *in vitro* studies, where a range of concentration of 5-FU was tested, 5-FU concentration-dependent % of cell growth inhibition is known. Therefore, in the model, 5-FU tissue concentration was associated to % of cell growth inhibition in

cancer cells. In other words, the % of cell growth inhibition is given depending on the concentration of anticancer drug in the tissue compartment over time. It's assumed that tumor tissue behaves the same way as other tissues grouped in tissue compartment, for simplification purposes.

With the *in vitro* studies with the A549 cell line, dose-response curves were obtained, as reported above. It's assumed that tumor tissue behaves the same way as other tissues grouped in tissue compartment, for simplification purposes. With the constants obtained from those curves, such as the lowest and highest effect achieved ("Bottom" and "Top" respectively), the steepness of the curve ("Steepness factor") and the drug concentration at which 50% of the maximum effect was obtained ("$EC_{50}$"), the effect over time can be determined through Equation 3.

The parameters from all the 4 dose-response curves were used in this model (one at a time) and for each, the AUC effect was evaluated:

- 5-FU alone
- 5-FU + Itraconazole 2 μM
- 5-FU + Itraconazole 4 μM
- 5-FU + Itraconazole 6 μM

All the variables, such as drug plasma concentration, drug tissue concentration, drug amount eliminated and % effect can be plotted in graph or table and evaluated over time.

For the simulation, 4 Runge–Kutta integration method was used, since it's the most accurate integration method available in STELLA®. Simulation length and h were chosen in a way that h was low enough to give accurate results and without compromising the speed of the simulation and simulation length long enough to allow the lower effect value to be reached. Therefore, h=0.02 and 200 min of simulation length were used.

In Figure 16 is shown the model for 5-FU without itraconazole (I=0 μM). For the three combinations of 5-FU with itraconazole, the exact same layout was used and only the "Bottom", "Top", "Steepness factor" and "$EC_{50}$" variables were changed, according to each situation.

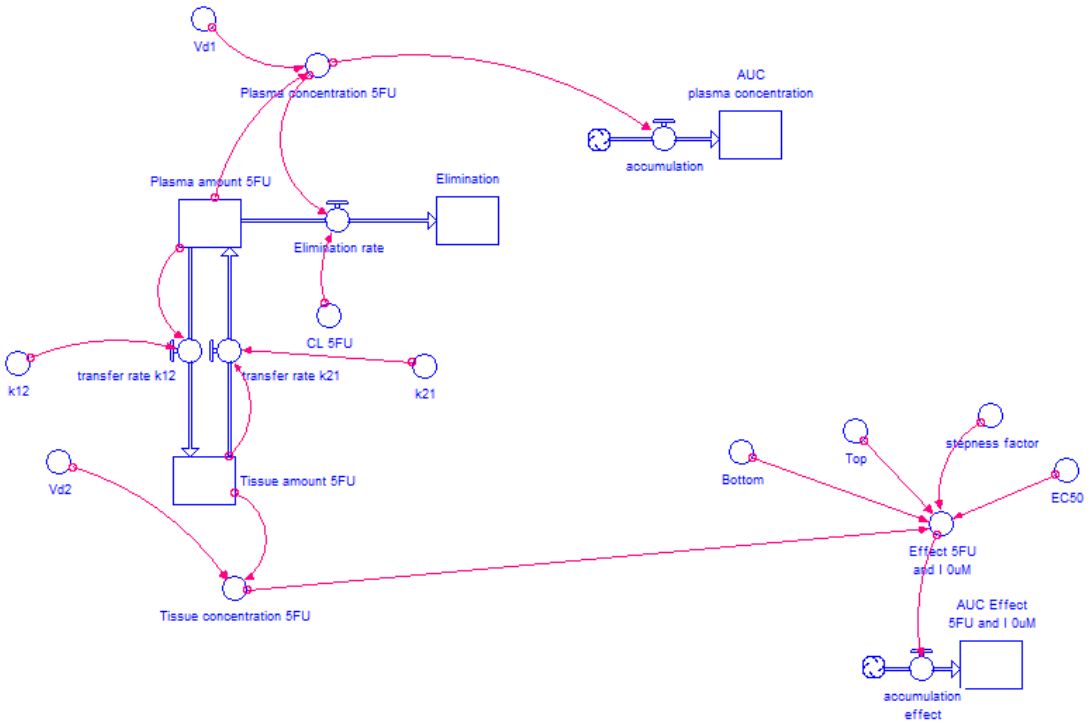


Figure 16 - **Two-compartment model of 5-FU intravenous injection administration.** The drug is injected into plasma compartment at a dose of 900 mg. The drug is transferred from plasma compartment to tissue compartment and vice versa at a rate defined by "$k_{12}$"*"Plasma amount 5-FU" and "$k_{21}$"*"Tissue amount 5-FU", respectively, where "$k_{12}$" and "$k_{21}$" are transfer rate constants. The drug is eliminated from plasma compartment to elimination compartment at a rate defined by "CL"*"Plasma concentration 5-FU", where "CL" is a constant and "Plasma concentration 5-FU" is a variable that changes over time. "Plasma concentration 5-FU" is the result of "Plasma amount 5-FU" divided by "$V_{d1}$" while "Tissue concentration 5-FU" results from "Tissue amount 5-FU" divided by "$V_{d2}$". "Plasma amount 5-FU" is the net result of the amount of drug that leaves plasma compartment (to elimination" or tissue compartment) and the amount that enters in this compartment (coming from tissue compartment). "AUC plasma concentration" is generated through Equation 2 where the variable in study is "Plasma concentration 5-FU". Considering Equation 3, "Tissue concentration 5-FU" and the four parameters obtained from 5-FU without itraconazole dose-response curve ("Bottom", "Top", "Steepness factor" and "$EC_{50}$"), the effect of 5-FU alone is modeled over time.

#### 3.4.2.2. Itraconazole's dose-dependent effect, when combined with gemcitabine or 5-FU, in humans

After quantification of each drug combination effect (through the determination of their AUC effect), where the main variable was ACD tissue concentration, itraconazole's dose-dependent effect was evaluated. At this stage of the work, the exact same four dose-response curves were considered:

- ACD alone
- ACD + Itraconazole 2 μM
- ACD + Itraconazole 4 μM
- ACD + Itraconazole 6 μM

The difference from the previous study lies in the addition of a second two-compartment model (this time for itraconazole) and the itraconazole dose-dependent effect evaluation. For this purpose, three different itraconazole doses were tested (100, 300 and 500 mg). ACD dose remained the same as the previous study (1884 mg of gemcitabine and 900 mg of 5-FU).

For % of cell growth inhibition prediction, in A549 cell line, when ACD is administered in combination with itraconazole, in humans, two-compartment PK models were built for each drug in study, in accordance with the literature information about the model that best fits their $C_p$-time data. The scheme used for ACD was the same as the one used in the previous study. For itraconazole, despite the most common administration route being oral, the intravenous infusion was selected to avoid the low bioavailability characteristic of this drug. Thus, with the literature human $C_p$-time data for intravenous infusion of itraconazole and WinNonLin program, all PK parameters need for two-compartment model construction were collected and the model was built.

Only the “Bottom” value of the ACD dose-response curve was found to be significantly affected by itraconazole concentration. Therefore, equations that relate the change of “Bottom” value with the concentration of itraconazole were included in “Bottom” Converter. In other words, % of cell growth inhibition is given taking into account not only ACD concentration (Equation 3) but also the influence of itraconazole concentration on “Bottom” value.

Equation 4 describes the change of “Bottom” value in gemcitabine + itraconazole dose-response curves and Equation 5 describes it for 5-FU + itraconazole combinations. x is itraconazole tissue concentration, in $\mu g.mL^{-1}$.

**Equation 4**

$$Bottom = 2.44x^2 - 1.95x - 1.06$$

**Equation 5**

$$Bottom = 2.15x^2 - 1.15x - 0.47$$

Regarding the other variables that describe dose-response curve (“Top”, “Steepness factor” and “$EC_{50}$”) average of the three values was used (the values relative to ACD + itraconazole 2, 4 and 6 μM dose-response curves).

The model for gemcitabine + itraconazole combination is shown in Figure 17. 5-FU + itraconazole combination model is shown in Figure 18. Once again, the exact same

layout was used to test three different doses of itraconazole and 5-FU dose remained the same.

All the variables, such as drug plasma concentration, drug tissue concentration, drug amount eliminated and % effect can be plotted in graph or table and evaluated over time.

For the simulation, 4 Runge–Kutta integration method was used, since it's the most accurate integration method available in STELLA®. Simulation length and h were chosen in a way that h was low enough to give accurate results and without compromising the speed of the simulation and simulation length long enough to allow the lower effect value to be reached. Therefore, for gemcitabine + itraconazole combination, h=0.02 and 400 min of simulation length were used and for 5-FU + itraconazole, h=0.02 and 200 min of simulation length were used.

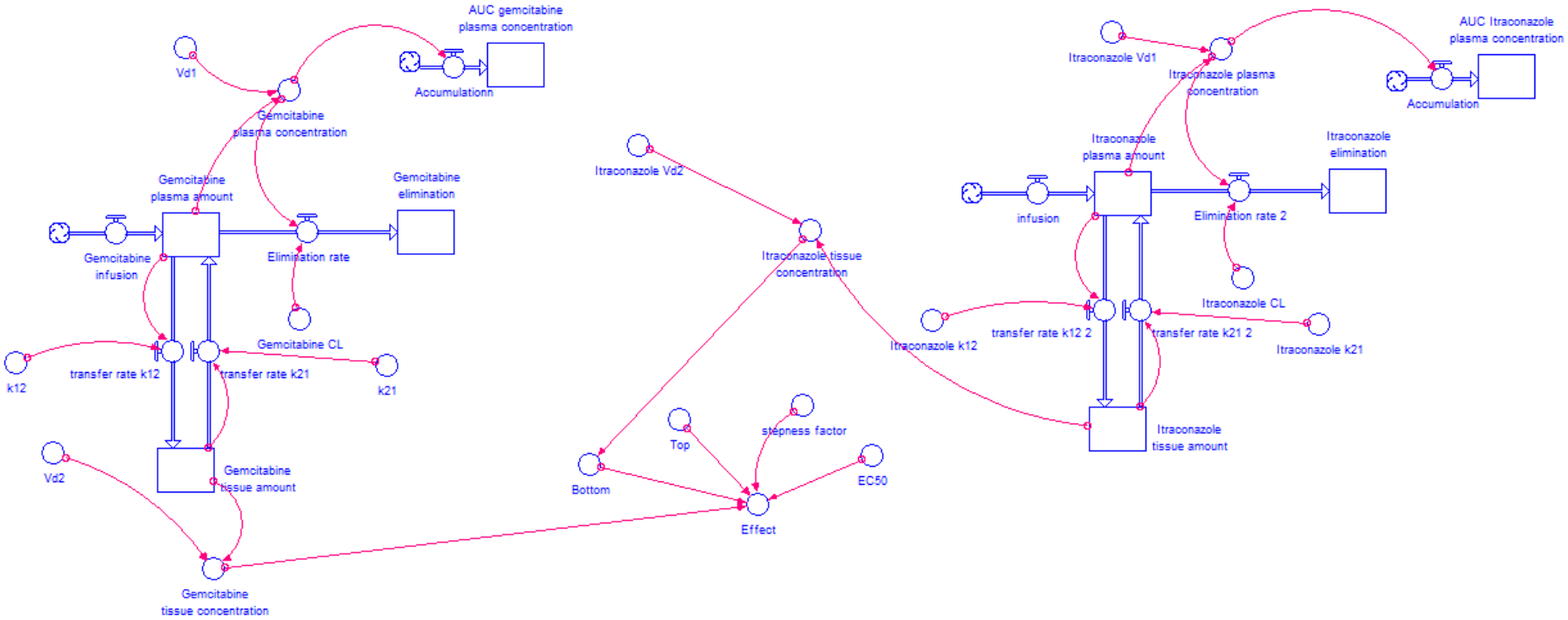


Figure 17 – **Two-compartmental PK model for gemcitabine with iv infusion, two-compartment PK model for itraconazole with iv infusion and the relation of their tissue concentration with % of cell growth inhibition in A549 cancer cell line**. Gemcitabine's model has been described in Figure 15. In itraconazole compartment model drug is infused to plasma compartment at a rate of 8.3, 5 or 1.7 mg.min$^{-1}$ during 1h (500, 300 or 100 mg doses, respectively). It is transferred from plasma compartment to tissue compartment and vice versa at a rate defined by "$k_{12}$"*"Itraconazole plasma amount" and "$k_{21}$"*" Itraconazole tissue amount", respectively, where "$k_{12}$" and "$k_{21}$" are transfer rate constants. Drug is eliminated from plasma compartment to elimination compartment at a rate defined by "CL"*" Itraconazole plasma concentration", where "CL" is a constant and "Itraconazole plasma concentration" is a variable that changes over time. "Itraconazole plasma concentration" is the result of "Itraconazole plasma amount" divided by "$V_{d1}$" while "Itraconazole tissue concentration" results from "Itraconazole tissue amount" divided by "$V_{d2}$". "Itraconazole plasma amount" is the net result of the amount of drug that leaves plasma compartment (to elimination and tissue compartment) and the amount that enters in this compartment (coming from infusion and tissue compartment). "AUC plasma concentration" is generated through Equation 2 where variable in study is "Itraconazole plasma concentration".

Considering Equation 3, "Gemcitabine tissue concentration", the average of gemcitabine + itraconazole dose-response curve parameters "Top", "Steepness factor" and "$EC_{50}$", and Equation 4, Itraconazole dose-dependent Effect was modelled.

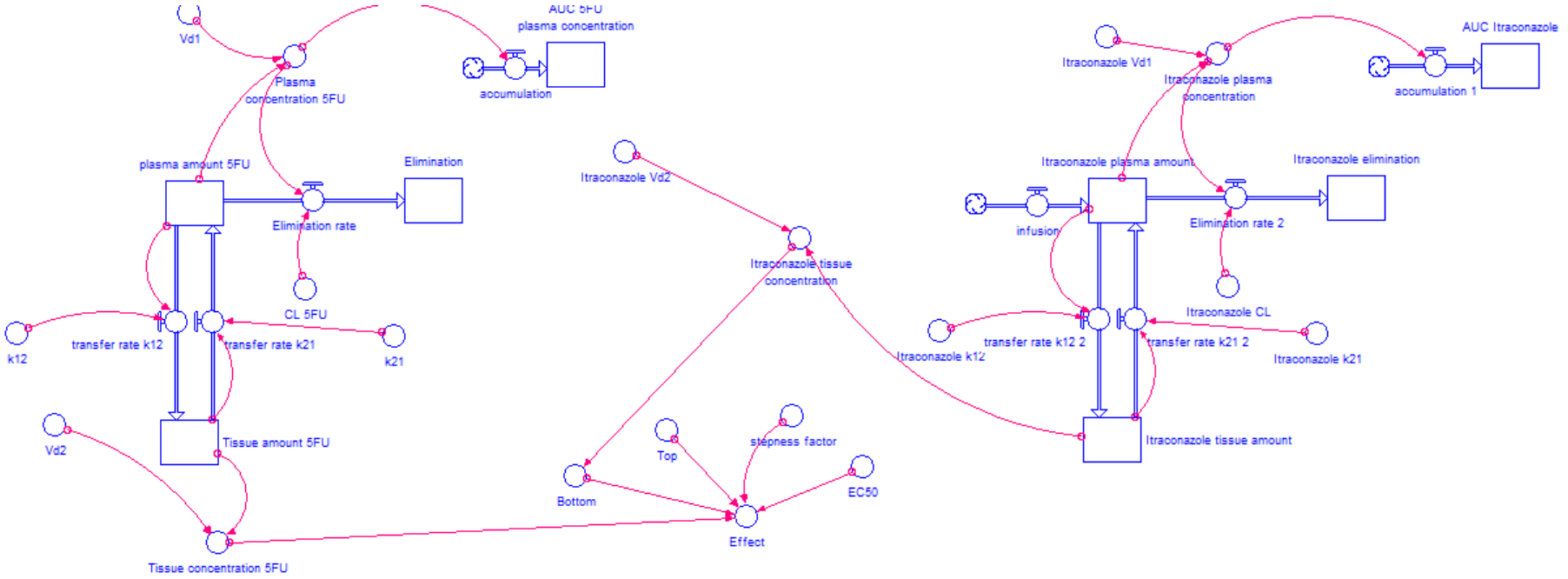


Figure 18 - **Two-compartmental PK model for 5-FU with iv injection (described in Figure 16), two-compartment model for itraconazole with iv infusion and the relation of their tissue concentration with % of cell growth inhibition in A549 cancer cell line.** In itraconazole compartment model drug is infused to plasma compartment at a rate of 8.3, 5 or 1.7 mg.min$^{-1}$ during 1h (500, 300 or 100 mg doses, respectively). It is transferred from plasma compartment to tissue compartment and vice versa at a rate defined by "$k_{12}$"*"Itraconazole plasma amount" and "$k_{21}$"*" Itraconazole tissue amount", respectively, where "$k_{12}$" and "$k_{21}$" are transfer rate constants. Drug is eliminated from plasma compartment to elimination compartment at a rate defined by "CL"*" Itraconazole plasma concentration", where "CL" is a constant and "Itraconazole plasma concentration" is a variable that changes over time. "Itraconazole plasma concentration" is the result of "Itraconazole plasma amount" divided by "$V_{d1}$" while "Itraconazole tissue concentration" results from "Itraconazole tissue amount" divided by "$V_{d2}$". "Itraconazole plasma amount" is the net result of the amount of drug that leaves plasma compartment (to elimination and tissue compartment) and the amount that enters in this compartment (coming from infusion and tissue compartment). "AUC plasma concentration" is generated through Equation 2 where variable in study is "Itraconazole plasma concentration".

Considering Equation 3, "Tissue concentration 5-FU", the average of 5-FU + itraconazole dose-response curve parameters "Top", "Steepness factor" and "$EC_{50}$", and Equation 5, Itraconazole dose-dependent Effect was modelled.

## 3.5. Model validation

In order to understand if two-compartment models were well constructed or if there were no errors in parameter inputs, two assessments were done. First, STELLA generated $C_p$-time curves were plotted against literature $C_p$-time data and general shape of the curve and fitting was evaluated. The other parameter used to evaluate the accuracy of the models was AUC plasma concentration. Thus, using the exact same dosages and routes of administration as the ones used in the literature experiments, $C_p$-time curve and AUC plasma concentration were determined and compared with literature data.

## 3.6. Schematic representation of the project

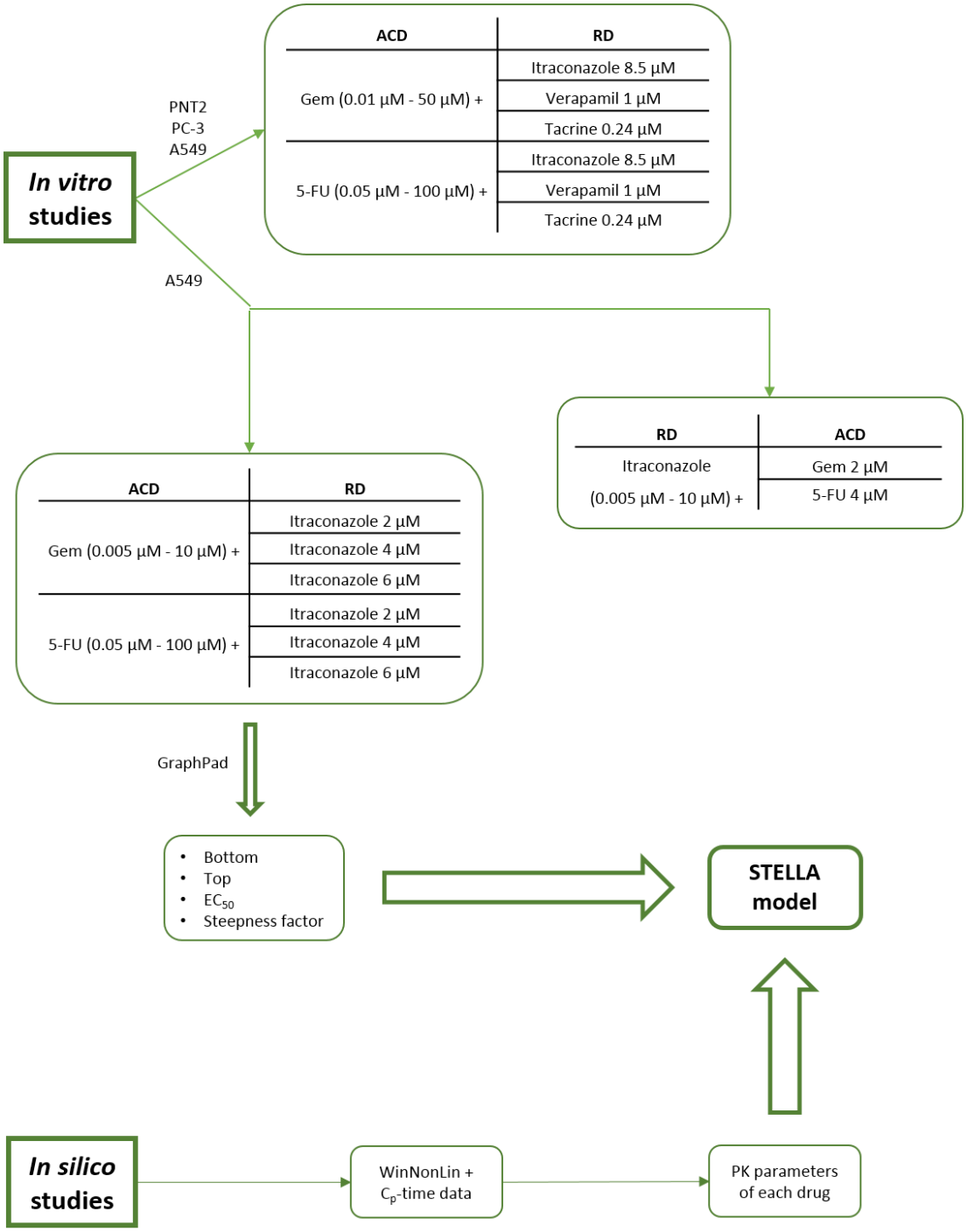


Figure 19 - **Schematic representation of the project.** First, MTT assay was performed in normal human prostate epithelial cell line PNT-2, human prostate adenocarcinoma cell line PC-3 and human lung carcinoma cell line A549. The range of concentrations of the anticancer drug (ACD) was used in combination with a fixed concentration of repurposed drug (RD). Second, MTT assay was performed in A549 cell line. One of the assays consisted in testing a range of concentrations of itraconazole in combination with a fixed concentration of ACD, and the other comprised testing a range of concentrations of anticancer drug (ACD) in combination with a fixed concentration of itraconazole (three different concentrations were tested). Results of last in vitro assay were treated in GraphPad and "Bottom", "Top", "$EC_{50}$" and "Steepness factor" parameters were obtained. In the meantime, $C_p$-time data of gemcitabine, 5-FU, and itraconazole were obtained from literature and PK analysis was performed through WinNonLin program. PK parameters obtained for each drug and the four parameters obtained from GraphPad were then used in STELLA model construction.

# 4. RESULTS AND DISCUSSION

## 4.1. *In vitro* experiments

In order to evaluate the effect of several drug combinations in cell proliferation, MTT assay was performed following 72 h treatment in human lung carcinoma A549 cell line, human prostate adenocarcinoma PC-3 cell line and normal human prostate epithelium PNT2 cell lines. For this study, the drug combinations used were the following:

Table 9 - Drug combinations used in cell proliferation studies.

| ACD | RD |
|---|---|
| Gem + | Itraconazole |
| | Verapamil |
| | Tacrine |
| 5-FU + | Itraconazole |
| | Verapamil |
| | Tacrine |

Range of ACD concentrations + fixed concentration of RD

Firstly, several ACD concentrations (gemcitabine or 5-FU) were tested with or without RD (itraconazole, verapamil or tacrine) at a fixed concentration.

Figure 20 shows the dose-response curve of gemcitabine combinations and gemcitabine alone in each one of the cell lines. As shown in this results, all the cell lines are sensitive to gemcitabine but to different degrees. Gemcitabine alone dose-response curve is approximately the same as gemcitabine in combination with verapamil or tacrine, in A549 and PNT2 cell lines (Figure 20 A and C, respectively), with an $IC_{50}$ rounding 0.01 and 0.04 μM respectively. The major difference between those combinations and gemcitabine alone is in PC-3 cell line where $IC_{50}$ ranged from 0.06 to 0.59 μM, but the difference was not considered to further studies. On the other hand, itraconazole combination improved substantially the overall effect, comparing to ACD alone. In healthy and cancer prostate cell lines (PNT2 and PC-3, respectively), itraconazole effect

is noticeable when gemcitabine concentration is low (<0.5 µM in PNT2 and <0.1 µM in PC-3 cell lines). At higher concentrations, Gem + I curve matches the control line suggesting that the overall effect is due to gemcitabine. In A549 cell line itraconazole considerably enhanced % of cell growth inhibition in all gemcitabine concentrations tested.

Although the concentration chosen for RD is a concentration reported as safe for clinical use,[74, 93, 105] PNT2 healthy cell line was used as a control. As shown in Figure 20 C, at gemcitabine's lowest concentration, % of cell growth inhibition is about 30% with or without RD (expect for itraconazole). Considering this, verapamil and tacrine are expected not to be at a cytotoxic concentration. However, RD should have been used alone for control purposes. Lacking this control, conclusions about itraconazole toxicity cannot be taken.

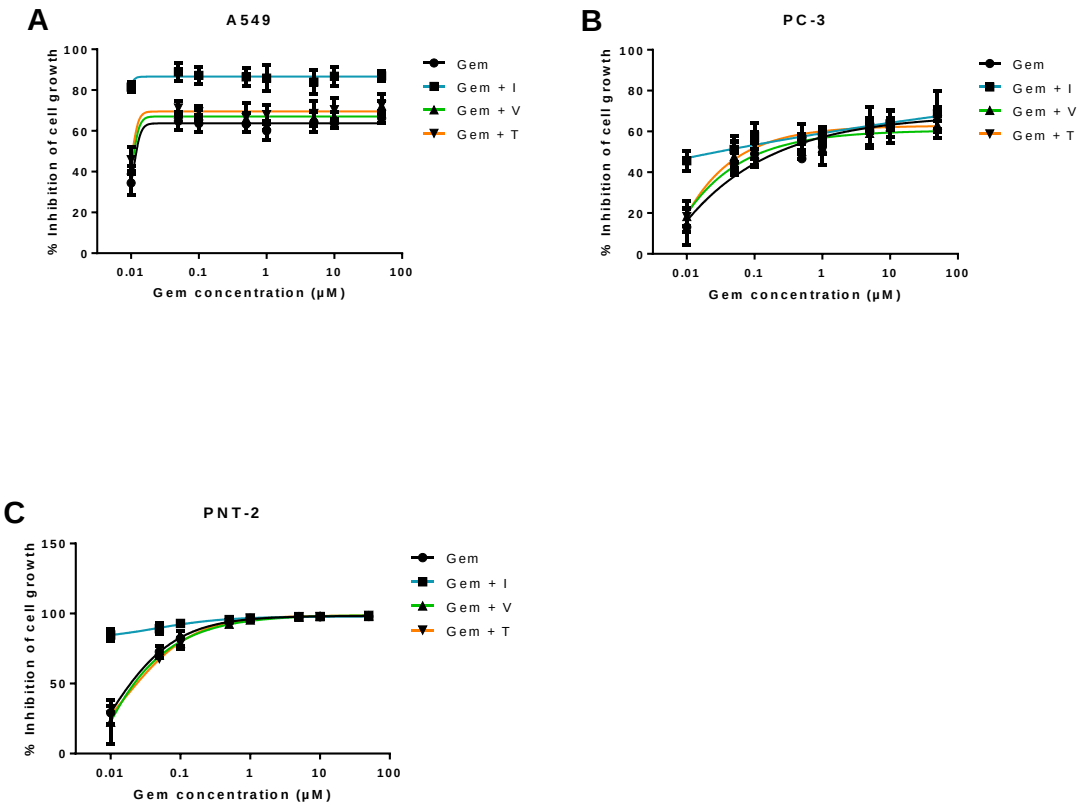


Figure 20 - **Dose-response curve of gemcitabine in combination with RD.** Percentage of cell growth inhibition of human lung carcinoma A549 cell line (A – left top), human prostate adenocarcinoma PC-3 cell line (B – right top) and normal human prostate epithelium PNT2 cell line (C – left bottom), treated with wide range of concentrations of gemcitabine (Gem) alone (black line) or Gem in combination with a fixed concentration of RD (verapamil (V) (green line), itraconazole (I) (blue line) or tacrine (T) (orange line)), during 72h, determined with MTT assay. Results are the mean of at least three independent experiments. The DMSO control did not present toxicity to the cells (data not shown).

Figure 21 shows the results for 5-FU combinations and 5-FU alone. As shown in this results, 5-FU alone dose-response curve is approximately the same as 5-FU in combination with verapamil or tacrine, in all the tested cell lines. Slight differences between 5-FU alone $IC_{50}$ and drug combinations $IC_{50}$ were detected within each cell line ($IC_{50}$ values ranging from 2.15 to 5.8 μM in A549 cell line, rounding 13 μM in PC-3 and rounding 12 μM in PNT2 cell line).

As verified in gemcitabine experiments, itraconazole in combination with 5-FU also improved substantially the overall effect, comparing to ACD alone. In fact, according to this results, the overall effect of 5-FU + I combination is almost independent on 5-FU concentration, suggesting that the observed response is mostly due to itraconazole effect. However, this conclusion cannot be validated due to the lack in RD alone control.

Concerning the use of PNT2 healthy cell line as control, in this study case, verapamil and tacrine concentration doesn't seem to be cytotoxic. As shown in Figure 21 C, at 5-FU lowest concentration % of cell growth inhibition was about 2% with or without RD (except for itraconazole). Considering this, verapamil and tacrine are expected not to be at a cytotoxic concentration. However, as explained before, RD should have been used alone for control purposes. Lacking this control, conclusions about itraconazole toxicity cannot be taken.

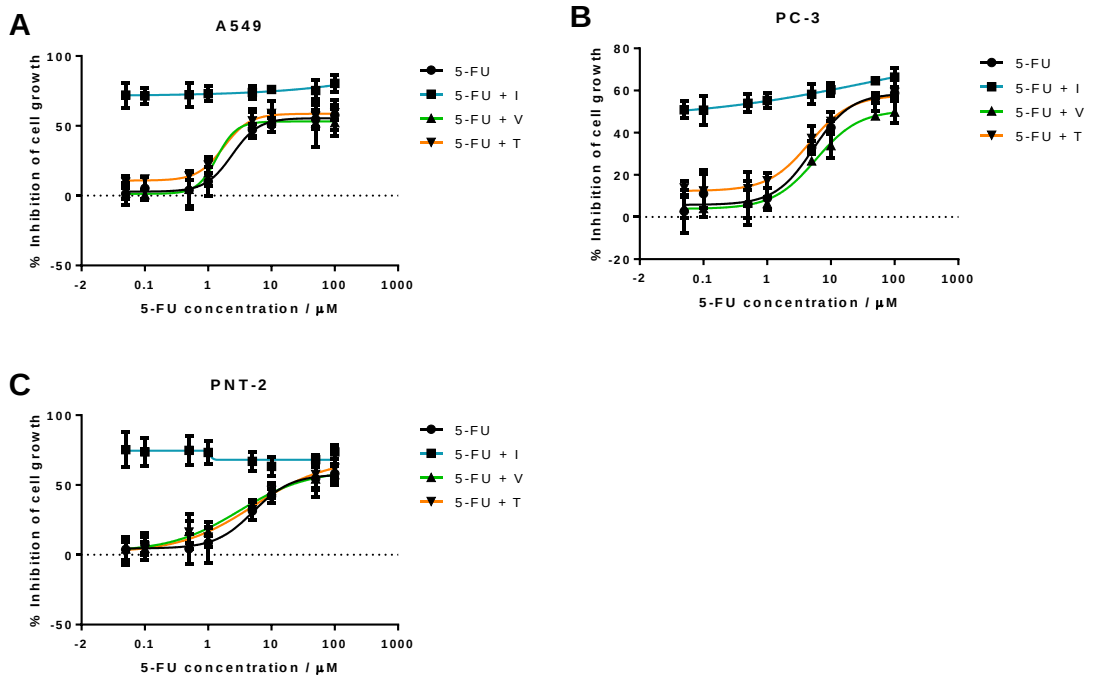


Figure 21 - **Dose-response curve of 5-FU in combination with RD.** Percentage of cell growth inhibition of human lung carcinoma A549 cell line (**A** – left top), human prostate adenocarcinoma PC-3 cell line (**B** – right top) and normal human prostate epithelium PNT2 cell line (**C** – left bottom), treated with wide range of concentrations of 5-fluorouracil (5-FU) alone (black line) or 5-FU in combination with a fixed concentration of RD (verapamil (V) (green line), itraconazole (I) (blue line) or tacrine (T) (orange line)), during 72h, determined with MTT assay. Results are the mean of at least three independent experiments. The DMSO control did not present toxicity to the cells (data not shown).

The three selected repurposed drugs were expected to show noticeable improvement in % of cell growth inhibition when combined with gemcitabine or 5-FU. However, tacrine and verapamil didn't reveal promising activity.

The former, tacrine, has been reported to enhance tumor suppressor's activity, such as caspase, Bax, and p53 in mouse hepatocytes,[69] as stated earlier. However, when used in combination with gemcitabine or 5-FU, at a concentration of 1 µM, in A549, PC-3, and PNT2 cell lines it didn't reveal significant improvement in % cell inhibition, comparing to the control (ACD alone).

The latter, verapamil, is known to promote intracellular chemotherapeutic drugs accumulation. It has been study in multiple types of cancer cell lines, such as lymphoma, myeloma, non-small cell lung cancer, colorectal carcinoma, leukemia, and neuroblastoma cell lines, in combination with multiple ACD such as vincristine, vinblastine, doxorubicin, daunorubicin and paclitaxel and have proven efficacy in reversing multidrug resistance through inhibition of P-gp, one of the main responsible proteins for drug extrusion in cancer.[113-118] In a recent study has also been tested

Verapamil in combination with gemcitabine, in chemotherapy-resistant pancreatic cancer side population (SP) cells, showing not only enhancement of cytotoxicity when used in combination with this chemotherapeutic agent, but also apoptosis induction of stem-like SP cells in L3.6pl and AsPC-1 pancreatic carcinoma models and significant inhibition of pancreatic cancer tumor growth *in vivo* potentially by targeting stem-like side population cells.[119]

Although the first-generation inhibitor of P-gp and possible capability of inducing apoptosis and inhibiting tumor growth, verapamil didn't show significant improvement in drug combinations tested against PNT2, PC-3, and A549 cell lines.

As shown in the results above, itraconazole was the only RD significantly increasing the % of cell growth inhibition when combined with an ACD (gemcitabine or 5-FU). Itraconazole has been extensively studied in cancer research and several anticancer mechanisms of action have been identified, which include the ability to inhibit Hedgehog pathway and angiogenesis, both mechanisms related to cancer development (Figure 12), autophagy induction and reversal of multidrug resistance.[53-58] Therefore, enhancement of cell growth inhibition may be explained by the targeting of an additional pathway in cell division.

To understand how the itraconazole concentration did affect the % of cell growth inhibition, lower itraconazole concentrations were tested, since the concentration tested in the previous experiments was the maximum plasma concentration recommended.

Range of itraconazole concentrations + fixed concentration of ACD

A range of concentrations of itraconazole was either tested alone (control) or in combination with a fixed concentration of ACD. ACD was also tested alone as a control.

Figure 22 shows itraconazole dose-response curve (black line), where improvement of cell growth is achieved at concentrations lower than 2 μM. Concentrations higher than this value drove to cell growth inhibition in a dose-dependent manner. In I + 5-FU combination dose-response curve (green line), 5-FU alone effect (first value of the curve) is almost insignificant. Itraconazole effect for concentration up to 2 μM is also null in drug combination effect improvement. Only itraconazole concentrations higher than 2 μM, enhance % of cell growth inhibition in I + 5-FU drug combination. However, the dose-response curve overlaps itraconazole alone dose-response curve. Hereupon, this data is not enough to understand if itraconazole is improving 5-FU effect or if the result is only due to itraconazole itself. In I + Gem combination dose-response curve (blue line),

gemcitabine alone effect (first value of the curve) is about 50% and this value doesn't change when itraconazole concentrations are lower than 2 μM. At higher concentrations, the drug combination effect is higher than itraconazole or gemcitabine effect alone.

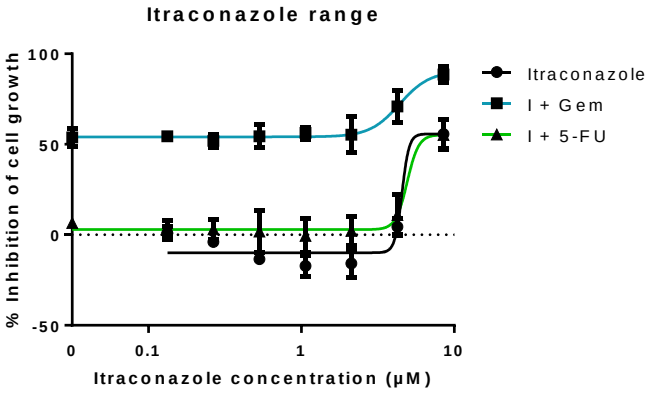


Figure 22 - **Dose-response curve of itraconazole in combination with ACD.** Percentage of cell growth inhibition of human lung carcinoma A549 cell line treated with a range of concentrations of itraconazole alone (black line) or itraconazole in combination with a fixed concentration of ACD (Gem (blue line) or 5-FU (green line)), during 72h, determined with MTT assay. Results are mean of at least three independent experiments. The DMSO control did not present toxicity to the cells (data not shown).

As shown in Figure 22, only itraconazole concentrations above 2 μM enhanced the % of cell growth inhibition, when in combination with an ACD (Figure 22). Thus, in order to evaluate the itraconazole concentration effect in ACD dose-response curve, further experiments were done.

Range of ACD concentrations + fixed concentration of itraconazole

ACD range of concentrations was tested with or without a fixed concentration of itraconazole. Three different concentrations of itraconazole were tested: 2, 4 and 6 μM. Itraconazole was also tested alone as a control.

Figure 23 shows gemcitabine + itraconazole (A) and 5-FU + itraconazole (B) dose-response curves. According to the results, itraconazole concentration doesn't significantly affect the highest % of cell growth inhibition ("Top" value), but it strongly affects the lowest value of the curve ("Bottom" value). In other words, the highest effect ("Top" value) achieved with gemcitabine or 5-FU alone is approximately the same as drug combinations, values rounding 73% (Table 10) and 59% (Table 11), respectively. Thus, it was concluded that itraconazole different concentrations don't affect the "Top" value of the drug combinations dose-response curve. On the other hand, the lowest %

of cell growth inhibition ("Bottom" value) strongly depends on itraconazole concentration, varying in a dose-dependent manner. Again and as stated above, when itraconazole concentration is low (2 μM), % of cell growth is enhanced, comparing to the control (ACD alone) for unknown reasons. Increasing itraconazole concentration to 4 and 6 μM increases "Bottom" value from 0 (control) to about 13% and 33%, respectively, in both combination groups (Figure 23 A and B).

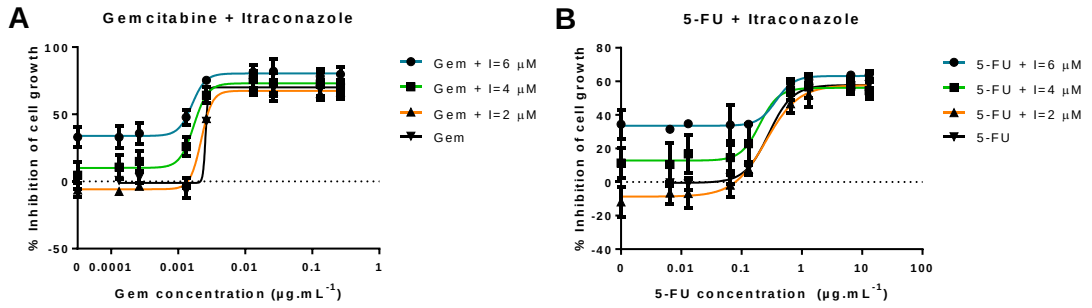


Figure 23 - **Dose-response curves of ACD in combination with itraconazole. A:** Percentage of cell growth inhibition of human lung carcinoma A549 cell line treated with wide range of concentrations of gemcitabine (Gem) alone (control) or Gem in combination with a fixed concentration of itraconazole (I), during 72h, determined with MTT assay; **B:** Percentage of cell growth inhibition of human lung carcinoma A549 cell line, treated with wide range of concentrations of 5-FU alone (control) or 5-FU in combination with a fixed concentration of I, during 72h, determined with MTT assay. Results are the mean of at least three independent experiments. The DMSO control did not present toxicity to the cells (data not shown).

In Table 10 are presented the four parameters that describe, through Equation 3, every dose-response curve for gemcitabine and itraconazole combinations (Figure 23 A), obtained from GraphPad Prism 6. "Bottom" values were used in Equation 4 construction. However, in order to obtain scientifically meaningful equation, Gem + I=2 "Bottom" value was excluded.

Average value of "Top", "Steepness factor" and "$EC_{50}$" parameters were used in STELLA model converters (Figure 17). However, since GraphPad fits a model to experimental data, obtained parameters may have big errors associated. Therefore, Gem + I=0 "Steepness factor" was not included in average "Steepness factor" measurement.

Table 10 - Dose-response curve parameters for gemcitabine and itraconazole combinations, obtained from GraphPad. (N.A.: non applicable.)

| Gem + … | Bottom (%) | Top (%) | Steepness Factor | $EC_{50}$ ($\mu g.mL^{-1}$) |
|---|---|---|---|---|
| **I=6 µM** | 34.33 ± 2.43 | 80.39 ± 1.71 | 4.30 ± 1.30 | $0.0016 \pm 3.2x10^{-7}$ |
| **I=4 µM** | 12.83 ± 2.79 | 73.07 ± 1.97 | 4.37 ± 0.99 | $0.0018 \pm 3.1x10^{-7}$ |
| **I=2 µM** | -5.51 ± 1.83 | 67.47 ± 1.29 | 5.35 ± 1.12 | $0.0022 \pm 1.6x10^{-7}$ |
| **I=0 µM** | -1.06 ± 2.35 | 70.12 ± 1.67 | $23.14 \pm 4.20x10^{5}$ | $0.0026 \pm 2.2x10^{5}$ |
| **Average** | N.A. | 72.76 | 4.67 | 0.0021 |

In Table 11 are presented the four parameters that describe, through Equation 3, every dose-response curve for 5-FU and itraconazole combinations (Figure 23 B), obtained from GraphPad Prism 6. “Bottom” values were used in Equation 5 construction. However, similarly to what was done in the previous situation, in order to obtain scientifically meaningful equation, 5-FU + I=2 “Bottom” value was excluded. Average value of “Top”, “Steepness factor” and “$EC_{50}$” parameters were used in STELLA model converters (Figure 18).

Table 11 – Dose-response curve parameters for 5-FU and itraconazole combinations, obtained from GraphPad. (N.A.: non applicable.)

| 5-FU + … | Bottom (%) | Top (%) | Steepness factor | $EC_{50}$ ($\mu g.mL^{-1}$) |
|---|---|---|---|---|
| **I=6 µM** | 33.22 ± 1.58 | 63.24 ± 1.62 | 2.77 ± 1.23 | 0.3615 ± 0.0122 |
| **I=4 µM** | 13.42 ± 3.09 | 56.05 ± 2.87 | 2.90 ± 2.40 | 0.2018 ± 0.0071 |
| **I=2 µM** | -6.99 ± 2.14 | 57.52 ± 2.11 | 1.70 ± 0.26 | 0.2663 ± 0.0016 |
| **I=0 µM** | -0.47 ± 1.32 | 57.80 ± 1.32 | 2.19 ± 0.27 | 0.2812 ± 0.0009 |
| **Average** | N.A. | 58.65 | 2.39 | 0.2777 |

## 4.2. WinNonLin: PK analysis

The concentration-time curves of gemcitabine in plasma were evaluated by compartmental analysis (Phoenix WinNonLin (64-bit, version 7.00)). The best fitting was achieved with a two-compartmental model (Figure 24) and PK parameters were obtained through PK analysis (Table 12). The precision of the measurements are expressed in % of the coefficient of variation (%CV) and are also presented in Table 12.

In spite of WinNonLin prediction (blue line) don't fit all experimental values (red circles), $k_{10}$, AUC, $C_{max}$ and CL values obtained are in accordance with the literature (Table 12). However, transfer rate constants $k_{12}$ and $k_{21}$ and tissue compartment volume of distribution ($V_{d2}$) measurements are not very precise, but, since no more accurate data was available, the values were included in STELLA model.

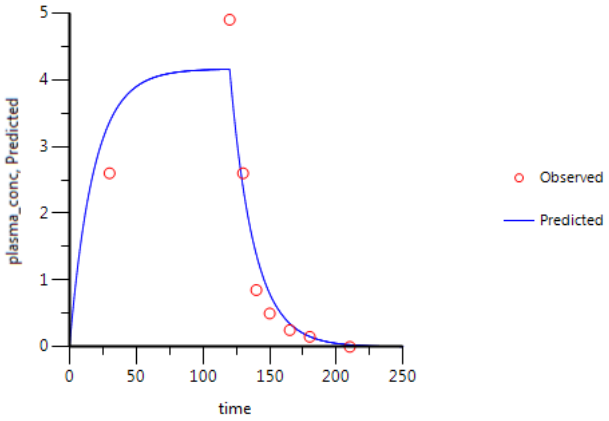


Figure 24 - **Gemcitabine $C_p$-time curve prediction through two-compartmental model fitting of its observed $C_p$-time data.** Red circles correspond to the experimental data, obtained from the literature, and the continuous blue line corresponds to the in silico $C_p$-time curve prediction. Plasma concentration is given in $\mu g.mL^{-1}$ and time in minutes.

Table 12 - Gemcitabine PK parameters obtained from WinNonLin.

| Gemcitabine parameters | Estimate | CV (%) | Literature values[108] |
|---|---|---|---|
| $k_{10}$ ($min^{-1}$) | $5.54x10^{-2}$ | 144.9 | $7.00x10^{-2}$ |
| $k_{12}$ ($min^{-1}$) | $6.64x10^{-4}$ | 45998.6 | - |
| $k_{21}$ ($min^{-1}$) | $1.02x10^{-1}$ | 29203.6 | - |
| AUC ($\mu g.mL^{-1}.min$) | 499.58 | 10.3 | 453.00 |
| $C_{max}$ ($\mu g.mL^{-1}$) | 4.16 | 10.5 | 4.92 |
| CL ($mL.min^{-1}$) | 3771.20 | 10.3 | 3940.05 |
| $V_{ss}$ (mL) | 68464.40 | 37.4 | - |
| $V_{d1}$ (mL) | 68019.62 | 148.8 | - |
| $V_{d2}$ (mL) | 444.79 | 19137.5 | - |

$k_{10}$: elimination rate constant; $k_{12}$: transfer rate constant from central compartment to tissue compartment; $k_{21}$: transfer rate constant from tissue compartment to central compartment; AUC: area under the plasma concentration-time curve; $C_{max}$: maximum plasma concentration; CL: clearance; $V_{ss}$: steady state volume of distribution; $V_{d1}$: volume of distribution of central compartment; $V_{d2}$: volume of distribution of tissue compartment.

The concentration-time curves of 5-FU in plasma were evaluated by compartmental analysis (Phoenix WinNonLin (64-bit, version 7.00)). The best fitting was achieved with a two-compartmental model (Figure 25) and PK parameters were obtained through PK analysis (Table 13). The precision of the measurements are expressed in % of the coefficient of variation (%CV) and are also presented in the table.

As shown in Figure 25, WinNonLin prediction (blue line) fits almost perfectly all experimental values (red circles). All PK parameters obtained are also in accordance with literature values (Table 13).

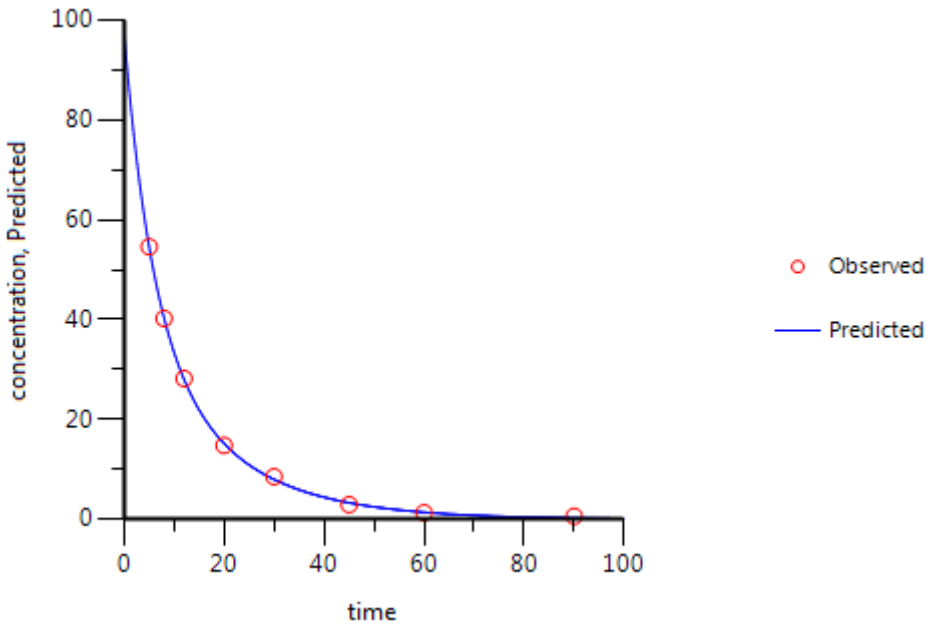


Figure 25 - **5-FU $C_p$-time curve prediction through two-compartmental model fitting of its observed $C_p$-time data.** Red circles correspond to the experimental data, obtained from the literature, and the continuous blue line corresponds to the in silico $C_p$-time curve prediction. Plasma concentration is given in $\mu g.mL^{-1}$ and time in minutes.

Table 13 - 5-FU PK parameters obtained from WinNinLin.

| **5-FU parameters** | **Estimate** | **CV (%)** | **Literature values[109]** |
|---|---|---|---|
| $k_{10}$ ($min^{-1}$) | $9.17x10^{-2}$ | 4.9 | - |
| $k_{12}$ ($min^{-1}$) | $3.21x10^{-2}$ | 29.5 | - |
| $k_{21}$ ($min^{-1}$) | $1.07x10^{-1}$ | 28.1 | - |
| AUC ($\mu g.mL^{-1}.min$) | 1058.81 | 1.6 | 926.80 |
| $C_{max}$ ($\mu g.mL^{-1}$) | 97.14 | 5.1 | - |
| CL ($mL.min^{-1}$) | 850.01 | 1.6 | 1069.20 |
| $V_{ss}$ (mL) | 12056.99 | 4.9 | 15912.00 |
| $V_{d1}$ (mL) | 9265.14 | 5.1 | - |
| $V_{d2}$ (mL) | 2791.84 | 14.2 | - |

$k_{10}$: elimination rate constant; $k_{12}$: transfer rate constant from central compartment to tissue compartment; $k_{21}$: transfer rate constant from tissue compartment to central compartment; AUC: area under the plasma concentration-time curve; $C_{max}$: maximum plasma concentration; CL: clearance; $V_{ss}$: steady state volume of distribution; $V_{d1}$: volume of distribution of central compartment; $V_{d2}$: volume of distribution of tissue compartment.

The concentration-time curves of itraconazole in plasma were evaluated by compartmental analysis (Phoenix WinNonLin (64-bit, version 7.00)). The best fitting was achieved with a two-compartmental model (Figure 25) and PK parameters were obtained through PK analysis (Table 14). The precision of the measurements are expressed in % of the coefficient of variation (%CV) and are also presented in the table.

Although the steady-state volume of distribution ($V_{ss}$) is quite lower than the volume of distribution reported in literature source, WinNonLin prediction (blue line) fits almost perfectly all experimental values (red circles) and % CV is quite low in all parameters determined. Therefore, WinNonLin prediction was assumed to be reliable. In fact, the volume of distribution parameter determined in the literature is $V_{darea}$,[106] which means that it was determined during the elimination phase and not at steady-state, as in WinNonLin prediction.[120] Therefore, parameters cannot be compared.

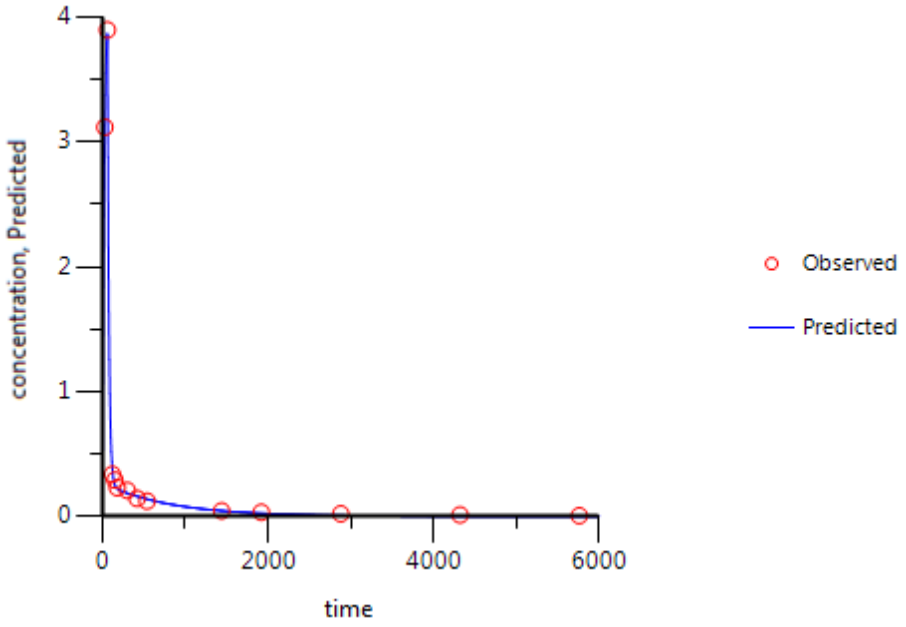


Figure 26 - **Itraconazole $C_p$-time curve prediction through two-compartmental model fitting of its observed $C_p$-time data.** Red circles correspond to the experimental data, obtained from the literature, and the continuous blue line corresponds to the in silico $C_p$-time curve prediction. Plasma concentration is given in $\mu g.mL^{-1}$ and time in minutes.

Table 14 - Itraconazole PK parameters obtained from WinNonLin.

| Itraconazole parameters | Estimate | CV (%) | Literature values[106] |
|---|---|---|---|
| $k_{10}$ ($min^{-1}$) | $2.80x10^{-2}$ | 8.8 | $2.66x10^{-2}$ |
| $k_{12}$ ($min^{-1}$) | $2.38x10^{-2}$ | 9.4 | - |
| $k_{21}$ ($min^{-1}$) | $2.34x10^{-3}$ | 15.3 | - |
| AUC ($\mu g.mL^{-1}.min$) | 437.73 | 7.9 | 449.88 |
| $C_{max}$ ($\mu g.mL^{-1}$) | 3.88 | 0.6 | - |
| CL ($mL.min^{-1}$) | 228.45 | 7.9 | 246.67 |
| $V_{ss}$ (mL) | 90922.24 | 20.9 | 558000 |
| $V_{d1}$ (mL) | 8145.37 | 2.6 | - |
| $V_{d2}$ (mL) | 82776.88 | 22.9 | - |

$k_{10}$: elimination rate constant; $k_{12}$: transfer rate constant from central compartment to tissue compartment; $k_{21}$: transfer rate constant from tissue compartment to central compartment; AUC: area under the plasma concentration-time curve; $C_{max}$: maximum plasma concentration; CL: clearance; $V_{ss}$: steady state volume of distribution; $V_{d1}$: volume of distribution of central compartment; $V_{d2}$: volume of distribution of tissue compartment.

## 4.3. STELLA® models

### 4.3.1. Input data for the model

For the models described in the experimental section, two types of parameters were used: 1) the parameters related with the drug in study obtained through WinNonLin (Table 12, Table 13 and Table 14), which were used as constants without further modification, and 2) the parameters obtained from the in vitro studies (Table 10 and Table 11).

### 4.3.2. Model validation

In order to evaluate the model accuracy, $C_p$-time curve was determined, through STELLA model, and compared with the experimental values.

Figure 27 shows that gemcitabine STELLA model (Figure 15) is quite accurate in predicting gemcitabine's plasma concentration over time. Since the input values came from WinNonLin, and WinNonLin $C_p$-time curve prediction don't fit all experimental values, then $C_p$-time curve predicted through STELLA won't fit them all as well.

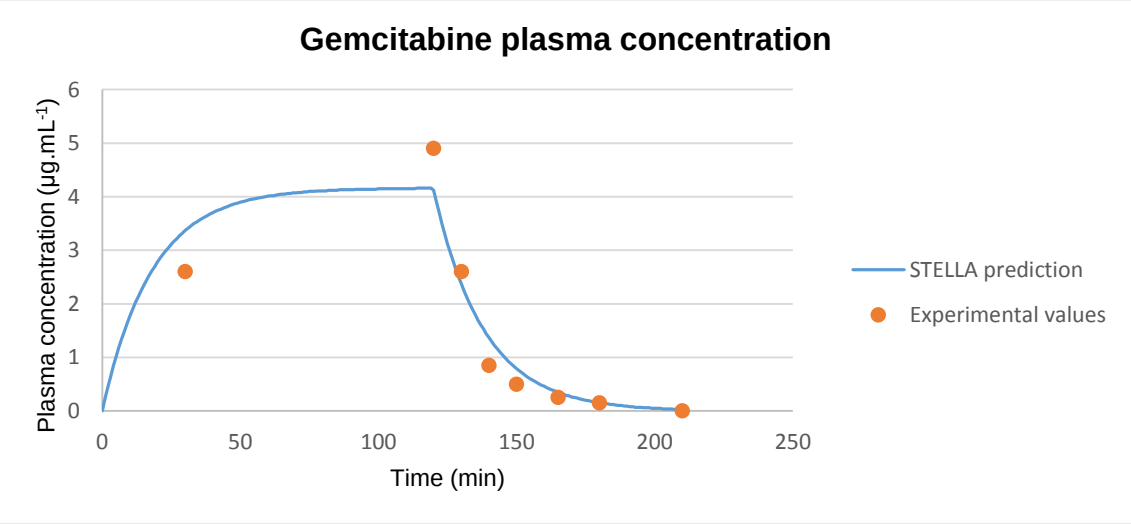


Figure 27 - **Graphical representation of experimental $C_p$-time data of gemcitabine and $C_p$-time curve generated *in silico* for this drug over 210 minutes.**

For the 5-FU STELLA model, Figure 28 demonstrates $C_p$-time curve predicted with STELLA (blue line) fitting all the experimental values (orange circles). Thus, one can assume that the model is accurately predicting 5-FU's plasma concentration over time.

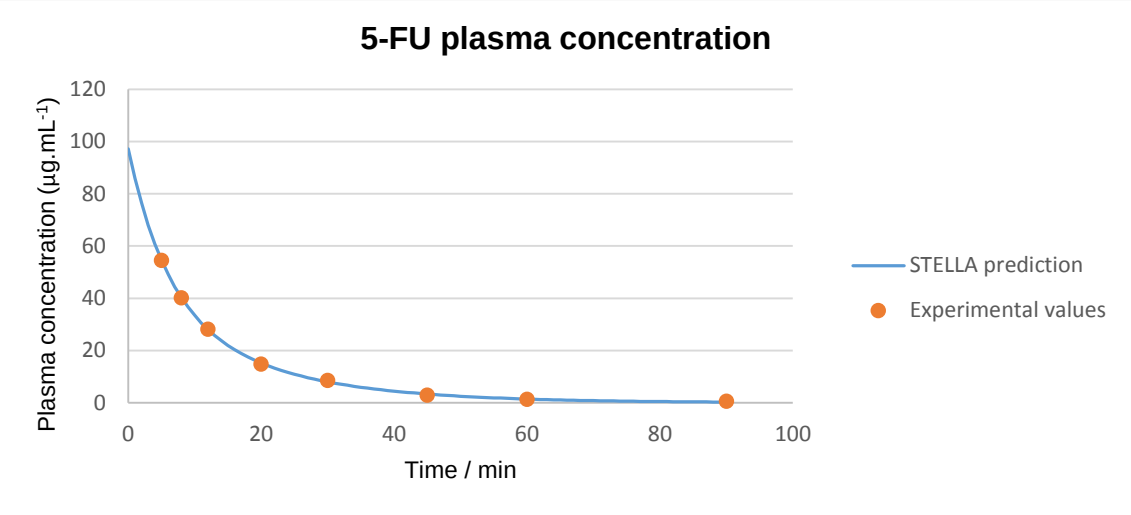


Figure 28 - **Graphical comparison between experimental $C_p$-time data of 5-FU and $C_p$-time curve generated *in silico* for this drug over 90 minutes.**

Similarly to the previous case, itraconazole $C_p$-time curve predicted with STELLA (blue line) is also fitting all the experimental values (orange circles) (Figure 29). Once more, one can assume that the model is accurately predicting itraconazole plasma concentration over time.

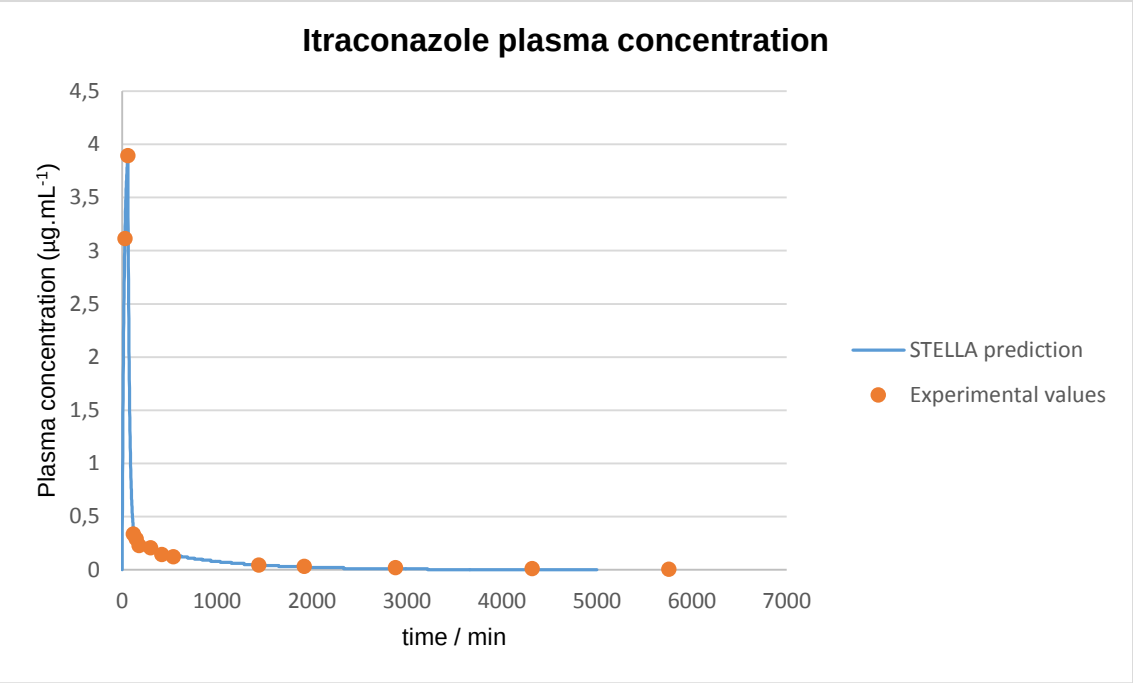


Figure 29 - **Graphical comparison between experimental $C_p$-time data of itraconazole and $C_p$-time curve generated *in silico* for this drug over 5000 minutes.**

Besides $C_p$-time curve graphical analysis, in order to validate STELLA models, AUC value was determined and compared with literature source.

In Figure 30, three AUC values are depicted for each drug: AUC calculated from experimental data (literature value), WinNonLin PK analysis, and STELLA model simulation prediction. As expected, for each drug, STELLA prediction is in perfect accordance with WinNonLin PK analysis, showing the exact same AUC value. Literature value is slightly different from STELLA and WinNonLin values probably because integration method used for AUC calculation was different (all literature sources used trapezoidal rule, while STELLA and WinNonLin predictions resorted to $4^{th}$ order Runge-Kutta method).

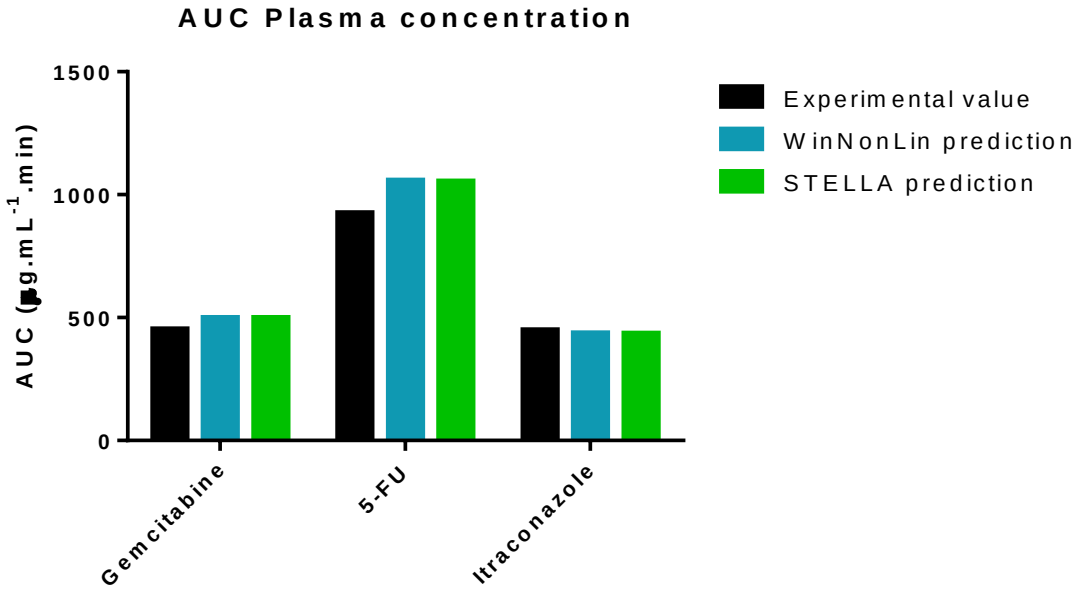


Figure 30 - **Graphical representation of AUC plasma concentration of gemcitabine, 5-FU, and itraconazole when determined experimentally, through WinNonLin or STELLA models.**

### 4.3.3. AUC effect: Drug combination effect comparison

To compare drug combination effect in A549 cancer cell line, AUC of effect was determined in STELLA®. The effect is calculated through Equation 3, where the only variable is ACD tissue concentration. All the other parameters are constants and characterize the dose-response curve obtained from *in vitro* studies. In other words, depending on ACD tissue concentration, and the parameters introduced in model converters (Table 10 and Table 11), "Effect" gets a certain value over time. AUC effect quantifies the overall effect during simulation.

According to the results (Figure 31), and in accordance with the *in vitro* experimental results (Figure 23), the higher the itraconazole concentration, the higher is the AUC effect value. In gemcitabine combinations, when itraconazole tissue concentration is 4 μM and 6 μM, $AUC_{Effect}$ is about 9% and 22% higher than control (gemcitabine without itraconazole), respectively. In 5-FU combinations, these values reach 12% and 34% improvement relative to control (5-FU without itraconazole), respectively. However, when itraconazole concentration is 2 μM, AUC effect is lower than control, in both combination groups, for unknown reasons.

Although gemcitabine and 5-FU elimination half-life ($t_{1/2}$) is identical (10 and 12 minutes, respectively),[108-109] the former is infused at a rate of 15.7 mg per minute, over 2 hours, which represents a total dose of 1884 mg, while the latter is administered through 1 minute i.v. injection at a dose of 900 mg. Therefore, the AUC effect of 5-FU is expected to be much smaller than gemcitabine's, due to a reduced exposure time of 5-FU in tissue.

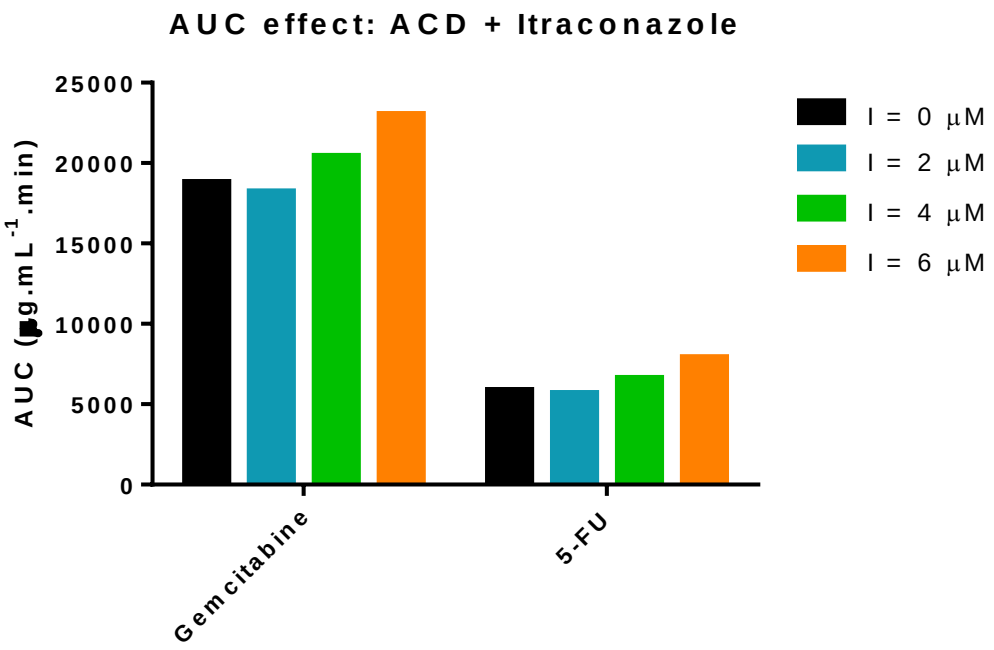


Figure 31 - **Graphical representation of AUC for gemcitabine + itraconazole and 5-FU + itraconazole combinations.**

Besides the AUC effect, further analysis was done regarding itraconazole dose-dependent effect. This time, instead of one only variable (ACD concentration), as in the previous study, % effect will also depend on itraconazole tissue concentration over time. "% Effect" is still calculated through Equation 3, where ACD tissue concentration is the main variable, but "Bottom" parameter is now an equation dependent on itraconazole tissue concentration, instead of being a constant (Equation 4 and Equation 5).

In Figure 36 are presented five different graphs that enable the evaluation of drug concentration in the tissue compartment and its relationship with % effect over time. Graphs A and B show effect-time curve of ACD and itraconazole drug combination. Using constant ACD dose administration and three different doses of itraconazole,

differences between effect-time curves can be seen. According to Figure 36 A and B, depending on itraconazole dose administration, the final part of the curve is different.

For gemcitabine + itraconazole drug combination (Figure 36 A), first, “% Effect” remains constant, at a level of 73% of cell growth inhibition. Then, at minute 260 “Effect” starts dropping abruptly. This drop can be explained with a deeper analysis of Equation 3. Gemcitabine concentration affects “% Effect” through exponential function described by Equation 6, where x is gemcitabine tissue concentration. According to this equation, at very high concentrations, gemcitabine tissue concentration influence on “% Effect” can be despised because f(x) will result in a very low value (Equation 6). Then, this value will be summed to 1 and divided to (“Top”-“Bottom”) values. When this concentration is reduced to a value lower than 0.008 μg.mL$^{-1}$, f(x) increases exponentially reducing “% Effect” abruptly. Figure 36 C shows gemcitabine tissue concentration-time curve. Figure 32 is a graphical representation of Equation 6, for better understanding.

**Equation 6**

$$f(x) = \left(\frac{x}{0.0019}\right)^{-4.67}$$


Figure 32 - **Graphical representation of Equation 6, using desmos.com calculator.**

After the drop in “% Effect” value, slight differences between effect-time curves start to be noticed. At this point, itraconazole tissue concentration plays the main role in the

overall effect, since “% Effect” equals “Bottom” value (Equation 3), which is directly dependent on itraconazole tissue concentration.

In Figure 36 E, itraconazole tissue concentration is shown for the three studied doses. According to the results, itraconazole concentration is slowly eliminated from the tissue compartment and will maintain % of cell growth inhibition relatively constant while it is been eliminated from the tissue compartment. In fact, if higher values of itraconazole tissue concentration were considered, “% Effect” would be equally higher. This can be mathematically explained through Equation 4 analysis. Figure 33 is a graphical representation of Equation 4, where the x-axis is itraconazole tissue concentration and the y-axis is “Bottom” value. Since the highest itraconazole concentration value used in Equation 4 formulation was 4.2 $\mu g.mL^{-1}$ (6 μM), higher concentrations were not considered for graphical representation.

Itraconazole multiple dosing simulation was tried in the STELLA® simulation program, with the objective of increasing itraconazole tissue concentration, but limitations in the software's builtin functions did not allow the study.

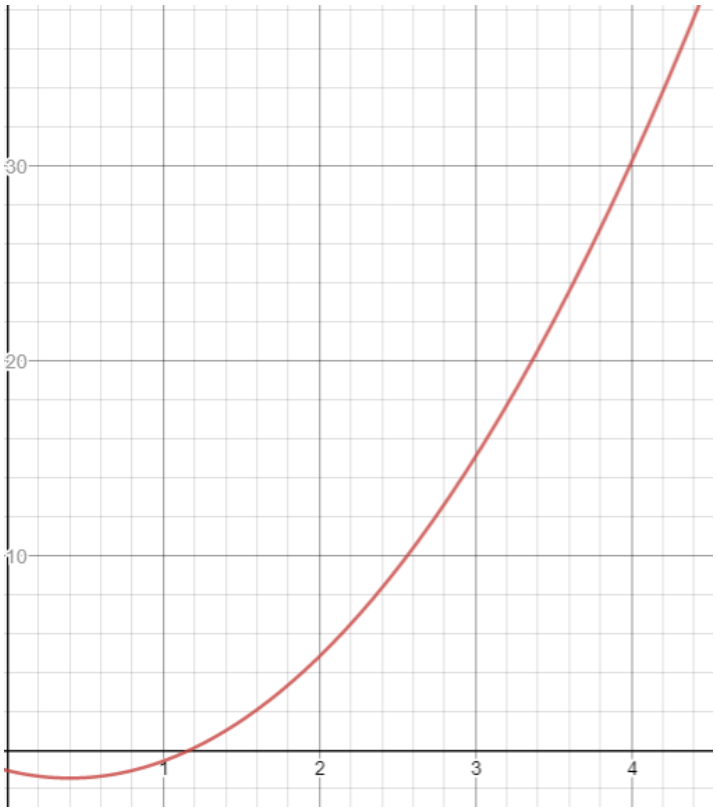


Figure 33 - **Graphical representation of equation 4, using desmos.com calculator**. The x-axis is itraconazole tissue concentration in $\mu g.mL^{-1}$ and the y-axis is “Bottom” value in %.

For 5-FU + itraconazole drug combination (Figure 36 A), first, “% Effect” remains constant, at a level of 59% of cell growth inhibition. Then, at minute 70 effect starts dropping abruptly. This drop can be explained with deeper analysis of Equation 3. 5-FU concentration influences “% Effect” through exponential function described by Equation 7, where x is 5-FU tissue concentration. According to this equation, at very high concentrations 5-FU tissue concentration influence on “% Effect” can be despised because f(x) will result in a very low value. Then, this value will be summed to 1 and divided to (“Top”-“Bottom”) values. When this concentration is reduced to a value lower than 0.5 μg.mL$^{-1}$, f(x) increases exponentially reducing “% Effect” abruptly. Figure 36 D shows 5-FU tissue concentration-time curve. Figure 34 is a graphical representation of Equation 7, for better understanding.

**Equation 7**

$$f(x) = \left(\frac{x}{0.28}\right)^{-2.62}$$

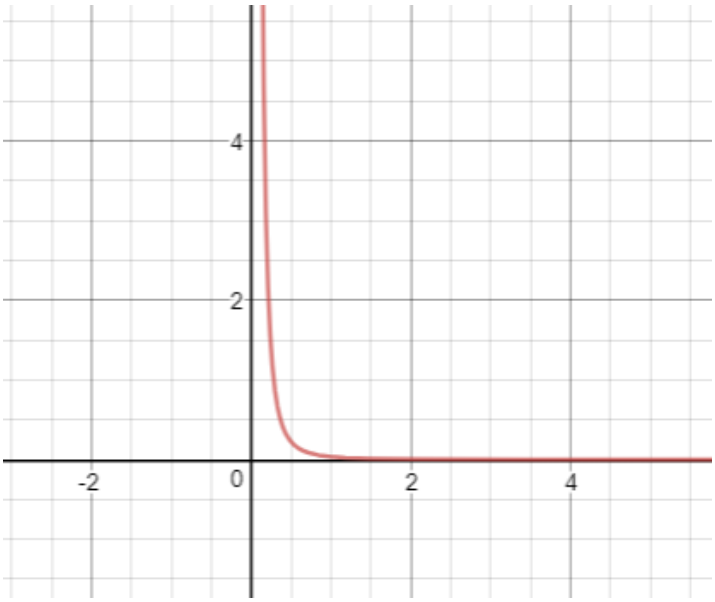


Figure 34 - **Graphical representation of Equation 7, using desmos.com calculator.**

When the drop in “% Effect” value starts, slight differences between effect-time curves start to be noticed. At this point, itraconazole tissue concentration plays the main role in the overall effect, since “% Effect” equals “Bottom” value (Equation 3), which is directly dependent on itraconazole tissue concentration. As stated above, if higher values of

itraconazole tissue concentration were considered, “% Effect” would be equally higher. This can be mathematically explained through Equation 5 analysis. Figure 35 is a graphical representation of Equation 5, where the x-axis is itraconazole tissue concentration and the y-axis is “Bottom” value. Since the highest itraconazole concentration value used in Equation 5 formulation was 4.2 $\mu g.mL^{-1}$ (6 µM), higher concentrations were not considered for graphical representation.

Itraconazole multiple dosing simulation was tried in the STELLA® simulation program, with the objective of increasing itraconazole tissue concentration, but limitations in the software's builtin functions did not allow the study.

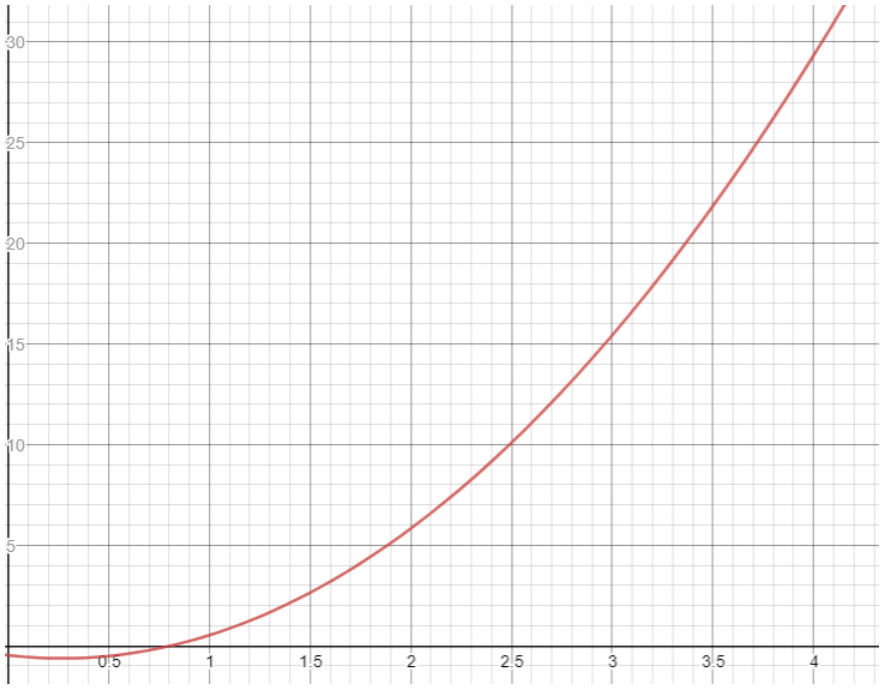


Figure 35 - **Graphical representation of Equation 5, using desmos.com calculator**. The x-axis is itraconazole tissue concentration in $\mu g.mL^{-1}$ and the y-axis is “Bottom” value in %.

While drug dose-response curve enables the establishment of a relationship between drug concentration and % of cell growth inhibition, this kind of approach enables the study of drug concentration-% of cell growth inhibition relationship over time. In other words, one can be elucidated about how long a drug will exert its maximum effect when administered at a certain dose until metabolization reduces drug concentration to a non-therapeutic level.

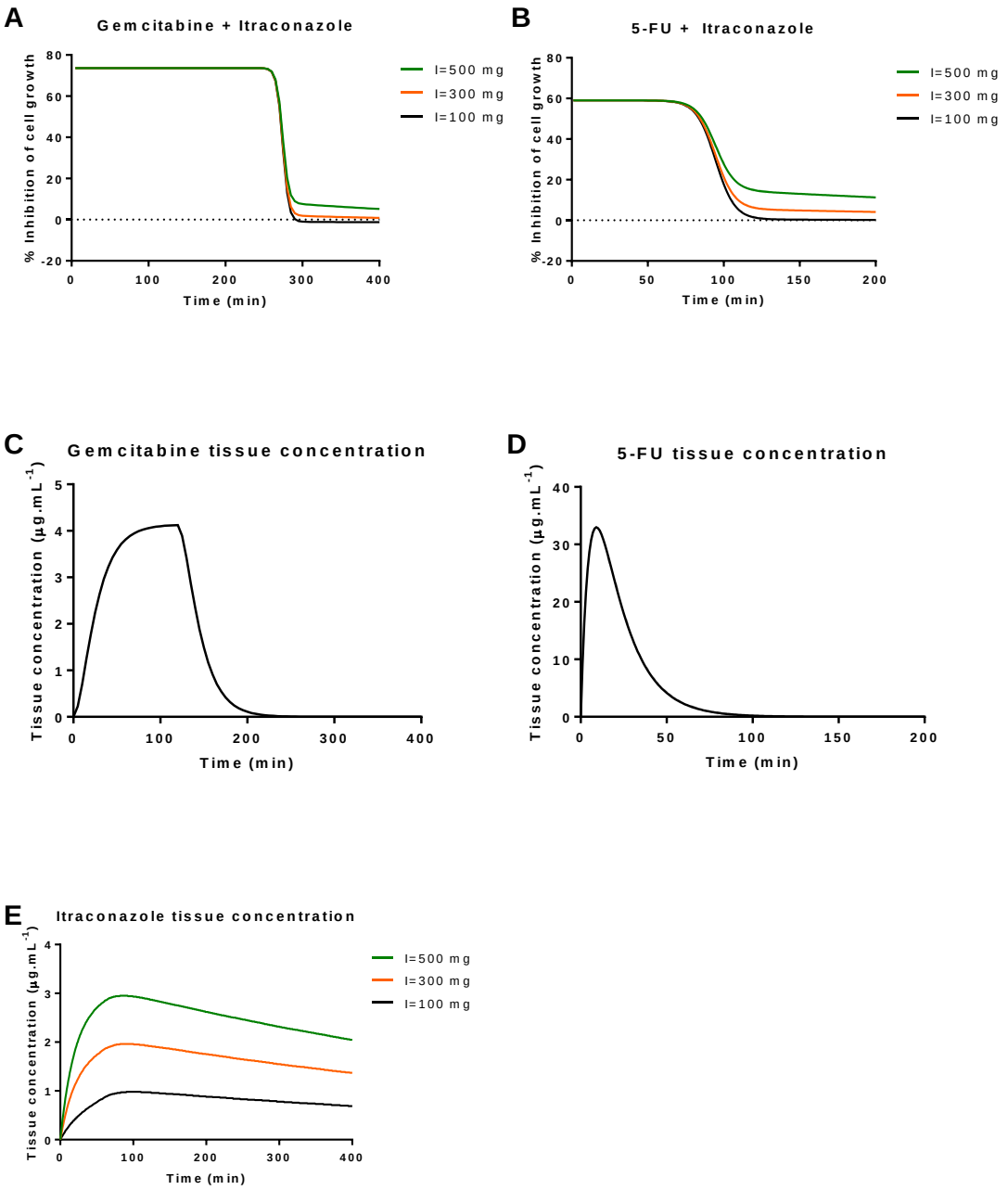


Figure 36 - **ACD + itraconazole combination STELLA simulation. A** and **B**: Effect curves for gemcitabine + itraconazole and 5-FU + itraconazole combinations, respectively. Three itraconazole doses were tested; **C** and **D**: Tissue concentration-time curves of gemcitabine and 5-FU, when intravenously administered at a dose of 1884 mg (infusion) and 900 mg (injection), respectively; **E**: Tissue concentration-time curve of itraconazole for three different doses of intravenous infusion.

## 4.4. Limitations in pharmacokinetics modeling

The work developed in this project was innovative and well succeeded. However, some difficulties were detected during the project, for example, the impossibility to make multiple dosing regimen (for iv infusion) in the STELLA® simulation program.

As mentioned in section 4.3.3., itraconazole concentration in the tissue compartment was not high enough to significantly influence the overall "% Effect". The idea of using multiple dosing regimen was to reach steady-state plasma concentration ($C_{ss}$), increasing itraconazole accumulation in tissue compartment, and thus, to predict the influence of itraconazole in % cell growth, in multiple dosing regimen. Thus, alternatives to the STELLA® simulation program were explored to overcome this problem, which included the use of Gastroplus™ simulation software and Microsoft Excel.

GastroPlus™ has a module that enables, through the upload of a drug's molecular structure, the prediction of several physicochemical and pharmacokinetic properties of that drug. With the input of those parameters, it is possible to run a simulation in GastroPlus™ simulation module and predict drug's plasma concentration profile for different administration routes and dosing regimens. Although the sophistication of the program, not all the parameter values predicted correctly represent real values. Thus, when available, experimental data is preferable for model construction.

In this project, an attempt to replicate experimental $C_p$-time data of itraconazole, in GastroPlus was made, but neither uploading itraconazole molecular structure nor inputting experimental parameters could replicate the concentration plasma profile reported in the literature. As shown in Figure 37, itraconazole $C_{max}$ predicted through this program, for 100 mg, 1 h iv infusion, is about 0.095 $\mu g.mL^{-1}$, while the equivalent value reported in the literature, for the same dosing regimen, is 3.9 $\mu g.mL^{-1}$.

GastroPlus™ is a complex software and it is not solely ruled by simple pharmacokinetics equations. To run a simulation in this program the input of a few parameters is needed. Apart from common parameters input as dose, dosage form, solubility and the pH at which it was measured, logP and pKa's (if any), it is also required knowledge about particle radius, particle density and diffusion coefficient. In the simulation presented in Figure 37, most of the parameters used were predicted through itraconazole structure upload. Therefore, even with the input of some experimental values, itraconazole $C_p$-time is quite different from the reported one. Thus, it was impossible to validate the model and multiple dosing regimen could not be evaluated.

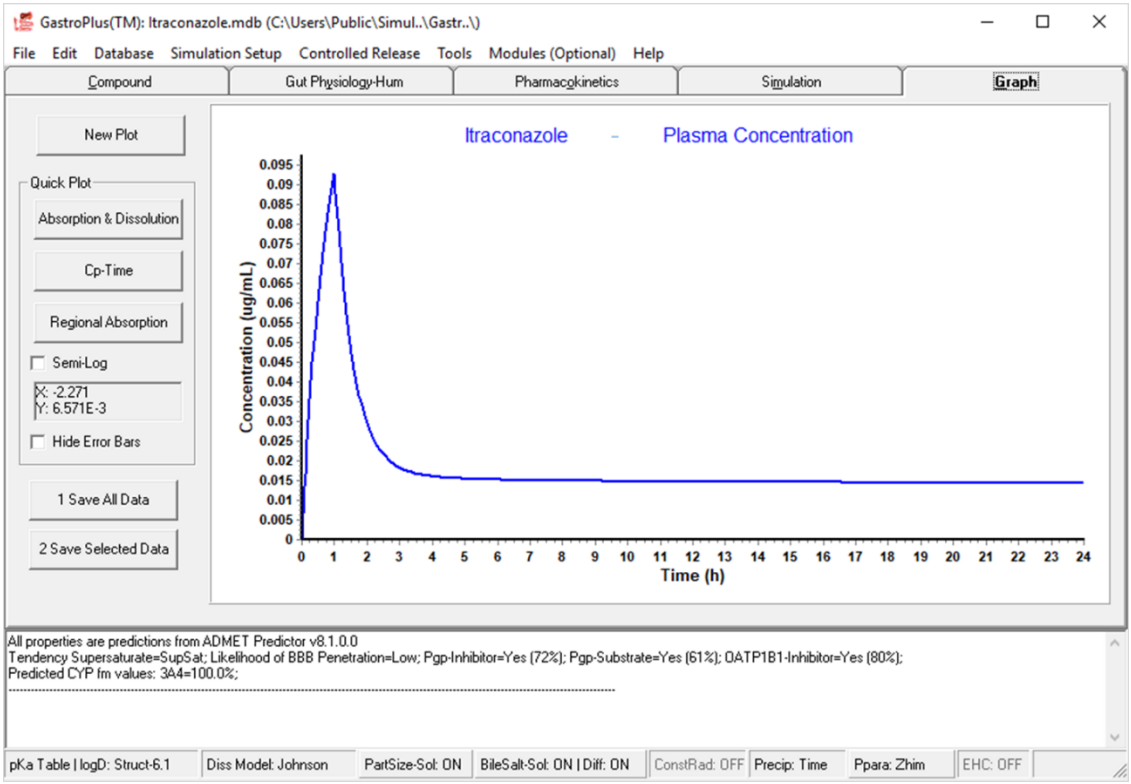


Figure 37 - **Itraconazole $C_p$-time profile predicted through GastroPlus™ simulation software.**

Given the circumstances, the study of itraconazole's multiple dosing regimen was done in Microsoft Excel. The literature $C_{ss}$ value was used as the itraconazole plasma concentration. The transfer rate constants $k_{12}$ and $k_{21}$ previously obtained through WinNonLin were used to simulate itraconazole flow between plasma and tissue compartment. Then the "Bottom" value was calculated at every time point, which is dependent on itraconazole tissue concentration on that specific time point (Equation 4 or Equation 5). Finally, "% Effect" was calculated through Equation 3. Figure 38 is the graphical representation of "% Effect" over time, for 5-FU + itraconazole combination, when itraconazole plasma concentration is maintained constant. For "Bottom" value calculation, Equation 5 was used since it is the equation that relates itraconazole tissue concentration with "Bottom" value in 5-FU + itraconazole combinations. Gemcitabine + itraconazole combination are not presented since the only difference is the equation used in "Bottom" determination, and the equivalent equation would demonstrate similar results.

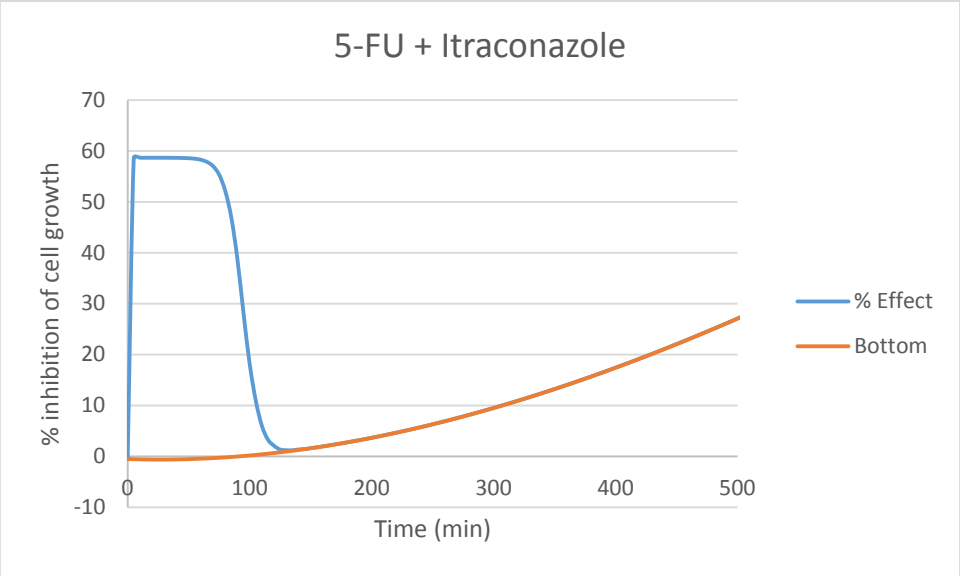


Figure 38 - **5-FU + itraconazole combination effect calculated through Microsoft Excel.** Itraconazole plasma concentration is maintained at a concentration reported as steady-state when 300 mg of itraconazole are administered at 24 h dosing interval. This enables itraconazole accumulation in the tissue compartment and subsequent increase in % inhibition of cell growth.

Figure 39 schematizes the general idea of the itraconazole multidose study using GastroPlus™.

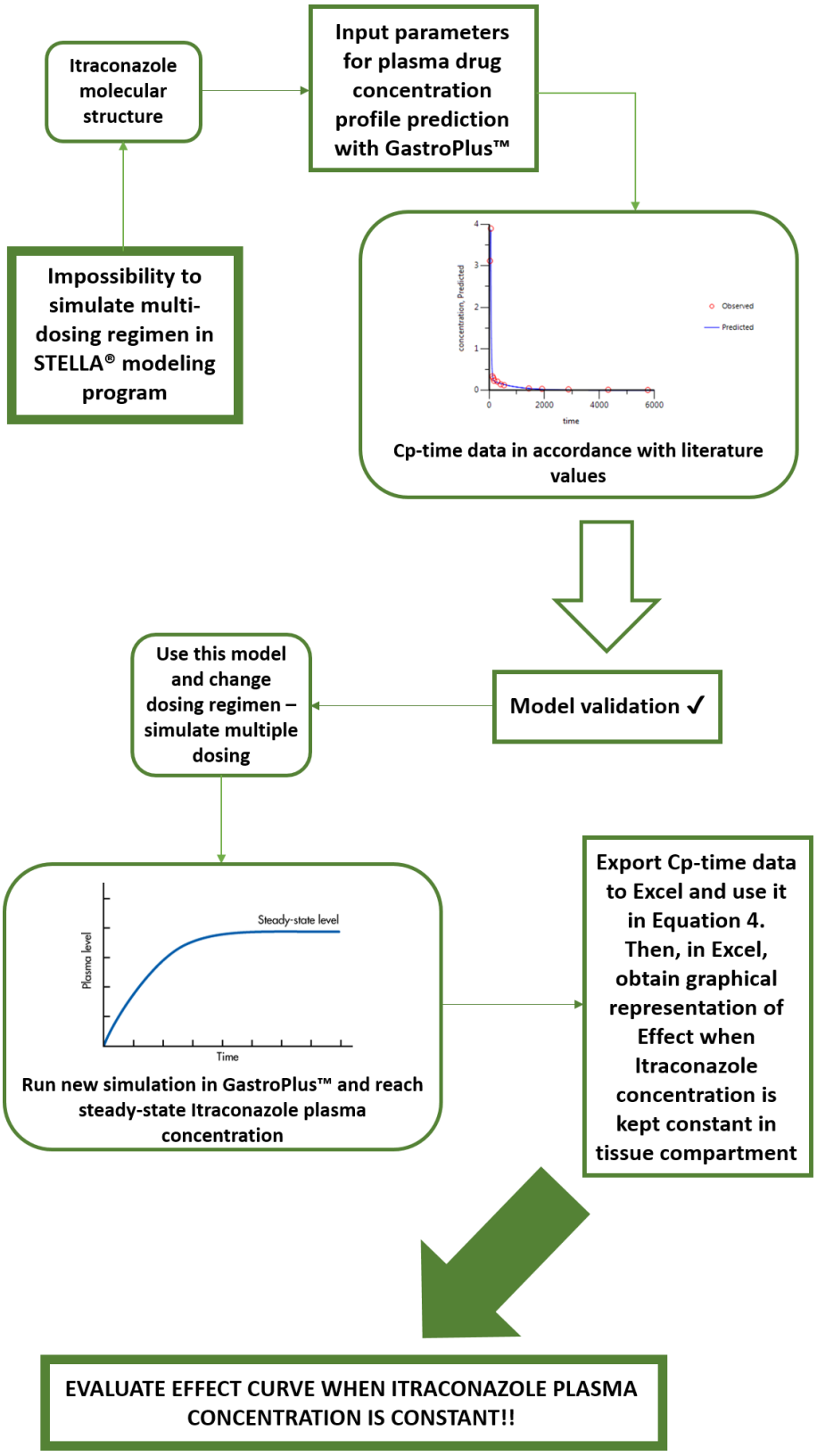


Figure 39 - **Schematic representation of itraconazole multi-dosing idealized study.** First, the impossibility to simulate multi-dosing iv infusion in STELLA® simulation software led to the use of GastroPlus™ modeling program. The idea started with itraconazole structure input for the prediction of mandatory parameters to run a simulation, complementing the information with experimental data. Then, if itraconazole plasma profile was coincident with experimental data, the model would be validated and dosing regimen could be changed to multiple dosing iv infusion. Running a new simulation, steady-state itraconazole plasma concentration would be obtained and data could be exported to Microsoft Excel for further treatment. Finally, effect could be evaluated when itraconazole plasma concentration is constant.

There are several potential benefits in employing *in silico* models in the process of drug R&D. However, reliable results require complex and data-intensive models. Furthermore, the use of complex models in drug development requires adequate resources and well-qualified researchers with a good understanding of the ADME data required to drive the models.

STELLA models developed in this work are simple but innovative. Ideally, parameters used in the model structure should be more consistent, but for a first idea of the general behavior of the drug combinations in human body the data used is quite appropriate. For example, starting with $C_p$-time data origin, the two-compartment model built for gemcitabine is reproducing drug disposition in a Chinese cancer patient, while the two-compartment model for Itraconazole is reproducing drug disposition in a healthy Dutch patient. Moreover, the tumor is assumed to behave like the tissues grouped into a tissue compartment but no such assumption was confirmed or validated. Nevertheless, this studies might be useful for comparative effect purposes and to provide mechanistic predictions of dosing regimens.

Keeping the simplicity of this models, small adjustments can be done in future experiments, like as:

- $C_p$-time data could be obtained from an associate Hospital, for example, ensuring that all the data comes from the same source;
- Ideally and if possible, rate transfer constant between tumor tissue and plasma, as well as tumor volume of distribution should be measured;
- Drug combinations could be tested in primary cancer cell lines corresponding to the cancer type in study, from where transfer rate constants and volume of distribution were determined.

# 5. CONCLUSIONS AND FUTURE PERSPECTIVES

At the end of this project, the defined goals were accomplished. Insight into GastroPlus™ and STELLA® modeling programs was achieved, *in vitro* experiments were done successfully and drug combination modeling was possible. Not all *in vitro* studies resulted in favorable data for further modeling but gladly itraconazole combinations showed workable results. Models were developed and drug combination effect was simulated in *in silico* human model. Itraconazole multiple-dosing iv infusion could not be studied through STELLA® or GastroPlus™ softwares but the most important calculations could be done in Microsoft Excel.

In summary, the results of the present study provide a new possible combination for lung and prostate cancer treatment and a new tool to quantify drug combinations effect, the area under the dose-response-time curve, or $AUC_{effect}$. Furthermore, the innovative idea developed in this work resides in an *in silico* study that enables the coupling of cell viability assay data with human drug disposition. Thus, it is now possible to study tissue drug concentration-% of cell growth inhibition relationship over time. In other words, one can be elucidated about how long a drug will exert its maximum effect when administered at a certain dose until metabolization reduces drug concentration to a non-therapeutic level.

For the future, other drug combinations can be tested in cell models, and % effect can be evaluated over time through similar models. However, some limitations and inconsistencies were found in the developed models, which may require some upgrading. Furthermore, future experiments may need different model construction, depending on the context in which they are inserted, but understanding how STELLA® modeling program works, one can “play” with the data and build the most convenient model in pharmacology.

# 6. BIBLIOGRAPHY

1. Dasgupta, A., *Therapeutic Drug Monitoring: Newer Drugs and Biomarkers*. Elsevier Science: 2012.

2. Jambhekar, S.; Breen, P. J., *Basic Pharmacokinetics*. Pharmaceutical Press: 2009.

3. Lees, P.; Cunningham, F. M.; Elliott, J., Principles of pharmacodynamics and their applications in veterinary pharmacology. *J. Vet. Pharmacol. Ther.* **2004,** *27* (6), 397-414.

4. Kaitin, K. I.; DiMasi, J. A., Pharmaceutical innovation in the 21st century: new drug approvals in the first decade, 2000-2009. *Clin. Pharmacol. Ther.* **2011,** *89* (2), 183-8.

5. DiMasi, J. A.; Feldman, L.; Seckler, A.; Wilson, A., Trends in risks associated with new drug development: success rates for investigational drugs. *Clin. Pharmacol. Ther.* **2010,** *87* (3), 272-7.

6. DiMasi, J. A.; Hansen, R. W.; Grabowski, H. G., The price of innovation: new estimates of drug development costs. *J. Health Econ.* **2003,** *22* (2), 151-85.

7. Shargel, L.; Wu-Pong, S.; Yu, A., *Applied Biopharmaceutics & Pharmacokinetics, Fifth Edition*. Mcgraw-hill: 2004.

8. Box, G. E. P.; Draper, N. R., *Empirical model-building and response surfaces*. Wiley: 1987.

9. Rooney, K. F.; Snoeck, E.; Watson, P. H., Modelling and simulation in clinical drug development. *Drug Discov. Today* **2001,** *6* (15), 802-806.

10. Gieschke, R.; Steimer, J. L., Pharmacometrics: modelling and simulation tools to improve decision making in clinical drug development. *Eur. J. Drug Metab. Pharmacokinet.* **2000,** *25* (1), 49-58.

11. Zhuang, X.; Lu, C., PBPK modeling and simulation in drug research and development. *Acta Pharm Sin B* **2016,** *6* (5), 430-440.

12. de Biasi, J.; Rekik, L., Four compartment mammillary model applied to the pharmacokinetics of a spiroarsorane administered orally to rabbits. *J. Biomed. Eng.* **1991,** *13* (5), 439-40.

13. Gabrielsson, J.; Weiner, D., *Pharmacokinetic and Pharmacodynamic Data Analysis: Concepts and Applications, Third Edition*. Taylor & Francis: 2001.

14. Paalzow, L. K., Torsten Teorell, the father of pharmacokinetics. *Ups. J. Med. Sci.* **1995,** *100* (1), 41-6.

15. Teorell, T., Kinetics of distribution of substances administered to the body, I: the extravascular modes of administration. *Archives internationales de pharmacodynamie et de therapie* **1937,** *57*, 205-225.

16. Sawada, Y.; Hanano, M.; Sugiyama, Y.; Iga, T., Prediction of the disposition of nine weakly acidic and six weakly basic drugs in humans from pharmacokinetic parameters in rats. *J. Pharmacokinet. Biopharm.* **1985,** *13* (5), 477-92.

17. Chapra, S., *Numerical Methods for Engineers*. 2014.

18. Otsuka, K.; Wagner, C.; Selen, A.; Dressman, J., Prediction of in-vivo pharmacokinetic profile for immediate and modified release oral dosage forms of furosemide using an in-vitro-in-silico-in-vivo approach. *J Pharm Pharmacol* **2015,** *67* (5), 651-65.

19. Vellonen, K. S.; Soini, E. M.; Del Amo, E. M.; Urtti, A., Prediction of Ocular Drug Distribution from Systemic Blood Circulation. *Mol Pharm* **2016,** *13* (9), 2906-11.

20. Hargrove, J. L.; Hulsey, M. G.; Summers, A. O., From genotype to phenotype: computer-based modeling of gene expression with STELLA II. *Biotechniques* **1993,** *15* (6), 1096-101.

21. Yu, L. X.; Amidon, G. L., A compartmental absorption and transit model for estimating oral drug absorption. *Int J Pharm* **1999,** *186* (2), 119-25.

22. DeVita, V. T., Jr., Single agent versus combination chemotherapy. *CA Cancer J. Clin.* **1975,** *25* (3), 152-8.

23. Perelson, A. S.; Essunger, P.; Cao, Y.; Vesanen, M.; Hurley, A.; Saksela, K.; Markowitz, M.; Ho, D. D., Decay characteristics of HIV-1-infected compartments during combination therapy. *Nature* **1997,** *387* (6629), 188-91.

24. Armand, J. P.; Dormont, J.; Schwebig, A., [Recommendations for the study of drug combination therapy for the treatment of AIDS and cancer. Round Table No 7 at Giens XIII]. *Therapie* **1998,** *53* (4), 385-9.

25. Ai, N.; Fan, X.; Ekins, S., In silico methods for predicting drug-drug interactions with cytochrome P-450s, transporters and beyond. *Adv Drug Deliv Rev* **2015,** *86*, 46-60.

26. Tallarida, R. J., An overview of drug combination analysis with isobolograms. *J. Pharmacol. Exp. Ther.* **2006,** *319* (1), 1-7.

27. Chou, T. C., Drug combination studies and their synergy quantification using the Chou-Talalay method. *Cancer Res.* **2010,** *70* (2), 440-6.

28. Skeel, R. T.; Khleif, S. N., *Handbook of Cancer Chemotherapy*. Lippincott Williams & Wilkins: 2011.

29. Moysan, E.; Bastiat, G.; Benoit, J. P., Gemcitabine versus Modified Gemcitabine: a review of several promising chemical modifications. *Mol Pharm* **2013,** *10* (2), 430-44.

30. Liu, F.; Gore, A. J.; Wilson, J. L.; Korc, M., DUSP1 is a novel target for enhancing pancreatic cancer cell sensitivity to gemcitabine. *PLoS One* **2014,** *9* (1), e84982.

31. Hu, G.; Li, F.; Ouyang, K.; Xie, F.; Tang, X.; Wang, K.; Han, S.; Jiang, Z.; Zhu, M.; Wen, D.; Qin, X.; Zhang, L., Intrinsic gemcitabine resistance in a novel pancreatic cancer cell line is associated with cancer stem cell-like phenotype. *Int. J. Oncol.* **2012,** *40* (3), 798-806.

32. Karampelas, T.; Argyros, O.; Sayyad, N.; Spyridaki, K.; Pappas, C.; Morgan, K.; Kolios, G.; Millar, R. P.; Liapakis, G.; Tzakos, A. G.; Fokas, D.; Tamvakopoulos, C., GnRH-Gemcitabine conjugates for the treatment of androgen-independent prostate cancer: pharmacokinetic enhancements combined with targeted drug delivery. *Bioconjug. Chem.* **2014,** *25* (4), 813-23.

33. Dasari, M.; Acharya, A. P.; Kim, D.; Lee, S.; Lee, S.; Rhea, J.; Molinaro, R.; Murthy, N., H-gemcitabine: a new gemcitabine prodrug for treating cancer. *Bioconjug. Chem.* **2013,** *24* (1), 4-8.

34. Ryu, J. S.; Raucher, D., Anti-tumor efficacy of a therapeutic peptide based on thermo-responsive elastin-like polypeptide in combination with gemcitabine. *Cancer Lett* **2014,** *348* (1-2), 177-84.

35. Jin, S. F.; Fan, Z. K.; Pan, L.; Jin, L. M., Gemcitabine-based combination therapy compared with gemcitabine alone for advanced pancreatic cancer: a meta-analysis of nine randomized controlled trials. *Hepatobiliary Pancreat. Dis. Int.* **2017,** *16* (3), 236-244.

36. Longley, D. B.; Harkin, D. P.; Johnston, P. G., 5-fluorouracil: mechanisms of action and clinical strategies. *Nat. Rev. Cancer* **2003,** *3* (5), 330-8.

37. Johnston, P. G.; Kaye, S., Capecitabine: a novel agent for the treatment of solid tumors. *Anticancer Drugs* **2001,** *12* (8), 639-46.

38. Diasio, R. B.; Harris, B. E., Clinical pharmacology of 5-fluorouracil. *Clin. Pharmacokinet.* **1989,** *16* (4), 215-37.

39. Wohlhueter, R. M.; McIvor, R. S.; Plagemann, P. G., Facilitated transport of uracil and 5-fluorouracil, and permeation of orotic acid into cultured mammalian cells. *J. Cell. Physiol.* **1980,** *104* (3), 309-19.

40. Gorlick, R.; Bertino, J. R., *Clinical Pharmacology and Resistance to Dihydrofolate Reductase Inhibitors. In: Jackman A.L. (eds) Antifolate Drugs in Cancer Therapy. Cancer Drug Discovery and Development.* Humana Press, Totowa, NJ: 1999.

41. Pantziarka, P.; Bouche, G.; Meheus, L.; Sukhatme, V.; Sukhatme, V. P.; Vikas, P., The Repurposing Drugs in Oncology (ReDO) Project. *Ecancermedicalscience* **2014,** *8*, 442.

42. Sleire, L.; Forde, H. E.; Netland, I. A.; Leiss, L.; Skeie, B. S.; Enger, P. O., Drug repurposing in cancer. *Pharmacol. Res.* **2017,** *124*, 74-91.

43. Bertolini, F.; Sukhatme, V. P.; Bouche, G., Drug repurposing in oncology--patient and health systems opportunities. *Nat. Rev. Clin. Oncol.* **2015,** *12* (12), 732-42.

44. Belpomme, D.; Gauthier, S.; Pujade-Lauraine, E.; Facchini, T.; Goudier, M. J.; Krakowski, I.; Netter-Pinon, G.; Frenay, M.; Gousset, C.; Marie, F. N.; Benmiloud, M.; Sturtz, F., Verapamil increases the survival of patients with anthracycline-resistant metastatic breast carcinoma. *Ann. Oncol.* **2000,** *11* (11), 1471-6.

45. Rudin, C. M.; Brahmer, J. R.; Juergens, R. A.; Hann, C. L.; Ettinger, D. S.; Sebree, R.; Smith, R.; Aftab, B. T.; Huang, P.; Liu, J. O., Phase 2 study of pemetrexed and itraconazole as second-line therapy for metastatic nonsquamous non-small-cell lung cancer. *J. Thorac. Oncol.* **2013,** *8* (5), 619-23.

46. Dirix, L.; Swaisland, H.; Verheul, H. M.; Rottey, S.; Leunen, K.; Jerusalem, G.; Rolfo, C.; Nielsen, D.; Molife, L. R.; Kristeleit, R.; Vos-Geelen, J.; Mau-Sorensen, M.; Soetekouw, P.; van Herpen, C.; Fielding, A.; So, K.; Bannister, W.; Plummer, R., Effect of Itraconazole and Rifampin on the Pharmacokinetics of Olaparib in Patients With Advanced Solid Tumors: Results of Two Phase I Open-label Studies. *Clinical therapeutics* **2016,** *38* (10), 2286-2299.

47. Antonarakis, E. S.; Heath, E. I.; Smith, D. C.; Rathkopf, D.; Blackford, A. L.; Danila, D. C.; King, S.; Frost, A.; Ajiboye, A. S.; Zhao, M.; Mendonca, J.; Kachhap, S. K.; Rudek, M. A.; Carducci, M. A., Repurposing itraconazole as a treatment for advanced prostate cancer: a noncomparative randomized phase II trial in men with metastatic castration-resistant prostate cancer. *The oncologist* **2013,** *18* (2), 163-73.

48. Hendrick, A. M.; Harris, A. L.; Cantwell, B. M., Verapamil with mitoxantrone for advanced ovarian cancer: a negative phase II trial. *Ann. Oncol.* **1991,** *2* (1), 71-2.

49. Karsy, M.; Hoang, N.; Barth, T.; Burt, L.; Dunson, W.; Gillespie, D. L.; Jensen, R. L., Combined Hydroxyurea and Verapamil in the Clinical Treatment of Refractory Meningioma: Human and Orthotopic Xenograft Studies. *World Neurosurg.* **2016,** *86*, 210-9.

50. Panda, N. K., Itraconazole - a potent antifungal drug. *Indian J Otolaryngol Head Neck Surg* **1997,** *49* (3), 293-4.

51. Vanden Bossche, H.; Marichal, P.; Gorrens, J.; Coene, M. C., Biochemical basis for the activity and selectivity of oral antifungal drugs. *Br. J. Clin. Pract. Suppl.* **1990,** *71*, 41-6.

52. Berg, J. M.; Tymoczko, J. L.; Stryer, L., *Biochemistry*. W.H. Freeman: 2002.

53. Chong, C. R.; Xu, J.; Lu, J.; Bhat, S.; Sullivan, D. J., Jr.; Liu, J. O., Inhibition of angiogenesis by the antifungal drug itraconazole. *ACS Chem. Biol.* **2007,** *2* (4), 263-70.

54. Kim, J.; Tang, J. Y.; Gong, R.; Kim, J.; Lee, J. J.; Clemons, K. V.; Chong, C. R.; Chang, K. S.; Fereshteh, M.; Gardner, D.; Reya, T.; Liu, J. O.; Epstein, E. H.; Stevens,

D. A.; Beachy, P. A., Itraconazole, a commonly used antifungal that inhibits Hedgehog pathway activity and cancer growth. *Cancer Cell* **2010,** *17* (4), 388-99.

55. Kim, J.; Aftab, B. T.; Tang, J. Y.; Kim, D.; Lee, A. H.; Rezaee, M.; Kim, J.; Chen, B.; King, E. M.; Borodovsky, A.; Riggins, G. J.; Epstein, E. H., Jr.; Beachy, P. A.; Rudin, C. M., Itraconazole and arsenic trioxide inhibit Hedgehog pathway activation and tumor growth associated with acquired resistance to smoothened antagonists. *Cancer Cell* **2013,** *23* (1), 23-34.

56. Nacev, B. A.; Grassi, P.; Dell, A.; Haslam, S. M.; Liu, J. O., The antifungal drug itraconazole inhibits vascular endothelial growth factor receptor 2 (VEGFR2) glycosylation, trafficking, and signaling in endothelial cells. *J. Biol. Chem.* **2011,** *286* (51), 44045-56.

57. Liu, R.; Li, J.; Zhang, T.; Zou, L.; Chen, Y.; Wang, K.; Lei, Y.; Yuan, K.; Li, Y.; Lan, J.; Cheng, L.; Xie, N.; Xiang, R.; Nice, E. C.; Huang, C.; Wei, Y., Itraconazole suppresses the growth of glioblastoma through induction of autophagy: involvement of abnormal cholesterol trafficking. *Autophagy* **2014,** *10* (7), 1241-55.

58. Wang, E. J.; Lew, K.; Casciano, C. N.; Clement, R. P.; Johnson, W. W., Interaction of common azole antifungals with P glycoprotein. *Antimicrob. Agents Chemother.* **2002,** *46* (1), 160-5.

59. Xu, J.; Dang, Y.; Ren, Y. R.; Liu, J. O., Cholesterol trafficking is required for mTOR activation in endothelial cells. *Proc. Natl. Acad. Sci. U. S. A.* **2010,** *107* (10), 4764-9.

60. Stecca, B.; Ruiz, I. A. A., Context-dependent regulation of the GLI code in cancer by HEDGEHOG and non-HEDGEHOG signals. *J. Mol. Cell. Biol.* **2010,** *2* (2), 84-95.

61. Whitehouse, P. J.; Price, D. L.; Clark, A. W.; Coyle, J. T.; DeLong, M. R., Alzheimer disease: evidence for selective loss of cholinergic neurons in the nucleus basalis. *Ann. Neurol.* **1981,** *10* (2), 122-6.

62. Davis, K. L.; Thal, L. J.; Gamzu, E. R.; Davis, C. S.; Woolson, R. F.; Gracon, S. I.; Drachman, D. A.; Schneider, L. S.; Whitehouse, P. J.; Hoover, T. M.; et al., A double-blind, placebo-controlled multicenter study of tacrine for Alzheimer's disease. The Tacrine Collaborative Study Group. *N. Engl. J. Med.* **1992,** *327* (18), 1253-9.

63. Crismon, M. L., Tacrine: first drug approved for Alzheimer's disease. *Ann. Pharmacother.* **1994,** *28* (6), 744-51.

64. Watkins, P. B.; Zimmerman, H. J.; Knapp, M. J.; Gracon, S. I.; Lewis, K. W., Hepatotoxic effects of tacrine administration in patients with Alzheimer's disease. *JAMA* **1994,** *271* (13), 992-8.

65. Spaldin, V.; Madden, S.; Pool, W. F.; Woolf, T. F.; Park, B. K., The effect of enzyme inhibition on the metabolism and activation of tacrine by human liver microsomes. *Br J Clin Pharmacol* **1994,** *38* (1), 15-22.

66. O'Brien, J. T.; Eagger, S.; Levy, R., Effects of tetrahydroaminoacridine on liver function in patients with Alzheimer's disease. *Age Ageing* **1991,** *20* (2), 129-31.

67. Berson, A.; Renault, S.; Letteron, P.; Robin, M. A.; Fromenty, B.; Fau, D.; Le Bot, M. A.; Riche, C.; Durand-Schneider, A. M.; Feldmann, G.; Pessayre, D., Uncoupling of rat and human mitochondria: a possible explanation for tacrine-induced liver dysfunction. *Gastroenterology* **1996,** *110* (6), 1878-90.

68. Freudenreich, C. H.; Kreuzer, K. N., Localization of an aminoacridine antitumor agent in a type II topoisomerase-DNA complex. *Proc. Natl. Acad. Sci. U. S. A.* **1994,** *91* (23), 11007-11.

69. Mansouri, A.; Haouzi, D.; Descatoire, V.; Demeilliers, C.; Sutton, A.; Vadrot, N.; Fromenty, B.; Feldmann, G.; Pessayre, D.; Berson, A., Tacrine inhibits topoisomerases and DNA synthesis to cause mitochondrial DNA depletion and apoptosis in mouse liver. *Hepatology* **2003,** *38* (3), 715-25.

70. Haeusler, G., The effect of verapamil on the contractility of smooth muscle and on excitation-secretion coupling in adrenergic nerve terminals. *Angiologica* **1971,** *8* (3-5), 156-60.

71. Katz, A. M.; Hager, W. D.; Messineo, F. C.; Pappano, A. J., Cellular actions and pharmacology of calcium-channel blockers. *Am. J. Emerg. Med.* **1985,** *3* (6 Suppl), 1-9.

72. Singh, B. N., A fourth class of anti-dysrhythmic action? Effect of verapamil on ouabain toxicity, on atrial and ventricular intracellular potentials, and on other features of cardiac function. *Cardiovasc. Res.* **1972,** *6* (2), 109-19.

73. Singh, B. N.; Ellrodt, G.; Peter, C. T., Verapamil: a review of its pharmacological properties and therapeutic use. *Drugs* **1978,** *15* (3), 169-97.

74. Hamann, S. R.; Blouin, R. A.; McAllister, R. G., Jr., Clinical pharmacokinetics of verapamil. *Clin. Pharmacokinet.* **1984,** *9* (1), 26-41.

75. Verapamil Dosage. https://www.drugs.com/dosage/verapamil.html.

76. McAllister, R. G., Jr.; Kirsten, E. B., The pharmacology of verapamil. IV. Kinetic and dynamic effects after single intravenous and oral doses. *Clin. Pharmacol. Ther.* **1982,** *31* (4), 418-26.

77. Biedler, J. L.; Riehm, H., Cellular resistance to actinomycin D in Chinese hamster cells in vitro: cross-resistance, radioautographic, and cytogenetic studies. *Cancer Res.* **1970,** *30* (4), 1174-84.

78. Gros, P.; Ben Neriah, Y. B.; Croop, J. M.; Housman, D. E., Isolation and expression of a complementary DNA that confers multidrug resistance. *Nature* **1986,** *323* (6090), 728-31.

79. Li, J.; Pan, Y. Y.; Zhang, Y., Synergistic interaction between sorafenib and gemcitabine in EGFR-TKI-sensitive and EGFR-TKI-resistant human lung cancer cell lines. *Oncol. Lett.* **2013,** *5* (2), 440-446.

80. Li, J.; Wang, S.; Su, Z. F.; Yuan, Y., Synergistic effects of sorafenib in combination with gemcitabine or pemetrexed in lung cancer cell lines with K-ras mutations. *Contemp Oncol (Pozn)* **2016,** *20* (1), 33-8.

81. Ozturk, O. H.; Bozcuk, H.; Burgucu, D.; Ekinci, D.; Ozdogan, M.; Akca, S.; Yildiz, M., Cisplatin cytotoxicity is enhanced with zoledronic acid in A549 lung cancer cell line: preliminary results of an in vitro study. *Cell Biol. Int.* **2007,** *31* (9), 1069-71.

82. Zhang, Y. X.; Yuan, Y. Q.; Zhang, X. Q.; Huang, D. L.; Wei, Y. Y.; Yang, J. G., HMGB1-mediated autophagy confers resistance to gemcitabine in hormone-independent prostate cancer cells. *Oncol. Lett.* **2017,** *14* (5), 6285-6290.

83. Muenchen, H. J.; Quigley, M. M.; Pilat, M. J.; Lehr, J. E.; Brumfield, S. K.; Mahoney, M.; Pienta, K. J., The study of gemcitabine in combination with other chemotherapeutic agents as an effective treatment for prostate cancer. *Anticancer Res.* **2000,** *20* (2A), 735-40.

84. Yang, W.; Soares, J.; Greninger, P.; Edelman, E. J.; Lightfoot, H.; Forbes, S.; Bindal, N.; Beare, D.; Smith, J. A.; Thompson, I. R.; Ramaswamy, S.; Futreal, P. A.; Haber, D. A.; Stratton, M. R.; Benes, C.; McDermott, U.; Garnett, M. J., Genomics of Drug Sensitivity in Cancer (GDSC): a resource for therapeutic biomarker discovery in cancer cells. *Nucleic Acids Res.* **2013,** *41* (Database issue), D955-61.

85. Pan, X.; Zhang, X.; Sun, H.; Zhang, J.; Yan, M.; Zhang, H., Autophagy inhibition promotes 5-fluorouracil-induced apoptosis by stimulating ROS formation in human non-small cell lung cancer A549 cells. *PLoS One* **2013,** *8* (2), e56679.

86. Zhao, X.; Dong, W.; Gao, Y.; Shin, D. S.; Ye, Q.; Su, L.; Jiang, F.; Zhao, B.; Miao, J., Novel indolyl-chalcone derivatives inhibit A549 lung cancer cell growth through activating Nrf-2/HO-1 and inducing apoptosis in vitro and in vivo. *Sci. Rep.* **2017,** *7* (1), 3919.

87. Serova, M.; Bieche, I.; Sablin, M. P.; Pronk, G. J.; Vidaud, M.; Cvitkovic, E.; Faivre, S.; Raymond, E., Single agent and combination studies of pralatrexate and molecular correlates of sensitivity. *Br. J. Cancer* **2011,** *104* (2), 272-80.

88. Buur, A.; Bundgaard, H.; Falch, E., Prodrugs of 5-fluorouracil. IV. Hydrolysis kinetics, bioactivation and physicochemical properties of various N-acyloxymethyl derivatives of 5-fluorouracil. *Int. J. Pharm.* **1985,** *24* (1), 43-60.

89. Vogelpoel, H.; Welink, J.; Amidon, G. L.; Junginger, H. E.; Midha, K. K.; Moller, H.; Olling, M.; Shah, V. P.; Barends, D. M., Biowaiver monographs for immediate release solid oral dosage forms based on biopharmaceutics classification system (BCS) literature data: verapamil hydrochloride, propranolol hydrochloride, and atenolol. *J. Pharm. Sci.* **2004,** *93* (8), 1945-56.

90. Heykants, J.; Van Peer, A.; Van de Velde, V.; Van Rooy, P.; Meuldermans, W.; Lavrijsen, K.; Woestenborghs, R.; Van Cutsem, J.; Cauwenbergh, G., The clinical pharmacokinetics of itraconazole: an overview. *Mycoses* **1989,** *32 Suppl 1*, 67-87.

91. Yu, H.; Li, W. M.; Kan, K. K.; Ho, J. M.; Carlier, P. R.; Pang, Y. P.; Gu, Z. M.; Zhong, Z.; Chan, K.; Wang, Y. T.; Han, Y. F., The physicochemical properties and the in vivo AChE inhibition of two potential anti-Alzheimer agents, bis(12)-hupyridone and bis(7)-tacrine. *J Pharm Biomed Anal* **2008,** *46* (1), 75-81.

92. Yilmaz, B.; Kadioglu, Y. Y.; Aksoy, Y., Investigation of the pharmacokinetics of gemcitabine and 2',2'-difluorodeoxyuridine in human plasma by liquid chromatography. *Anal Biochem* **2004,** *332* (2), 234-7.

93. Madden, S.; Spaldin, V.; Park, B. K., Clinical pharmacokinetics of tacrine. *Clin. Pharmacokinet.* **1995,** *28* (6), 449-57.

94. Miura, K.; Kinouchi, M.; Ishida, K.; Fujibuchi, W.; Naitoh, T.; Ogawa, H.; Ando, T.; Yazaki, N.; Watanabe, K.; Haneda, S.; Shibata, C.; Sasaki, I., 5-fu metabolism in cancer and orally-administrable 5-fu drugs. *Cancers (Basel)* **2010,** *2* (3), 1717-30.

95. Kobayashi, Y.; Ohshiro, N.; Sakai, R.; Ohbayashi, M.; Kohyama, N.; Yamamoto, T., Transport mechanism and substrate specificity of human organic anion transporter 2 (hOat2 [SLC22A7]). *J Pharm Pharmacol* **2005,** *57* (5), 573-8.

96. Tsujie, M.; Nakamori, S.; Nakahira, S.; Takahashi, Y.; Hayashi, N.; Okami, J.; Nagano, H.; Dono, K.; Umeshita, K.; Sakon, M.; Monden, M., Human equilibrative nucleoside transporter 1, as a predictor of 5-fluorouracil resistance in human pancreatic cancer. *Anticancer Res.* **2007,** *27* (4B), 2241-9.

97. Ritzel, M. W.; Ng, A. M.; Yao, S. Y.; Graham, K.; Loewen, S. K.; Smith, K. M.; Ritzel, R. G.; Mowles, D. A.; Carpenter, P.; Chen, X. Z.; Karpinski, E.; Hyde, R. J.; Baldwin, S. A.; Cass, C. E.; Young, J. D., Molecular identification and characterization of novel human and mouse concentrative Na+-nucleoside cotransporter proteins (hCNT3 and mCNT3) broadly selective for purine and pyrimidine nucleosides (system cib). *J. Biol. Chem.* **2001,** *276* (4), 2914-27.

98. Mackey, J. R.; Mani, R. S.; Selner, M.; Mowles, D.; Young, J. D.; Belt, J. A.; Crawford, C. R.; Cass, C. E., Functional nucleoside transporters are required for gemcitabine influx and manifestation of toxicity in cancer cell lines. *Cancer Res.* **1998,** *58* (19), 4349-57.

99. Mackey, J. R.; Yao, S. Y.; Smith, K. M.; Karpinski, E.; Baldwin, S. A.; Cass, C. E.; Young, J. D., Gemcitabine transport in xenopus oocytes expressing recombinant plasma membrane mammalian nucleoside transporters. *J. Natl. Cancer Inst.* **1999,** *91* (21), 1876-81.

100. Govindarajan, R.; Leung, G. P.; Zhou, M.; Tse, C. M.; Wang, J.; Unadkat, J. D., Facilitated mitochondrial import of antiviral and anticancer nucleoside drugs by human equilibrative nucleoside transporter-3. *Am. J. Physiol. Gastrointest. Liver Physiol.* **2009,** *296* (4), G910-22.

101. Bergman, A. M.; Pinedo, H. M.; Talianidis, I.; Veerman, G.; Loves, W. J.; van der Wilt, C. L.; Peters, G. J., Increased sensitivity to gemcitabine of P-glycoprotein and multidrug resistance-associated protein-overexpressing human cancer cell lines. *Br. J. Cancer* **2003,** *88* (12), 1963-70.

102. Hopper-Borge, E.; Xu, X.; Shen, T.; Shi, Z.; Chen, Z. S.; Kruh, G. D., Human multidrug resistance protein 7 (ABCC10) is a resistance factor for nucleoside analogues and epothilone B. *Cancer Res.* **2009,** *69* (1), 178-84.

103. Imbert, F.; Jardin, M.; Fernandez, C.; Gantier, J. C.; Dromer, F.; Baron, G.; Mentre, F.; Van Beijsterveldt, L.; Singlas, E.; Gimenez, F., Effect of efflux inhibition on brain uptake of itraconazole in mice infected with Cryptococcus neoformans. *Drug Metab Dispos* **2003,** *31* (3), 319-25.

104. Mohamed, L. A.; Kaddoumi, A., Tacrine sinusoidal uptake and biliary excretion in sandwich-cultured primary rat hepatocytes. *J. Pharm. Pharm. Sci.* **2014,** *17* (3), 427-38.

105. De Beule, K.; Van Gestel, J., Pharmacology of itraconazole. *Drugs* **2001,** *61 Suppl 1*, 27-37.

106. Mouton, J. W.; van Peer, A.; de Beule, K.; Van Vliet, A.; Donnelly, J. P.; Soons, P. A., Pharmacokinetics of itraconazole and hydroxyitraconazole in healthy subjects after single and multiple doses of a novel formulation. *Antimicrob. Agents Chemother.* **2006,** *50* (12), 4096-102.

107. Milroy, R., A randomised clinical study of verapamil in addition to combination chemotherapy in small cell lung cancer. West of Scotland Lung Cancer Research Group, and the Aberdeen Oncology Group. *Br. J. Cancer* **1993,** *68* (4), 813-8.

108. Wang, L. R.; Huang, M. Z.; Xu, N.; Shentu, J. Z.; Liu, J.; Cai, J., Pharmacokinetics of gemcitabine in Chinese patients with non-small-cell lung cancer. *J Zhejiang Univ Sci B* **2005,** *6* (5), 446-50.

109. Heggie, G. D.; Sommadossi, J. P.; Cross, D. S.; Huster, W. J.; Diasio, R. B., Clinical pharmacokinetics of 5-fluorouracil and its metabolites in plasma, urine, and bile. *Cancer Res.* **1987,** *47* (8), 2203-6.

110. Soria, I.; Myhre, P.; Horton, V.; Ellefson, P.; McCarville, S.; Schmitt, K.; Owens, M., Effect of food on the pharmacokinetics and bioavailability of oral imiquimod relative to a subcutaneous dose. *Int. J. Clin. Pharmacol. Ther.* **2000,** *38* (10), 476-81.

111. Hoskin, P. J.; Hanks, G. W.; Aherne, G. W.; Chapman, D.; Littleton, P.; Filshie, J., The bioavailability and pharmacokinetics of morphine after intravenous, oral and buccal administration in healthy volunteers. *Br J Clin Pharmacol* **1989,** *27* (4), 499-505.

112. Nath, R. P.; Upton, R. A.; Everhart, E. T.; Cheung, P.; Shwonek, P.; Jones, R. T.; Mendelson, J. E., Buprenorphine pharmacokinetics: relative bioavailability of sublingual tablet and liquid formulations. *J. Clin. Pharmacol.* **1999,** *39* (6), 619-23.

113. Ince, P.; Appleton, D. R.; Finney, K. J.; Sunter, J. P.; Watson, A. J., Verapamil increases the sensitivity of primary human colorectal carcinoma tissue to vincristine. *Br. J. Cancer* **1986,** *53* (1), 137-9.

114. Merry, S.; Fetherston, C. A.; Kaye, S. B.; Freshney, R. I.; Plumb, J. A., Resistance of human glioma to adriamycin in vitro: the role of membrane transport and its circumvention with verapamil. *Br. J. Cancer* **1986,** *53* (1), 129-35.

115. Morrow, M.; Wait, R. B.; Rosenthal, R. A.; Gamelli, R. L., Verapamil enhances antitumor activity without increasing myeloid toxicity. *Surgery* **1987,** *101* (1), 63-8.

116. Tsuruo, T.; Iida, H.; Tsukagoshi, S.; Sakurai, Y., Overcoming of vincristine resistance in P388 leukemia in vivo and in vitro through enhanced cytotoxicity of vincristine and vinblastine by verapamil. *Cancer Res.* **1981,** *41* (5), 1967-72.

117. Ambudkar, S. V.; Dey, S.; Hrycyna, C. A.; Ramachandra, M.; Pastan, I.; Gottesman, M. M., Biochemical, cellular, and pharmacological aspects of the multidrug transporter. *Annu. Rev. Pharmacol. Toxicol.* **1999,** *39*, 361-98.

118. Wang, F.; Zhang, D.; Zhang, Q.; Chen, Y.; Zheng, D.; Hao, L.; Duan, C.; Jia, L.; Liu, G.; Liu, Y., Synergistic effect of folate-mediated targeting and verapamil-mediated P-gp inhibition with paclitaxel -polymer micelles to overcome multi-drug resistance. *Biomaterials* **2011,** *32* (35), 9444-56.

119. Zhao, L.; Zhao, Y.; Schwarz, B.; Mysliwietz, J.; Hartig, R.; Camaj, P.; Bao, Q.; Jauch, K. W.; Guba, M.; Ellwart, J. W.; Nelson, P. J.; Bruns, C. J., Verapamil inhibits tumor progression of chemotherapy-resistant pancreatic cancer side population cells. *Int. J. Oncol.* **2016,** *49* (1), 99-110.

120. Toutain, P. L.; Bousquet-Melou, A., Volumes of distribution. *J. Vet. Pharmacol. Ther.* **2004,** *27* (6), 441-53.